Effect of surface impurities and degradation on ice adhesion

Master of Science Thesis

Sara Caliari

Delft University of Technology

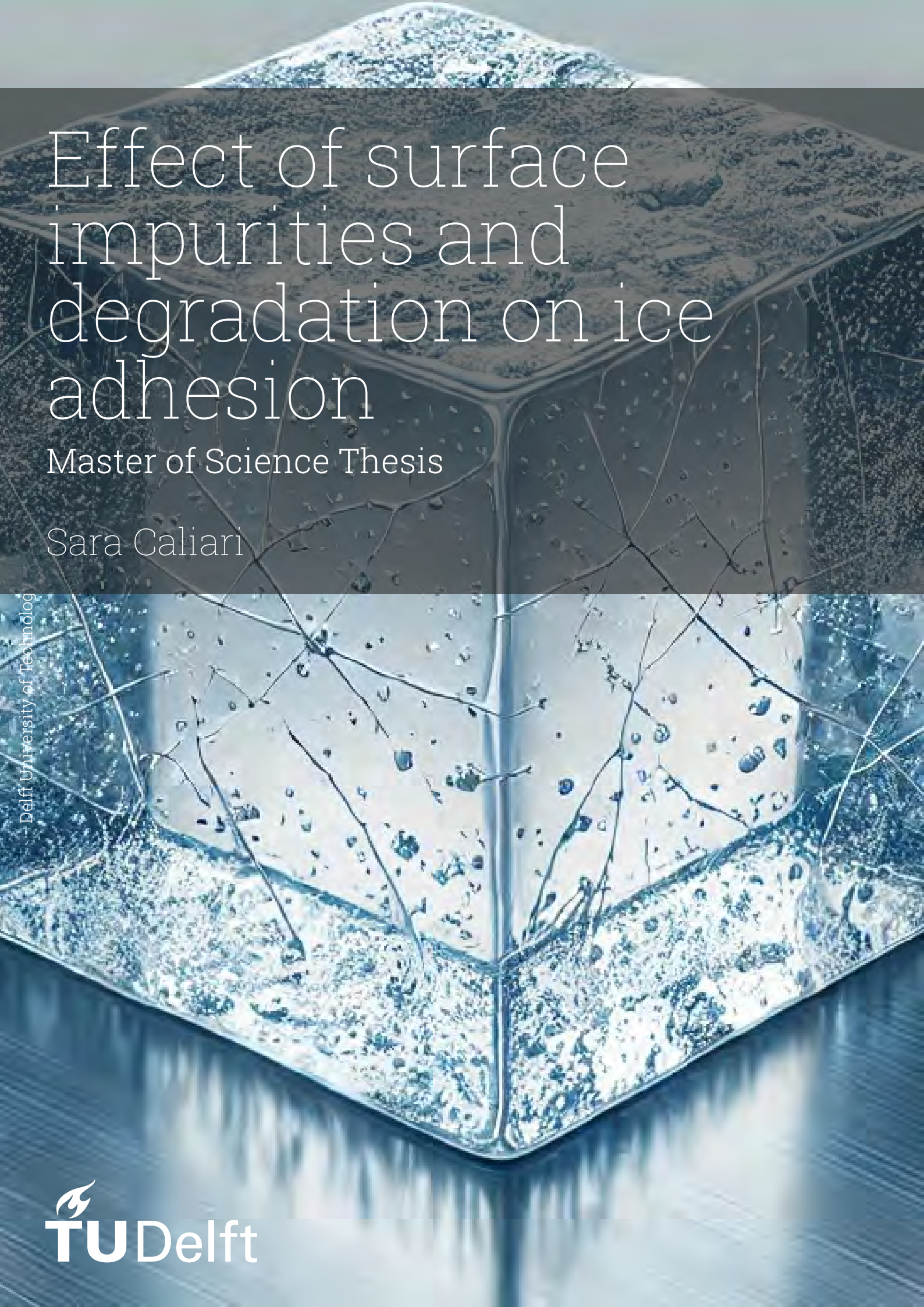

TU Delft

Effect of surface impurities and degradation on ice adhesion

Master of Science Thesis

by

Sara Caliari

to obtain the degree of Master of Science in Aerospace Engineering
at Delft University of Technology

To be defended publicly October 15th at 14:00 PM.

Student number:	5688574	
Supervisors:	Miisa J. Tavastsjerna	TU Delft, Aerospace faculty
	Dr. Santiago J. García Espallargas	TU Delft, Aerospace faculty
Thesis committee:	Dr.ir. Rene Alderliesten	TU Delft, Aerospace faculty
	Prof.dr.ir. Rinze Benedictus	TU Delft, Aerospace faculty

TU Delft

Acknowledgments

First of all, I would like to thank my main supervisor, Santiago, for providing invaluable guidance and insights, which helped me a lot throughout my thesis. Thanks to my daily supervisor, Miisa, for constant support and help. Your expertise has been crucial in completing this Master's thesis.

I owe my deepest gratitude to my family; without your unwavering support, I could not have reached this milestone. Your encouragement has been essential in helping me achieve this degree.

To my friends back in Italy - Giulia, Elisa, Anna, and Camilla - thank you for always being there for me and for believing in me. I wouldn't be the person I am today without you. To the friends I've made in the Netherlands, thank you for making me feel at home. The moments we've shared have been wonderful, and I am deeply grateful for the friendship we've built. A special thanks to Alice, who proofread my thesis multiple times.

Finally, I would like to thank Matej for his patience, understanding and encouragement. Your support and invaluable advice, especially during stressful times, has meant a lot to me. Without you, these past months would not have been as enjoyable and lovely.

Sara Caliari
October 2024, Delft

Abstract

In colder climates, ice formation and accumulation are a major safety hazard, which cause significant damage to infrastructure. These factors reduce operational efficiency and puts human safety at risk. For example, ice formation on aircraft wings can reduce aerodynamic performance, speed, and lift, and impede the movement of critical components, leading to unsafe situations.

Efficient anti-icing and de-icing methods are therefore essential to mitigate these risks. Anti-icing and de-icing techniques are generally divided into active and passive systems. Active systems require an external energy source and are usually very effective, but these methods have several drawbacks, including the need for continuous external energy and potential damage to aircraft materials. Alternatively, passive methods such as anti-icing fluids and icephobic coatings prevent ice formation without requiring external energy. However, anti-icing fluids are costly, environmentally harmful, and require frequent reapplication, increasing operating costs and labour. On the other hand, icephobic coatings use chemical or physical surface modification to impart anti-icing properties.

Within this context, icephobic coatings are one of the best solutions to prevent or inhibit ice formation and accumulation. However, designing effective and durable icephobic surfaces is a challenge due to the complex and varied nature of ice formation influenced by environmental conditions. To develop these coatings, it is important to have a deeper understanding of the mechanisms of adhesion between ice and surfaces, to compare different technologies to identify the best possible solution, and to quantify their efficacy. Ice adhesion strength is one of the key parameters used to assess ice adhesion to a particular surface. To determine ice adhesion strength, several mechanical test configurations have been developed, such as the tensile test, the centrifugal test, the vertical shear test and the horizontal shear test.

In the literature, the majority of tests have focused on understanding how surface topology affects ice adhesion strength, but no studies have focused on the effect of external factors or environmental degradation, even though both of these aspects are critical when considering the long-term durability and the real-world application of icephobic coatings.

The aim of this thesis is to address this gap with a systematic research approach. Four different materials were used; Teflon, polypropylene (PP), polyurethane (PU), and 6082 aluminium alloy (polished and unpolished). Particles of PVC and SiO_2 were introduced on the surfaces to simulate dust particles of different chemical nature, while silicone oil and UV radiation were used to simulate surface contamination and degradation. Ice adhesion strength was evaluated using a home-built horizontal shear test set-up.

The research revealed an increase in ice adhesion with the presence of dust particles at the interface between ice and the aluminium substrates. On the other hand, for the polymer substrates, the ice adhesion strength was influenced by the interaction between the dust particles and the substrates themselves. Finally, UV radiation degradation and oil contamination led, in most cases, to a decrease in ice adhesion strength. The results showed some unexpected behaviour, indicating that more attention should be paid to the effect of the environment on ice adhesion.

Contents

List of Figures

List of Tables

Nomenclature

Abbreviations

Abbreviation	Definition
AFPs	Anti-freezing proteins
APTES	(3-aminopropyl)triethoxysilane
CSH	Contact splitting hypothesis
DAQ	Data acquisition system
FTIR	Fourier Transform Infrared spectroscopy
HCl	Hydrochloric acid
Mn	Number average molar mass
Mw	Mass average molar mass
PC	Polycarbonate
PP	Polypropylene
PS	Polystyrene
PU	Polyurethane
PVC	Polyvinyl chloride
SAMs	Self-assembled monolayers
SiO_2	Silicon dioxide
SLIPS	Slippery liquid-infused porous surfaces
UV	Ultraviolet
WCA	Water contact angle

Symbols

Symbol	Definition
A	Area
D	Ice pillar diameter
E_{ice}	Modulus of ice
F	Peak removal force
f	Real fraction
g	Gravitational acceleration
H	Ice pillar height
h	Pushing height
L_c	Critical length
m	Mass
N	Normal force
r	Roughness factor
Sa	Arithmetical mean height of a surface
Sz	Maximum height of a surface
U	Energy loss due to plastic deformation

Symbol	Definition
$U_{friction}$	Energy dissipated by friction
V	Volume
W_A	Work of adhesion
$W_{A,P}$	Practical work of adhesion
Γ	Interfacial toughness
γ	Surface free energy
γ_i	Free energy of interface
γ^{lv}	Liquid surface free energy
γ^{sl}	Solid/liquid interfacial free energy
γ^{sv}	Solid surface free energy
$\Delta\theta$	Contact angle of hysteresis
ε	Dielectric constant
θ	Contact angle
θ_A	Advancing angle
θ_R	Receding angle
θ_w	Contact angle calculated with Wenzel's equation
θ_y	Contact angle calculated with Young's equation
ρ	Density
τ_{ice}	Ice adhesion strength
τ_{in}	Shear strength of the interface

1

Introduction

The unwanted formation of ice on surfaces can cause serious problems in a wide range of industries, such as telecommunications, power generation and distribution, infrastructure, offshore platforms, shipping and aviation, and all other forms of transport [1–4]. It has been reported that the problem of ice formation and accumulation is particularly prevalent in cold and mountainous areas such as Scandinavia, the Alps, North America, Russia, Japan, China and even South Africa [5, 6].

Ice accumulation can become a safety hazard to both instrumentation and people, as experienced by the Colgan Air Flight 3407 accident on 12 February 2009 involving a Bombardier Q400 [7]. The aircraft entered an aerodynamic stall due to a significant ice accretion on the wings and crashed into a house, killing a total of 50 people (all 49 passengers and crew on board and one person in the house). In terms of flight safety, the formation and accumulation of ice on external surfaces is to be considered one of the most dangerous risks to which an aircraft can be exposed. It can increase total weight, alter aerodynamics, and impact controllability of the aircraft, thereby seriously compromising flight safety [8]. In addition, critical instruments can be damaged by ice blockages in pitot-static systems, resulting in errors in airspeed, altimeter and vertical speed indicators. Before 1980, the number of aviation accidents caused by icing problems was approximately 500. As the number of commercial flights increased, so did the number of accidents. In the period 1982-2000, 583 aviation accidents in the USA alone identified icing as the primary cause, resulting in more than 800 fatalities [9]. In more recent years, with the development of anti-icing strategies, icing is still considered one of the major external causes of accidents in aviation [4].

Ice formation can also cause serious damage in other areas, as mentioned above. Excessive ice formation on wind turbines can increase structural loads, alter aerodynamic performance and reduce overall productivity [10] and the heavy loads caused by ice build-up on seagoing ships change the centre mass point of the ship and affects its manoeuvrability [11]. Increased loads on a structure due to ice also affect engineering structures, as happened in January 1998 in eastern Ontario and southern Quebec in Canada, where an ice storm and subsequent heavy ice load caused the collapse of 35000 distribution line structures and the destruction of 1300 high voltage power-line towers [12]. This event caused 25 deaths and left more than 2 million people without electricity for more than two weeks. The total cost of the damage was estimated to be in the magnitude of billions of dollars [12].

The problems caused by ice formation have shown how vulnerable modern societies are to ice and how difficult it is to predict the damage it can cause, both economically and socially. It is therefore essential to manage and reduce the risk of ice accretion, in order to increase safety and reduce the economic losses caused by failures and incidents. To

achieve this, it is necessary to develop effective methods for delaying or preventing the formation of ice on surfaces. These methods are discussed in section 1.1, with a special focus on icephobic coatings in section 1.2, where the mechanics of ice formation and the latest icephobic technologies are described. For the development of improved coatings, it is essential to measure their effectiveness accurately, which requires a universal test method. Existing test methods are described in section 1.3, along with the problem of lack of standardisation.

This thesis aims to gain a deeper understanding of how ice adheres to surfaces and how this adhesion is influenced by the presence of defects on the surfaces. The test results will be analysed to compare ice adhesion on different materials across various types of defects. The scope of this thesis is outlined in the last section of this chapter.

1.1. Ice protection

Various solutions to prevent ice accretion or to reduce ice adhesion strength on the structure have been developed and utilised. They can be divided in two main groups: anti-icing and de-icing systems [13]. The goal of anti-icing systems is to minimise nucleation and ice accumulation, while the main objective of de-icing systems is to minimise the energy required to remove ice from the surface, meaning ice is first formed and then removed. Each system is then divided into active and passive systems.

De-icing methods allow ice to accumulate on the surface before it is removed, so there are minimal passive methods that fall under this category. An example of this is the use of de-icing fluids on iced surfaces, as shown in **Figure 1.1**.

Figure 1.1: De-icing of an airplane with de-icing fluids [1].

[1] Source: www.airliners.net/photo/Aeroflot-Russian-Airlines/Airbus-A330-243/1710354

This is one of the most widely used methods for aircraft, but it can be very expensive. The cost and frequency of de-icing can vary depending on multiple factors [14]:

- Type of ice: if it is only a light layer of frost or snow, less fluid is required and the operation will be less expensive.
- Size of the aircraft: larger aircraft mean more fluid and higher overall costs.
- Geographical area: flights in colder regions will end up with more ice to remove and therefore the de-icing operation will be more expensive.
- Period of time in heavy ice conditions: for example, if the aircraft has been out all night, the de-icing operation will take more time and consequently be more expensive.
- Market conditions: the availability and cost of de-icing fluids, as well as labor costs, can fluctuate and impact the overall cost.

It has been estimated that the cost of de-icing an aircraft can range from $3,000 to $22,000.

Two other methods have been proposed, however their effectiveness has not yet been tested. The first method is called active pitching and can only be used in light conditions, as the idea behind this system is to expose the iced surface to the sun so that the ice melts or the ice load is released [15]. The second proposed method is based on flexible blades that help to shed the ice formed since they are flexible enough to crack the loose ice [16].

Active de-icing methods use thermal or mechanical techniques and include manual removal of ice [15]. An example of mechanical technique is flexible pneumatic boots, which remove ice by varying the profile of the surface when inflated. Instead, methods using thermal techniques are, for example, those based on utilising warm air or heating resistance (which can be classified as anti-icing methods if they are used during operation to prevent ice formation).

Active anti-icing methods use the same techniques as thermal de-icing systems [15], such as heating resistors and warm air. Passive anti-icing methods include chemicals (anti-icing fluids, which are more expensive than de-icing fluids but typically require less frequent application) and icephobic coatings designed to prevent or reduce the accumulation of ice on the surface before it forms.

Active systems consume energy to operate, which means they are expensive. They also add weight and require more restrictive design requirements, making them difficult to integrate into an efficient aircraft design. On the other hand, passive systems based on anti- and de-icing fluids also have disadvantages. De-icing fluids are expensive, time consuming, and can have a have a significant impact on the environment. They also gradually lose their effectiveness and can also corrode the surface they are designed to protect. Icephobic coatings are therefore one of the best options, as they require no energy or active components and protect the substrate. This makes them an attractive solution for preventing or delaying ice accumulation or reducing the ice adhesion strength on the substrate.

In recent years, research has increasingly focused on the latter solution [17–22], which when used in combination with active de-icing systems reduces energy consumption and weight. However, the production of durable icephobic surfaces is not simple. Ice formation is sensitive to the different environmental conditions that can occur, and these differences in ice formation make it difficult to develop consistent icephobic surfaces that work in every environment.

1.2. Icephobic coatings

In order to develop anti-icing surfaces, it is necessary to understand how ice adheres to a solid surface, the parameters that influence the adhesion, and the different ways in which ice can form on a surface. Ice adhesion to a solid surface is influenced by both the wettability of the surface and the interactions between the polar molecules of ice and the surface itself. Surface wettability is determined by the water contact angle (WCA), which depends on the surface free energy and the surface roughness, i.e. its micro- and nanostructure. The main physical mechanisms influencing ice adhesion are van der Waals forces, hydrogen bonding, and electrostatic interactions, with electrostatic interactions being the most important. To reduce ice adhesion to surfaces, it is necessary to minimise either the contact area or the electrostatic interactions between the ice and the surface. For the latter, low permittivity materials, such as low surface energy polymers, can be excellent candidates for icephobic coatings. Whereas to reduce the contact area, the surface morphology can be modified to change the hydrophobicity of the coating (i.e. the water contact angle). To achieve this, it is necessary to understand how surface free energy and surface roughness affect surface wettability. In this section, the factors that influence surface wettability are discussed (subsection 1.2.2), together with an overview of recent developments in icephobic coatings (subsection 1.2.3). This is preceded by a brief introduction to ice formation on surfaces (subsection 1.2.1).

1.2.1. Ice accretion on surfaces

Ice formation on surfaces is highly complex and is influenced by various environmental factors and surface conditions. Understanding how ice forms and the properties of ice is critical to selecting the best strategy for protecting surfaces from ice. Ice accretion is defined as the accumulation of ice or snow on surfaces [23]. Atmospheric icing can occur under three main conditions and can have different characteristics: in-cloud icing, precipitation and frost. The type of ice is an important factor in analysing the adhesion of ice to a surface, as the differences in density and microstructure result in different methods of adhering to a surface [24].

In-cloud icing occurs when supercooled water droplets collide with supercooled surfaces. The water droplets can be supercooled to temperatures as low as -30°C and, due to their size, are still in liquid form. The accumulation of ice due to cloud icing is influenced by the size of the water droplets, the number of droplets hitting the surface and the atmospheric conditions (such as wind speed and temperature). The latter factors determine the shape of the accumulated ice:

- Soft rime ice: usually has low adhesion and low density and typically forms when the size and number of water droplets are limited, i.e. when the water content is low and when the temperature is between -40°C and -20°C. It forms a thin layer of ice as a result of the small supercooled water droplets impacting the surface and freezing immediately.
- Hard rime ice: is more difficult to remove and has a higher density than soft rime. It forms when the water droplet size and the number of droplets are larger.
- Glaze ice: the temperatures at which it occurs are above -10°C and, as a result, the water droplets do not freeze immediately but run along the surface until they freeze, forming a dense layer of ice that has a strong adhesion to the surface.
- Mixed ice: has the characteristics of both rime and clear ice. Its aspect is rough and irregular and it forms when both small and large water droplets are present.

The difference between rime and glaze ice is shown in **Figure 1.2**.

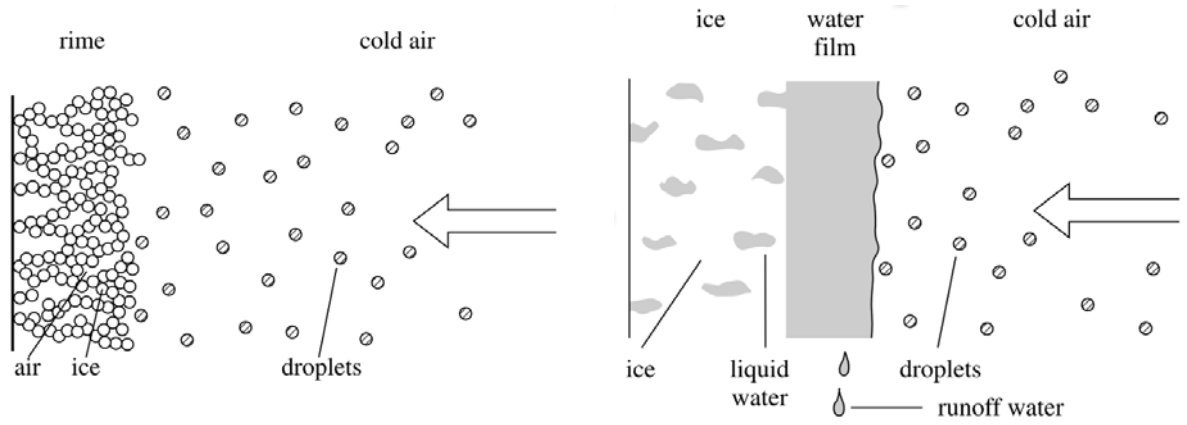

(a) Formation of rime ice [12].

(b) Formation of glaze ice [12].

Figure 1.2: Differences in the formation of rime ice (a) and glaze ice (b).

Ice accumulated from precipitation can cause more problems because it occurs at a higher rate. It can take two forms:

- Freezing rain: creates a dense, highly adhesive layer of ice and it forms when rain falls on supercooled surfaces and ice crystals nucleate.
- Wet snow: can be easily removed if it is not completely frozen, as snow can remain partially liquid between 0°C and -3°C. However, once fully frozen, it strongly adheres to the substrate.

The final way that ice can accumulate on a surface is through frost. This occurs when water vapor in the environment turns to ice when it touches supercooled surfaces. This happens when the wind speed is low. Frost can manifest itself in two different ways [25]:

- Desublimation frost: occurs when water vapor is converted directly into ice.
- Condensation frost: occurs when the water vapor first condenses into supercooled dew droplets, which then freeze.

Initially, the mechanism of condensation frosting was thought to be similar to that of icing, with supercooled droplets freezing by heterogeneous nucleation. The only perceived difference was that water is deposited in icing, and nucleated in freezing. However, it was discovered that heterogeneous nucleation is not the mechanism for condensation freezing. Instead, the primary mechanism is interdroplet ice bridging, a process in which ice bridges grow between frozen droplets and liquid droplets to form an interconnected ice network [26]. As a result, strategies developed for the icing problem are not necessarily the same for the frost problem. The process of condensation frosting can be divided into five distinct stages: (i) supercooled condensation, (ii) onset of freezing, (iii) frost halos, (iv) interdroplet ice bridging and dry zones, and (v) percolation clusters and frost densification. **Figure 1.3** shows the mechanisms of condensation frosting.

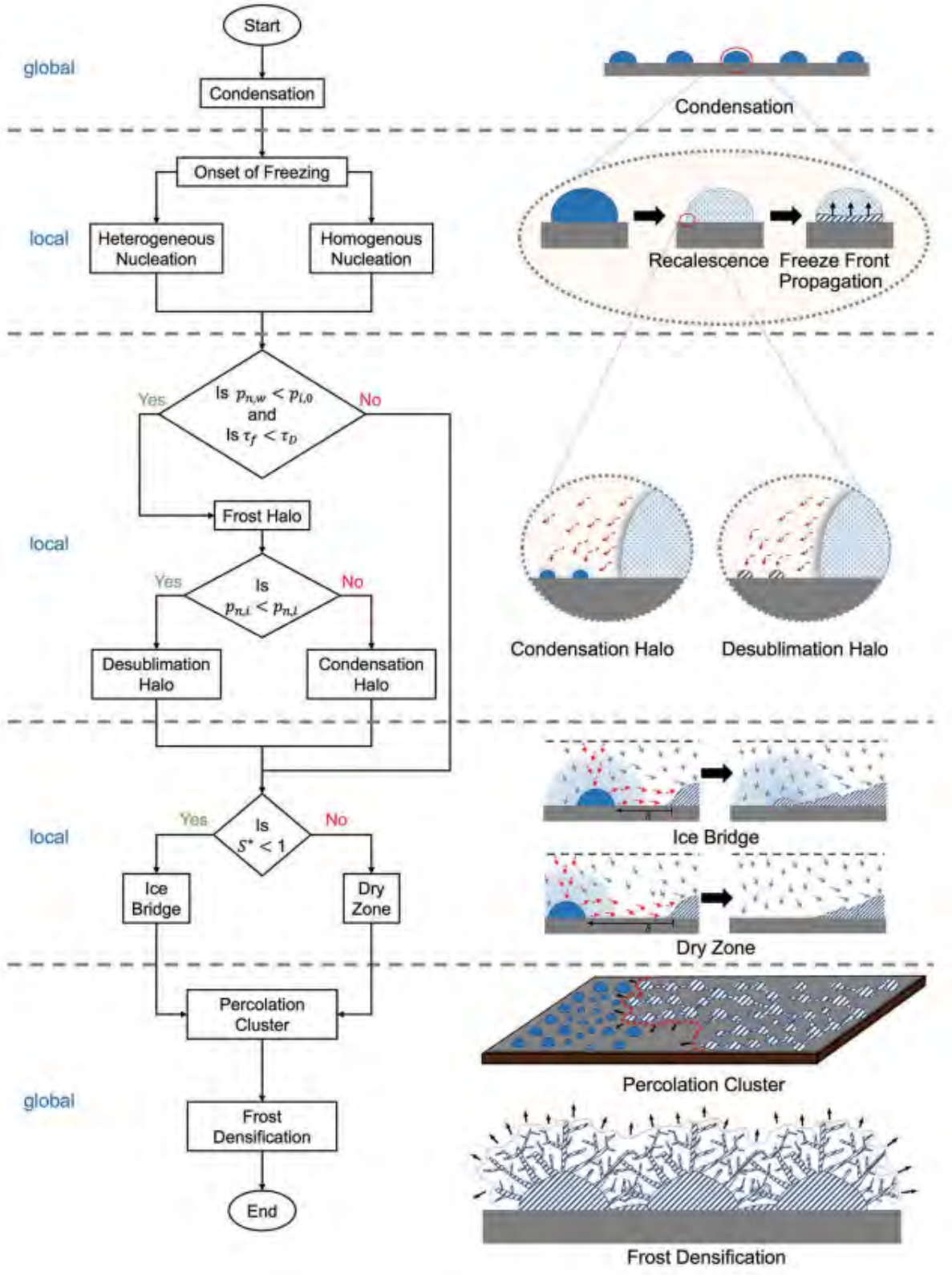

Figure 1.3: Process of condensation frosting. The parameters used in the diagram are further discussed in the review by Nath et al. [25].

1.2.2. Surface wettability

As discussed above, surface wettability is controlled by the water contact angle, which is directly related to the hydrophobicity (or hydrophilicity) of the surface itself. The term hydrophobic comes from the ancient Greek terms “húdro”, meaning water, and “phóbos”, meaning fear, literally “to be afraid of water”. The opposite term, hydrophilic, means “to love water”, from the ancient Greek “phílos”, meaning love. The hydrophobic effect is a molecular interaction mechanism that describes the tendency of nonpolar molecules to interact with other nonpolar molecules and thus displace water molecules from the interacting molecular surfaces. This effect explains the predisposition of nonpolar molecules to aggregate in water and to minimise the contact area between water and the nonpolar molecules involved. In thermodynamic terms, the hydrophobic effect is the positive change in the free energy of water. A positive change in the free energy of the solid in contact with water indicates hydrophobicity, while a negative change in free energy indicates hydrophilicity. This means that when a water droplet comes into contact with a surface, the surface may be completely wet or partially wet. If the surface is hydrophobic, its molecules will repel the water molecules and the water droplet will try to reform due to the cohesion force, which tends to form a shape that minimises energy. Conversely, if the surface is hydrophilic, the water droplet will spread on the surface due to the adhesive forces between the droplet and the surface. **Figure 1.4** shows the difference between the concept of a hydrophilic and a hydrophobic surface.

Figure 1.4: Difference between a hydrophilic and a hydrophobic surface.

The balance between the adhesive and cohesive forces gives the degree of wetting (wettability) of the surface, which is the physical property that characterises the ability of a liquid droplet to maintain contact with a solid surface and results from the intermolecular interactions between the solid and the liquid. The intermolecular forces between the solid surface and the liquid depend on the chemical structure of the solid. These interactions can be hydrogen bonding, van der Waals forces, electrostatic forces, dipole-dipole forces, or London dispersion forces.

The wetting tendency of the surface is quantified by the contact angle, which is the angle at which the liquid/vapour interface meets the solid substrate. Each system has a unique contact angle and it can be determined by the interactions between the three different phases, i.e. vapour, liquid and solid [27]. The first and most basic relationship describing wettability in terms of contact angle was given by Thomas Young in 1805 when he published “An Essay on the Cohesion of Fluid” in which he wrote that “for every combination of liquid and solid there is a corresponding angle of contact” [28]. This relationship is called Young’s equation (Equation 1.1), and it correlates the contact angle θ, the liquid surface free energy γ_{lv}, the solid/liquid interfacial free energy γ_{sl} and the solid surface free energy γ_{sv}. **Figure 1.5** shows the contact angle of a liquid droplet on a solid surface.

$$\gamma_{sv} - \gamma_{sl} = \gamma_{lv} cos\theta \tag{1.1}$$

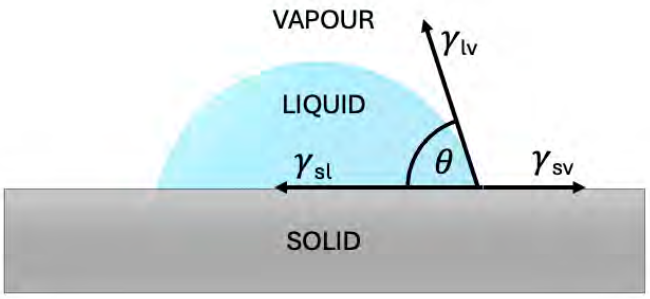

Figure 1.5: Contact angle θ of a liquid droplet on a solid surface and the free energies of the liquid surface γ_{lv}, the solid/liquid interface γ_{sl} and the solid surface γ_{sv}.

From Equation 1.1 the variables for hydrophobicity and hydrophilicity can be defined. If the contact angle is less than 90°, the surface is considered to be hydrophilic, and the solid surface free energy is high while the interfacial free energy is low. Therefore, when water tries to maximise the minimum energy state, the water-solid contact will be high. On the other hand, if the contact angle between 90° and 180°, the surface is considered hydrophobic and the surface free energy of the solid is low, while the interfacial free energy is high. This means that when water tries to maximise the minimum energy state, the solid-vapour contact will be high. Theoretically, when the contact angle is 180°, the droplet assumes a spherical shape.

However, Young's equation does not take into consideration the roughness of the surface. Robert N. Wenzel further developed Young's equation to account for roughness by introducing a roughness factor r, which is equal to the real wetted surface area over the apparent area. His assumption was that assuming a water droplet would penetrate the rough area of a surface. Wenzel's equation (Equation 1.2) uses θ_y, the contact angle calculated with Young's equation, to determine θ_w, the contact angle calculated taking into account the roughness of the surface.

$$cos\theta_w = rcos\theta_y \tag{1.2}$$

Wenzel's model correlates the wettability of a surface with its roughness. In fact, under hydrophilic conditions, a surface will become more hydrophilic as its roughness increases, meaning that θ_w will decrease, while under hydrophobic conditions, a surface will become even more hydrophobic as its roughness increases, meaning that θ_w will also increase.

On the other hand the Wenzel's equation cannot explain superhydrophobicity, which is a phenomenon that happens when a surface exhibits almost zero wetting [29, 30]. Superhydrophobic surfaces derive from a specific surface roughness and a specific surface free energy. They have a contact angle greater than 150° and a small contact angle of hysteresis ($\Delta\theta$), which can be defined as the difference between the advancing (θ_A) and receding (θ_R) angles when a droplet moves in a tilted surface.

Superhydrophobic surfaces can be observed on some natural tissues, such as the surface of lotus leaves, hence the name "lotus effect" (**Figure 1.6**). This effect is due to the presence of two types of roughnesses, microroughness and nanoroughness (**Figure 1.6b**), and a waxy material covering the surface, resulting in a high resistance to wetting and a contact angle slightly above 150°.

Therefore, superhydrophobicity can be achieved by creating a suitable roughness on the surface, which would reduce the contact area between water and the solid substrate. The fact that roughness affects the contact angle was extended by Archibald B. D. Cassie and Sydney Baxter in 1944, with Equation 1.3, which can explain superhydrophobicity by correlating the real fractions (f_1 and f_2) of the two components involved (solid surface and air) and the contact

(a) Water droplets on a lotus leaf [31].

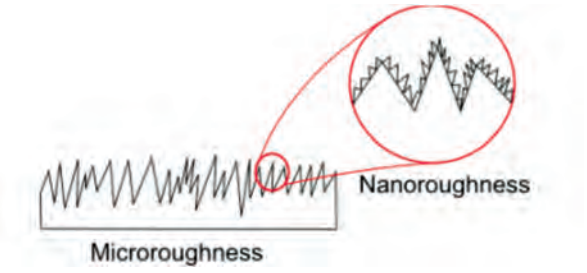

(b) Schematic representation of microroughness and nanoroughness [13].

Figure 1.6: The “Lotus effect”: (a) illustrates water droplets on a lotus leaf, and (b) shows a representation of microroughness and nanoroughness.

angles of the two components (θ_1 and θ_2) with the effective contact angle (θ_c).

$$cos\theta_c = f_1 cos\theta_1 - f_2 cos\theta_2 \tag{1.3}$$

Since f_2 represents the real fraction of air, it can be written as $1 - f_1$ and θ_2 can be set equal to 180°. The equation can therefore be written as:

$$cos\theta_c = f_1(cos\theta_1 + 1) - 1 \tag{1.4}$$

The latter equation explains why a rough surface with a large amount of air trapped between the surface irregularities has a very small fraction of the surface area in contact with water and can therefore be a superhydrophobic surface [32]. The difference between the Wenzel state (of a weak hydrophobic surface, where the cavities of the rough surface are fully wetted by the liquid and no air is trapped among them) and the Cassie-Baxter state (of a strong hydrophobic surface capable of trapping air in its cavities so the liquid rests in top of the roughness) is illustrated in **Figure 1.7**.

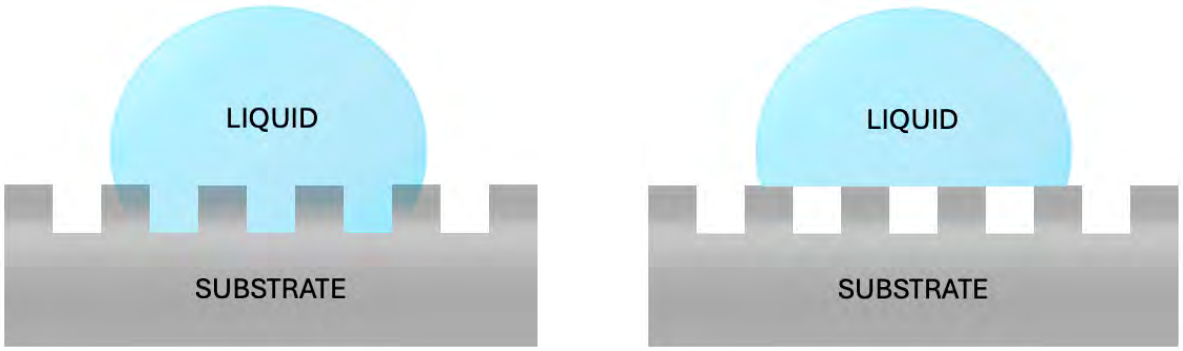

(a) **(b)**

Figure 1.7: Representation of the difference between the Wenzel state (a) and the Cassie-Baxter state (b).

In summary, the topology of a surface influences the contact angle, which in turn describes the surface’s wettability, indicating whether the surface is hydrophilic or hydrophobic. The Wenzel model explains that increasing surface roughness leads to greater hydrophobicity, with an apparent contact angle of up to 150°. On the other hand, the Cassie-Baxter model describes a particular surface structure that traps air below the surface, resulting in a low liquid-solid contact area and water repellency.

1.2.3. Icephobic coating technologies

Icephobic coatings aim to delay initial nucleation events, slow down ice growth, and/or lower ice adhesion strength [33]. Over the past 15 to 20 years, numerous attempts have been made to develop effective icephobic coatings, and the mechanisms by which these coatings work, together with the challenges they face, will now be briefly discussed.

The development of superhydrophobic surfaces is one of the most widely used approaches for realising icephobic coatings [23]. These surfaces can be created by combining micro- and nanoscale surface structures with low surface energy materials. This process typically involves two main procedures, where the first creates the micro- and nano-structure through various techniques such as deposition, etching, or lithography. Whereas, the second treats the surface with low surface energy materials that enhance hydrophobicity. This can be realised using techniques such as chemical modification or self-assembled monolayers (SAMs). However, developing superhydrophobic coatings for anti-icing applications may not be the optimal choice. There have been conflicting opinions about the effectiveness of superhydrophobic surfaces in reducing ice adhesion. Some studies have reported a reduction in ice adhesion on superhydrophobic surfaces compared to hydrophobic surfaces, which has been attributed to the increase in air entrapped in the surface structure in the Cassie-Baxter state after the water freezes on top of the surface [32, 34–37]. On the other hand, other studies report that superhydrophobic surfaces increase the adhesion of ice to the surface. This can be attributed to the fact that the smaller water droplets penetrate and freeze into the micro- and nano-structures of the surface, leading to the so-called Wenzel state, where the “mechanical interlock” between the ice and the superhydrophobic surface increases the adhesive force between the two [38–40]. This shows that the phenomenon of mechanical interlocking nullifies the icephobic effect of the surface, meaning that a higher water repellency does not imply better icephobic properties.

The main difference between these experiments was in the ice accretion on the surfaces, which strongly affects the ice adhesion properties of superhydrophobic surfaces. It has been found that frost forms within the superhydrophobic surface texture, meaning that the wettability state of the surface is not in the Cassie-Baxter state but in the Wenzel state [39, 40]. This means that ice will make contact with all available surfaces of the superhydrophobic coating texture, forming an ice layer. Therefore, ice adhesion of superhydrophobic surfaces will increase due to the mechanical interlock between the ice and the surface. In other words, depending on how ice forms on a surface, the surface itself changes its ice-resistance properties. In addition, the micro- and nanostructure of superhydrophobic surfaces can easily deteriorate during icing/deicing cycles, making these surfaces not durable enough for anti-icing purposes as they are subject to greater wear [33].

One method of improving anti-icing properties is to introduce a lubricating liquid into a porous surface, creating what are known as slippery liquid-infused porous surfaces (SLIPS), which have been shown to have better anti-icing properties than superhydrophobic surfaces [41]. These surfaces are inspired by a tropical pitcher plant called Nepenthes, which produces a liquid repellent, slippery layer on its surface. SLIPS have a solid micro-textured surface filled with a stable liquid matrix (as shown in **Figure 1.8**) and have been shown not to increase adhesion under different icing conditions. However, the durability of liquid-infused slippery surfaces may be the most challenging issue. The mechanism by which they delay ice formation is dependent on the availability of lubricant, which can be significantly reduced during flight due to abrasion, aerodynamic stresses, and icing/deicing cycles, making these coatings unsuitable for use on aircraft against icing.

One of the most effective techniques for icephobic coatings is to use low surface energy materials, thus materials with a low permittivity (i.e. with a low dielectric constant, ε). As

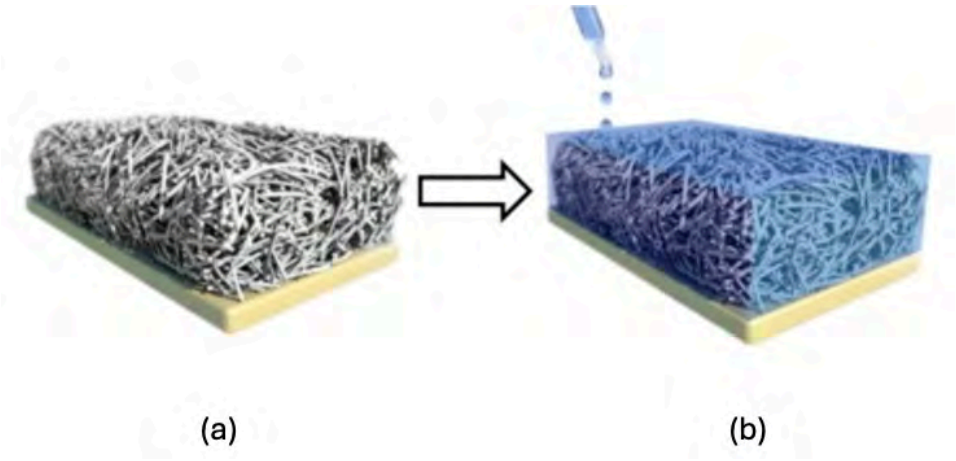

Figure 1.8: A porous surface (a) is infused with a lubricating liquid (b) to prepare a slippery liquid-infused porous surfaces [41].

mentioned above, a low permittivity material can reduce electrostatic interactions, resulting in a weaker bond between ice and the surface. Permittivity is also related to the surface energy of a material: lower permittivity materials typically have a lower surface energy, which reduces the attraction between the surface and the ice, making it harder for ice to adhere to the surface. This makes them suitable candidates for anti-icing applications. Compared to superhydrophobic coatings, they have a smoother surface and the effect of mechanical interlocking becomes negligible. These materials include fluoropolymers ($\varepsilon \approx$ 2.1), such as polytetrafluoroethylene (PTFE, commonly known as Teflon) and polysiloxanes. Fluoropolymers have been shown to significantly reduce ice adhesion under certain conditions and were considered good candidates as anti-icing materials [42]. However, they have raised several concerns about their potential harm to human health and the environment [43]. Their production and use is therefore restricted, except in essential cases. On the other hand, polysiloxanes exhibit good anti-icing properties due to the mismatch in mechanical and rheological properties between ice and silicone polymers. This originates from the low glass transition temperature (Tg) of the polysiloxanes, which causes their surface to be “soft”. On a soft surface, stresses are unevenly distributed and accumulate at the interface. When a force is applied to remove the ice, the stress at the interface creates a favorable path for easier ice release. However, their poor durability and mechanical properties make them unsuitable for anti-icing applications. Further developments to create icephobic surfaces focus on the combination of fluorinated and siloxane groups into synthetic materials.

Another icephobic material that was investigated is a stress-localized viscoelastic coating, which uses elastic energy localization at the ice-coating interface to induce shear stresses [44]. These stress-induced surfaces are developed by combining materials with hard and soft segments, which work together to create cracks at the interface when an external force is applied. As cracks form, localized stresses are generated, and the resulting shear stresses propagate the cracks along the interface. This ultimately leads to the detachment of ice from the coating.

In addition, recent research has shown that anti-freezing proteins (AFPs) could be used to develop anti-icing coatings based on them, as they can adhere to ice crystals and prevent them from expanding [23]. This effect is due to the interaction between ice and AFPs, which lowers the freezing point of water and inhibits the growth of ice crystals [45]. However, the durability of AFP-based coatings and their large-scale industrial applicability remain challenging and require further investigation. Moreover, the incorporation of AFPs into surfaces has not been

extensively studied and most of the knowledge of the working mechanisms of AFPs has been derived from studies in solutions, primarily in the field of biomedical applications [46].

Another novel strategy is based on patterned coatings, which work by a different mechanism and therefore do not have the same drawbacks as the previously described technologies. These coatings can, to some extent, control and influence how and what type of ice grows on the surface [47]. This reduces ice adhesion and prevents the formation of a thick layer of ice. Boreyko et al. studied the behaviour of chemical micropatterns on condensation frosting [48]. The mechanism is based on preventing ice bridging between droplets and the following ice growth by controlling the space between nucleation sites. This slows down and eventually stops ice bridging, thereby controlling the growth of condensation frost on a surface. It was found that condensate formed mainly on the hydrophilic zones and that water droplets were trapped by the hydrophilic zones before they could bridge, thus stopping the formation of a frost film and subsequently a layer of ice.

To summarize, there has been some research into passive anti-icing coatings in recent years, although none of these technologies have been developed for practical use. In order to advance these technologies, it is essential to quantify their effectiveness, durability, and applicability in areas where these anti-icing strategies are needed, such as aerospace or telecommunications. It is necessary to measure the ice adhesion of different surfaces in order to compare their anti-icing properties and to understand. For meaningful comparison and study, consistent test parameters and environmental conditions must be used to ensure that results are comparable and universal. The next chapter discusses the various ice adhesion testing technologies.

1.3. Ice adhesion testing

The development of a valid test method is essential for the progression of new anti-icing coatings, however testing the effectiveness of surfaces for ice adhesion is a major problem due to the difficulty of reproducing and controlling environmental conditions. The anti-icing efficacy of a surface can be evaluated by measuring the ice adhesion strength τ_{ice}. The ice adhesion strength is defined as the ratio between the peak removal force F and the interface area between the ice and the substrate A (**Equation 1.5**) [49].

$$\tau_{ice} = \frac{F}{A} \tag{1.5}$$

Using the ice adhesion strength τ_{ice} to characterize an interface implies that the force required to remove ice from the substrate scales with the area of the interface between them, meaning that structures with a large area exposed to ice formation may require extremely high forces to remove it. However it has been hypothesised that there is a critical length of the interface, L_c, beyond which the force required to separate the ice from the substrate becomes constant [50]. This was explained by the fact that the fracture mechanism can be either stress- or toughness-dominated. The shear strength of the interface τ_{in} controls the delamination when the length of the interface between the ice and the substrate is relatively small, meaning that $\tau_{ice} = \tau_{in}$. This implies that the fracture mechanism is stress-dominated and the fracture is sudden and spontaneous along the whole interface. On the other hand, when the interface is relatively large, the interfacial toughness (Γ), which quantifies the resistance to crack growth along the interface, controls the ice delamination and the fracture mechanism is toughness controlled. This indicates that there is a crack propagating along the interface and that the detachment is not sudden. The critical length L_c is the length of the interface where the transition between the two failure modes occurs and is given by **Equation 1.6**, where E_{ice}

is the modulus of ice and H is the ice pillar height [51].

$$L_c = \sqrt{2E_{ice}\Gamma\frac{H}{\tau_{in}^2}} \tag{1.6}$$

One of the most promising approaches to the development of icephobic surfaces is to reduce their ice adhesion strength. If a surface has a low adhesion strength to ice, the ice formed can be shed by its own weight, by wind, or by natural vibration. In order to reduce ice adhesion, it is essential to be able to test the adhesion between ice and a substrate. Various tests have been developed to determine the ice adhesion strength to a given surface.

When considering ice adhesion testing for aircraft, a distinction can be made between impact ice and non-impact ice. Impact ice has a non-zero initial velocity on contact with the surface, making it the most realistic type for testing as it closely simulates the real conditions under which ice forms on aircraft surfaces. In contrast, non-impact (or bulk) ice is easier to test as it is static and therefore easier to control and evaluate. The tests considered in this thesis all use non-impact ice.

The most common are the centrifugal test[2], the horizontal shear test, the vertical shear test, and the tensile test (**Figure 1.9**) [52].

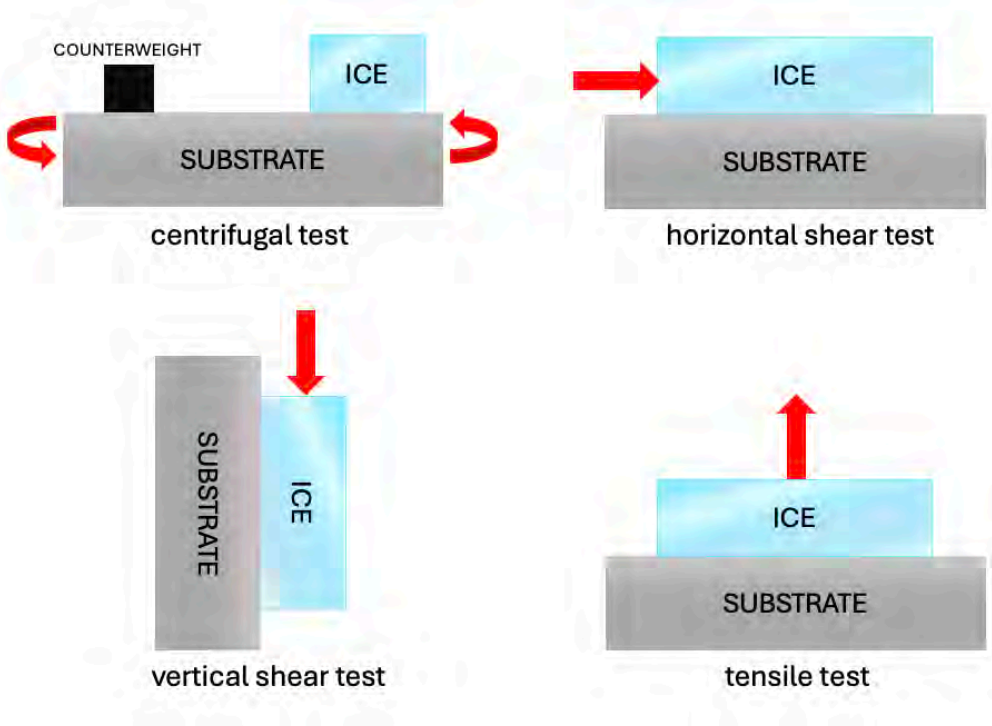

Figure 1.9: Illustration of the four most common tests to measure ice adhesion strength.

The centrifugal test is the only indirect mechanical test. The others can be described as direct mechanical tests, where the mechanical force is applied directly to the ice pillar (or to the mould containing the ice pillar). In a centrifugal test, an ice sample is placed on a beam and rotated with increasing acceleration, creating centripetal acceleration. By recording the angular velocity at the moment the ice pillar detaches from the surface, the detachment force can be determined. Shear tests, on the other hand, usually use a force probe to induce the ice

[2]Centrifugal test can be conducted for impact ice too, however the generation of the impact ice itself is much more complicated and prone to inconsistencies compared to the generation of bulk ice.

to detach from the substrate. The horizontal shear test (also known as the push test) is the most commonly used. In tensile tests, ice detachment is induced by pulling the ice perpendicular to the surface. More methods are found in literature but the two most two most common methods are the centrifuge test and the horizontal shear test [53]. Of these, the horizontal shear test is the simpler to set-up and allows more control over ice detachment from the substrate.

However, due to the large number of variables influencing the tests and the large number of different tests that have been carried out, there is a lack of standardised testing systems and test methods in literature, resulting in data that is not always comparable. In fact, the peak force is usually recorded and the ice adhesion strength is calculated, but there is no analysis of why these results are obtained, of what happens during the test, and of how certain variables and environmental conditions may affect the final results. It has been shown that several parameters are critical to an accurate assessment of ice adhesion and therefore need to be considered, although they are often neglected. These parameters include relative humidity, surface temperature, ice type, ice pillar size, cooling rate, freezing time, pushing height, and pushing speed [53].

1.4. Scope of master thesis

Ice adhesion is one of the most important parameters to quantify and study icephobic materials. Understanding the physics and mechanics of how ice adheres to surfaces and how this is influenced by environmental conditions, external factors, or surface defects is essential for the development of new techniques for anti-icing purposes. However, ice adhesion is a complex phenomenon that is not yet fully understood. Measuring ice adhesion in the laboratory is particularly challenging due to the sensitivity of ice to factors such as humidity and temperature changes, as well as the lack of standardisation, making it difficult to compare existing results.

Current research has focused primarily on reducing ice adhesion through the development of various materials and techniques, and on the impact that temperature variations and surface wettability have on ice adhesion. However, the tests used to measure ice adhesion are often conducted under different environmental conditions and with different types of ice, and the parameters used are not always reported, resulting in non-comparable results.

Moreover, research has largely overlooked how ice adhesion is affected by external factors or surface defects. Tests are usually conducted under ideal conditions, using clean and flawless surfaces, however, in reality surfaces are exposed to a variety of conditions that can cause surface damage and defects. These can be of various types:

- Mechanical defects: such as scratches on the surface and erosion.
- Chemical defects: such as exposure to UV radiation and solvents.
- Presence of dust or liquids (such as fuel or grease) on the surface.

Thus, despite ongoing research into new techniques to reduce ice adhesion, the influence of interfacial defects has not been thoroughly investigated in the literature. Exploring this aspect could provide valuable insights into the mechanisms by which ice adheres to surfaces and significantly contribute to the development of more effective anti-icing technologies. Moreover, a deeper understanding of ice-surface interactions can be achieved by analysing how the presence of surface defects alters ice adhesion.

After the previous discussion, the scope of this master thesis can be defined. The research questions that are wished to be answered during the thesis are the following:

Main question: How does the introduction of surface defects affect ice adhesion strength and how can this be explained?

Subquestions:

- How does the presence of different types of dust on the surface affect the ice adhesion strength of different materials?
- Does exposure to UV radiation affect the adhesion of ice to polymers?
- Does the presence of grease or oil affect the ice adhesion strength?
- Can the physics of ice adhesion be better understood?

Understanding the physics of ice adhesion, investigating the factors that contribute to influence ice adhesion, and understanding the influence of surface defects requires an accurate experimental approach, which allows repeatable and reliable results. This is essential for interpreting the results and drawing meaningful conclusions about the factors affecting ice adhesion strength. The results of this work will clarify whether interfacial defects, specifically impurities and UV radiation, affect ice adhesion strength, with the aim of improving the understanding of ice-surface interactions.

2

Materials and Experimental Methodology

This chapter describes the materials, sample preparation methods, characterisation techniques, and test procedures, used to analyse the ice adhesion strength of the substrates with different defects. The aim is to explain the steps taken to prepare, test, and analyse, the substrates to ensure the reproducibility of the experiments and the reliability of the results.

The following chapter is divided into four main sections. The first section describes the materials used. The second section focuses on the preparation of the samples, where specific defects (dust and oil contamination and UV exposure) were introduced to study their effects on the ice adhesion strength of the materials. The third section presents the results of the characterisation techniques, specifically Fourier Transform Infrared spectroscopy (FTIR), water contact angle (WCA), and surface roughness measurements. Finally, the fourth section explains the experimental set-up and procedure used to determine the ice adhesion strength of the substrates.

2.1. Materials and methods

The polyurethane (PU) substrates (product name: ALEXIT-ClearCoat 411-14 000U Colourless high gloss) were provided by AIRBUS. The Teflon, polypropylene (PP), and polyviynl chloride (PVC) substrates were purchased from S-Polytec GmbH. The aluminium alloy used for the substrates is AA6082. The dimensions of the samples are 20 mm x 20 mm x 1 mm. The glass surfaces were purchased from Carl Roth.

The PVC particles (average Mw $\approx$ 43,000, average Mn $\approx$ 22,000), SiO_2 particles (particle size: 40-63 μm), SiO_2 particles (particle size: 100 μm), hydrochloric acid (ACS reagent, 37%), (3-aminopropyl)triethoxysilane (purity $\geq$ 98%), and silicone oil were purchased from Sigma-Aldrich.

The solvents ethanol, methanol, and acetone, were purchased from Merck Sigma (analytical grade) and used as received.

2.1.1. Polishing of AA6082 substrates

The AA6082 samples were grinded with 1000, 2000, and 4000 grit size, and then polished with 3 μm and 1 μm diamond paste.

2.1.2. Surface modification of SiO_2particles

The method used is known as functionalization, a process that introduces new properties or functions to a material by altering its surface chemistry. Specifically, the technique used to increase the hydrophobicity of SiO_2 particles is called silanization. This method involves the modification of solid substrates through the deposition of organic monolayers composed of silane molecules. Silanes are a group of silicon-based compounds characterised by a silicon atom bonded to one or more organic groups and by reactive functional groups, such as alkoxy, amino, or chloro groups. The silanization process forms covalent bonds between the silane molecules and the SiO_2 particles surface, creating a controlled architecture that modifies the surface properties of the particles [54].

Before the process, the SiO_2 particles have a silanol-terminated surface, meaning that their surfaces contain silanol groups, which are functional groups with the connectivity Si-O-H. At the end of the process, the SiO_2 particles have an aminosilane-terminated surface. In this modified state, the amino groups (NH_2) are bonded to a siloxane (Si-O-Si), which increases the hydrophobicity of the particles. A schematic of the silanization process is depicted in **Figure 2.1**.

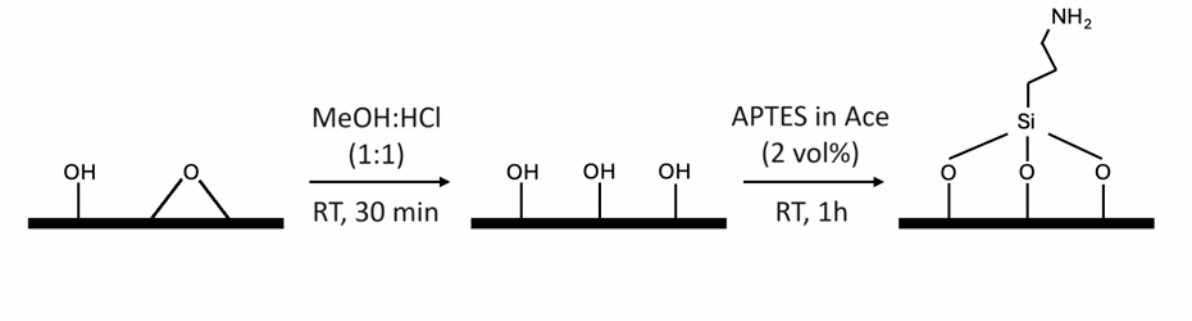

Figure 2.1: Schematic representation of the silanization process.

The modification of the SiO_2 particles is divided into two phases: the activation phase and the sol-gel silanization phase. The activation phase is necessary as it prepares the surface of the SiO_2 particles by introducing reactive functional groups essential to form strong bonds with the silane molecules. In the second phase the silane molecules, specifically (3-aminopropyl)triethoxysilane (APTES), are introduced to modify the surface of the particles. The silane molecules undergo a hydrolysis and condensation process, leading to the formation of stable bonds between the silane and the reactive groups introduced during the activation phase. This chemical modification results in an alteration of the particles surface, converting it to an aminosilane-terminated surface.

Activation phase: methodology

The activation phase requires methanol and hydrochloric acid (HCl) as well as the silica gel (size of the particles used: 63μm). The procedure for this phase is as follows:

- Dilution of hydrochloric acid: Place the SiO_2 particles in a container. Add 1:1 ratio of methanol and HCl to the silica particles (to dilute the acid, first pour the methanol and then the HCl).
- Magnetic stirring: Immerse a magnetic stirring bar in the container and place it on a magnetic stirrer. The latter is a device that uses a rotating magnetic field to cause the magnetic stirring bar to spin very rapidly, thus stirring the solution. The magnetic stirrer is set at 700 rpm for 30 minutes at room temperature.

- Separation of the SiO_2 particles: To separate the silica particles from the solution of methanol and hydrochloric acid, pour the content into a centrifuge tube and place it in a centrifuge. The centrifuge is set at 3000 rpm for 5 minutes. Then, the excess liquid is removed with a pipette.
- Cleaning of the particles: To obtain a clean powder, add deionized (DI) water to the particles and put the tube back into the centrifuge at 3000 rpm for 5 minutes. Remove the excess DI water and repeat this step until the DI water is clear after centrifugation.

At the end of this procedure, the particles will have no residue of the methanol and HCl solution and will be activated and ready for the second phase.

Sol-gel silanization phase: methodology

The second phase requires acetone and (3-aminopropyl)triethoxysilane (APTES). APTES is an organosilane molecule with three functional reactive ethoxy groups and one amine group per one silane molecule (**Figure 2.2**) [54].

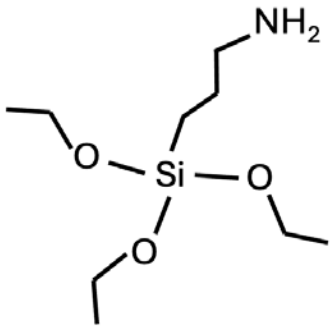

Figure 2.2: (3-aminopropyl)triethoxysilane (APTES) molecule.

The procedure for this phase is as follows:

- Formation of Si-O-Si bonds with the surface silanol groups: Place the SiO_2 particles in a container. Add 2% v/v of APTES in acetone to the silica particles. In acetone, the ethoxy groups of APTES hydrolyzes and then form the Si-O-Si bonds with the surface silanol groups.
- Magnetic stirring: Immerse a magnetic stirring bar in the container, place it on a magnetic stirrer and set it at 700 rpm for one hour at room temperature.
- Separation of the SiO_2 particles: To separate the silica particles, pour the content into a centrifuge tube and place it in a centrifuge at 3000 rpm for 5 minutes, then remove the excess liquid with a pipette.
- Cleaning of the particles: To obtain a clean powder, add acetone to the particles and put the tube back into the centrifuge at 3000 rpm for 5 minutes. Remove the excess acetone and repeat this step 2 more times to remove any unreacted APTES.

2.2. Sample preparation

This section describes the preparation of the samples with the introduction of dust particles and oil, as well as the method used to expose the samples to UV radiation.

2.2.1. Preparation of dust-contaminated surfaces

Dust is simulated using poly(vinyl chloride) (PVC) and silicon dioxide (SiO_2) particles. PVC particles were chosen because they are a common microplastic [55], while SiO_2 particles were selected because silicone dioxide is the main constituent of sand. Initially, SiO_2 particles with a size of 40-60 μm were used. Later, 100 μm SiO_2 particles were used, following the same procedure. The particles were observed using confocal microscopy, and can be seen in **Figure 2.3**.

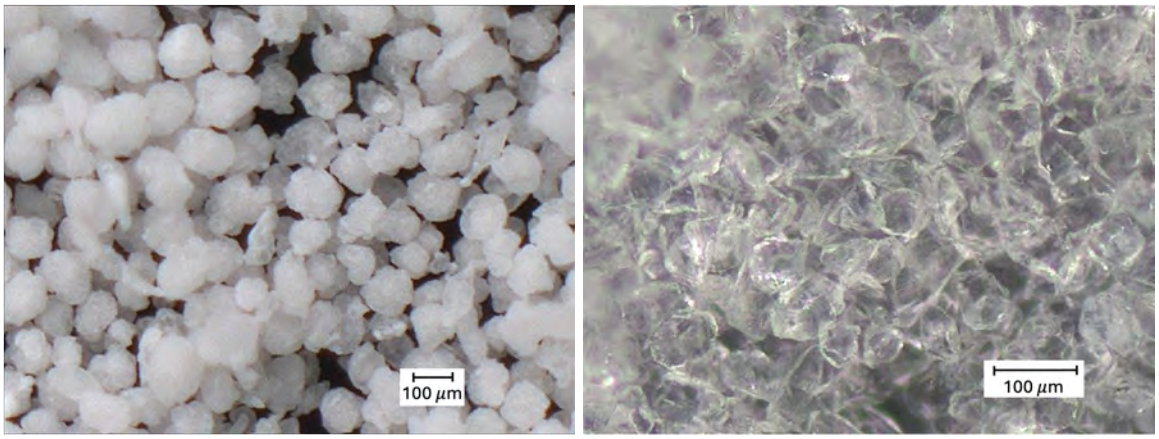

Figure 2.3: Confocal scanning microscope image of PVC (left) and SiO_2 (right) particles.

The particles were applied to the substrates using a spin coating technique, a process commonly used to create a uniform thin coating on flat surfaces. The spin coater employed for this process is a Laurell WS-400B-6NPP/LITE model. The particles are mixed with a solvent to create a solution that will be applied to the substrates. Ethanol is used for the PVC particles, while acetone is used for the SiO_2 particles. The substrates are secured in a spinning stage by vacuum and the solution is injected onto the surface. The spinning stage rotates at a set speed and time, and the solution is distributed over the substrate by centripetal forces. The PVC particles in ethanol are spin-coated at 3500 rpm for 15 seconds, while the SiO_2 particles in acetone are spin-coated at 500 rpm for 1 minute. The resulting surfaces were subjected to confocal scanning microscopy to determine the percentage of the surface area covered by dust. **Figure 2.4** and **Figure 2.5** illustrate two examples of how the percentage of area covered by the particles is determined by using ImageJ, a Java-based image processing program. These images show polyurethane surfaces covered with PVC and SiO_2 particles respectively.

2.2.2. Addition of oil droplets on the surfaces

The oil chosen for these experiments is silicone oil, a synthetic polymer consisting mainly of repeating units of siloxane (Si-O-Si) with organic groups attached to the silicon atoms, and with the chemical formula $(C_2H_6OSi)_n$. Silicone oil can withstand a wide range of temperatures, typically from -50°C to 100°C. It is known for its lubricating properties due to its low surface tension and hydrophobic nature, which is attributed to the presence of non-polar alkyl groups that are insoluble in water. In addition, its viscosity is relatively stable over a wide temperature range, making it suitable for a variety of applications. For example, it serves as a protective

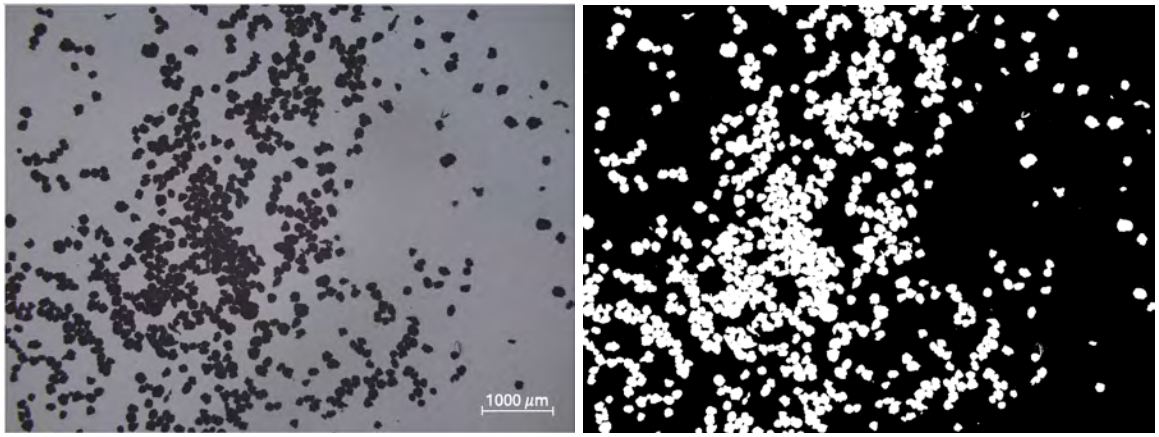

(a) Image from the confocal scanning microscope.

(b) Highlighting of PVC particles.

Summary

File Edit Font

Slice	Count	Total Area	Average Size	%Area	Mean
PU 1A 2.jpg	418	1202856	2877.646	21.498	255

(c) Percentage of area covered by dust (shown under %Area).

Figure 2.4: Determination of the percentage of the surface area that is covered by PVC particles.

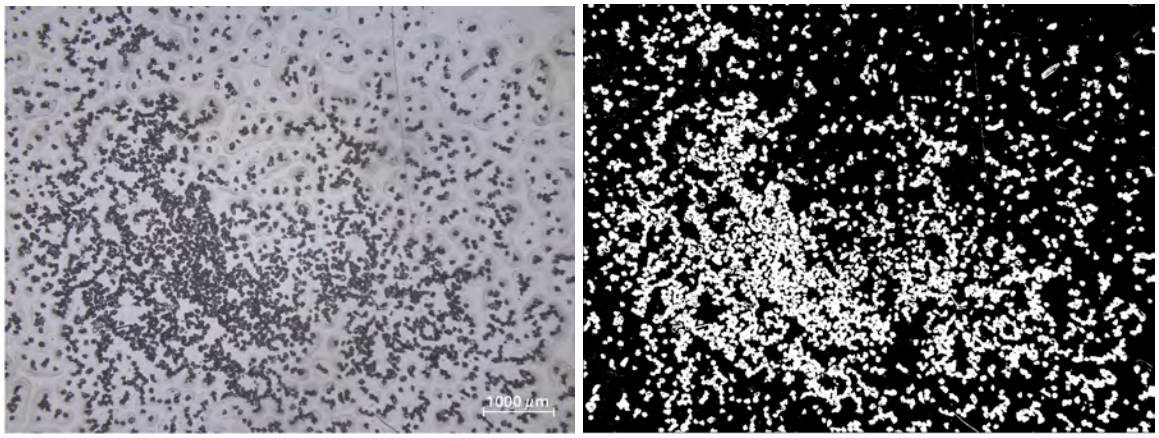

(a) Image from the confocal scanning microscope.

(b) Highlighting of SiO_2 particles

Summary

File Edit Font

Slice	Count	Total Area	Average Size	%Area	Mean
sio2 PU 1A 2.jpg	5513	1437545	260.755	25.693	255

(c) Percentage of area covered by dust (shown under %Area).

Figure 2.5: Determination of the percentage of the surface area that is covered by SiO_2 particles.

sheath for electrical components and wires, shielding from dust or ice that could infiltrate the inner workings of an aircraft.

A pipette is used to apply droplets of silicone oil to the surfaces. A few droplets are injected into the centre of the samples, where the ice will adhere. Images taken with a Dino-Lite digital microscope of the silicone oil droplets on the surfaces are shown in **Figure 2.6**. It is important to note that the way the droplets spread on the surface varies from substrate to substrate, even though the same technique was used.

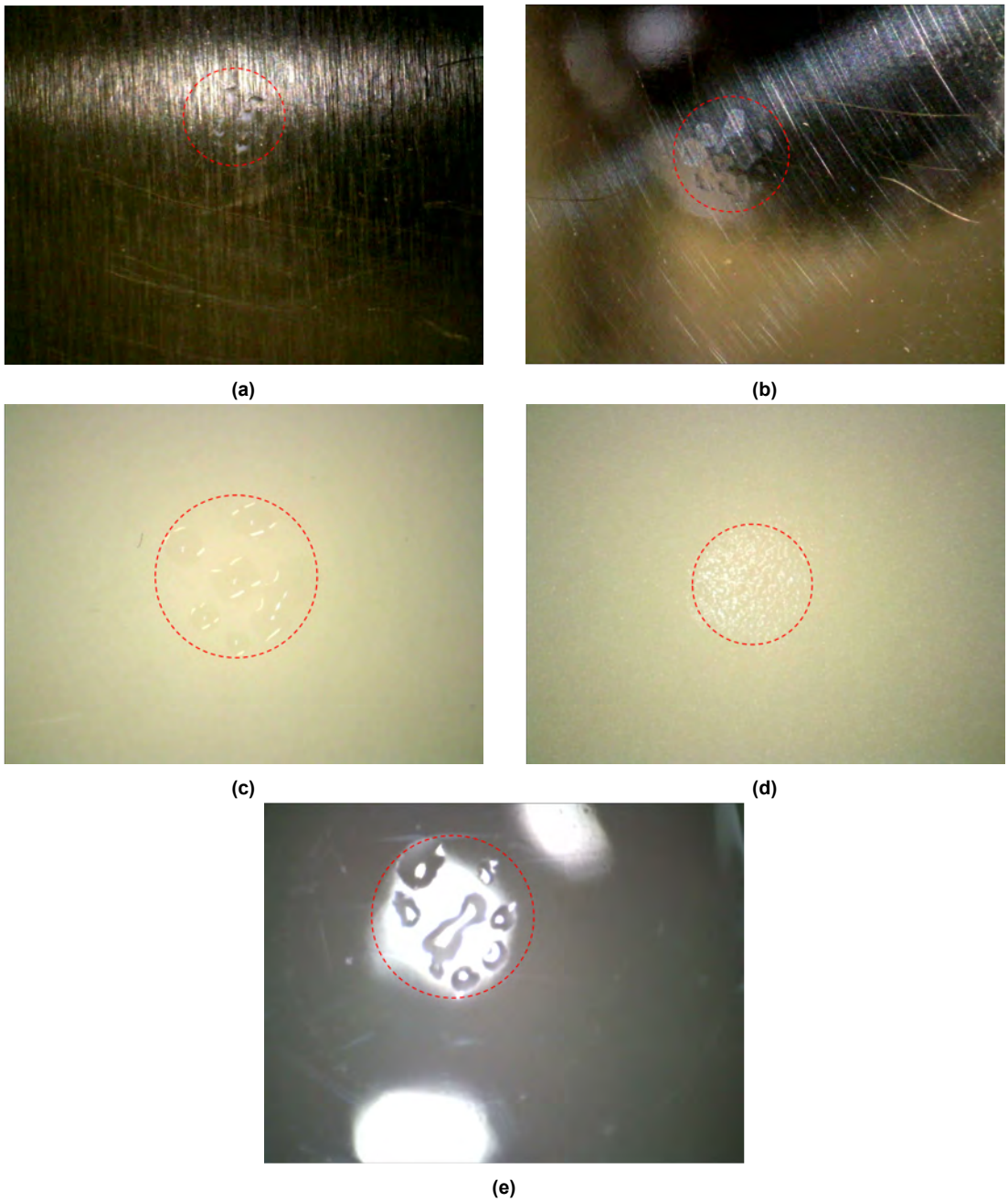

Figure 2.6: Silicone oil droplets on (a) unpolished AA6082, (b) polished AA6082, (c) Teflon, (d) polypropylene, and (e) polyurethane.

2.2.3. UV radiation exposure method

The OmniCure S1500 UV curing system was used to investigate the effect of UV radiation on polypropylene samples. The PP samples were first cleaned and dried to ensure that there were no contaminants on the surface. The UV lamp was set up in a designated area with appropriate safety measures and the PP samples were placed at a fixed distance from the lamp to ensure consistent and uniform UV exposure over the entire surface.

Each polypropylene sample was exposed to UV radiation for a total of 10 hours, divided into smaller intervals to monitor how the chemical and physical properties changed as the exposure time increased.

2.3. Characterisation techniques

This section describes the characterisation techniques used to analyse the samples and presents the results of the Fourier Transform Infrared spectroscopy (FTIR), the water contact angle (WCA) and surface roughness measurements.

2.3.1. Fourier Transform Infrared spectroscopy

Fourier Transform Infrared spectroscopy (FTIR) is a non-destructive technique used to determine the chemical composition of materials through an infrared spectrum of absorption or emission. In this technique, infrared (IR) radiation is passed through the sample being analysed and, depending on the nature of its bonds and molecular composition, specific IR wavelengths are absorbed by the sample. A Spectrum 100 FTIR spectrometer (Perkin Elmer) is used to measure the chemical composition of the PP and PU samples before and after UV radiation exposure. The spectrum produced ranges from 4000 to 600 cm^{-1} and an average of 32 scans is taken.

The difference in the infrared spectrum of the polypropylene samples before and after exposure is shown in **Figure 2.7**. The blue curve represents the spectrum before exposure, the red curve represents the spectrum after 5 hours of UV radiation exposure, and the green curve represents the spectrum after 10 hours of UV radiation exposure. UV radiation exposure causes the formation of new functional groups, which are hydroxyl groups (appearing between 3100 cm^{-1} and 3500 cm^{-1}) and carbonyl groups (appearing between 1500 cm^{-1} and 1800 cm^{-1}) [56]. The other noticeable peaks in the spectrum are summarized in **Table 2.1** [57, 58].

Table 2.1: FTIR transmission bands and their corresponding assignments for PP after 10 hours of UV radiation.

Wavenumber [cm^{-1}]	**Assignment**
3100-3500	O-H
2952, 2918, and 2838	C-H stretching
2720	CH bending and CH_3 stretching
1530-1840	Carbonyl group
1456 and 1376	CH_3 asymmetric deformation
1376	CH_3 symmetric deformation
1165	Tertiary carbon bending
974, 841, and 808	C-H deformation out-of-plane

Figure 2.8 shows the difference in the infrared spectrum of the polyurethane samples before and after 10 hours of UV radiation exposure.

In this spectrum, the transmission band in the range of 2858−2929 cm^{-1} is attributed to the stretching vibration of C–H [59]. The characteristic transmission peak at 3336 cm^{-1} and

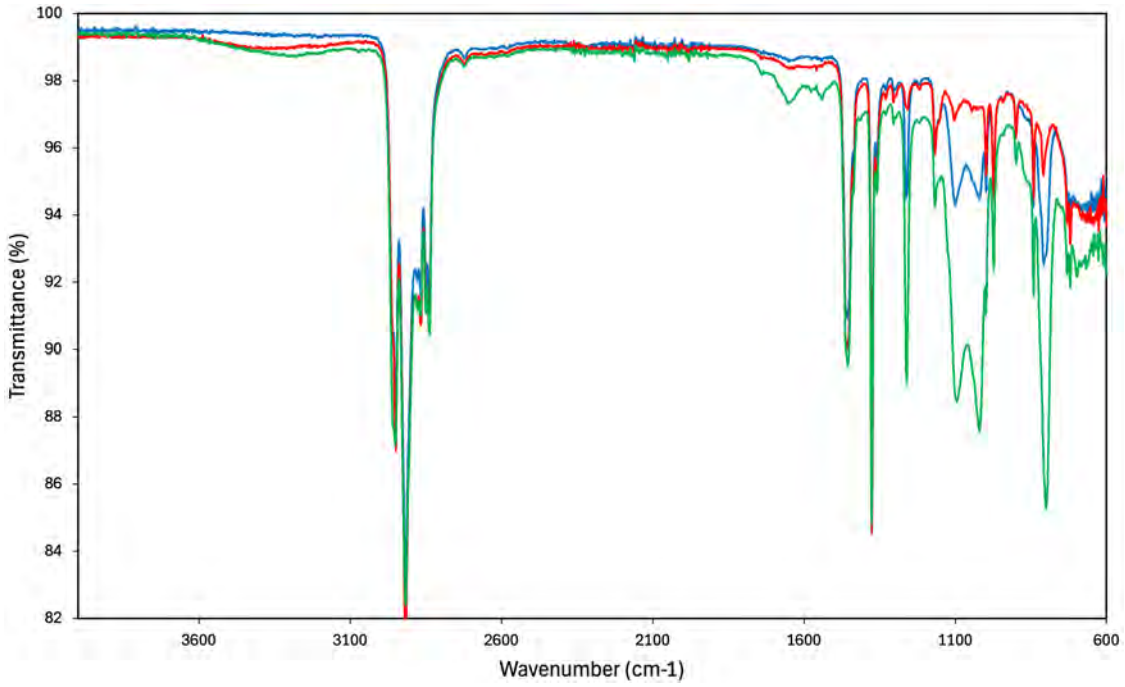

Figure 2.7: FTIR spectra of PP before (blue curve), after 5 hours (red curve), and after 10 hours (green curve) of UV radiation exposure.

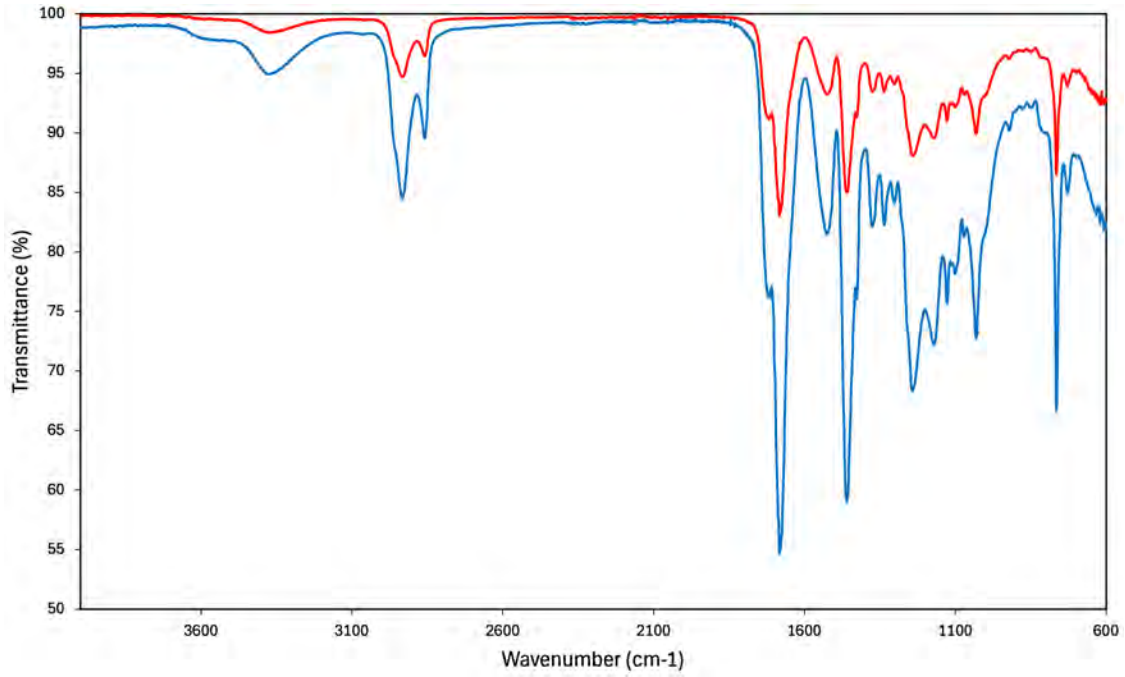

Figure 2.8: FTIR spectra of PU before (red curve) and after 10 hours (blue curve) of UV radiation exposure.

1540 cm^{-1} is related to the stretching vibration transmission of N–H in the urethane group, and the peak at 1714 cm^{-1} is due to the C–O bond.

2.3.2. Water contact angle measurements

Water contact angle (WCA) measurements determine the contact angle formed between a droplet of water and a surface, as defined in **Figure 1.5**. The WCA provides information about the wettability and the surface energy.

Table 2.2: Water contact angles of materials.

Material	Water Contact Angle [°]
AA-6082 unpolished	84
AA-6082 polished	98
Teflon	111
Polypropylene	101
Polyurethane	87
Polyvinyl chloride	96
SiO_2	28
Surface modified SiO_2	47
PP after 5h of UV	86
PP after 10h of UV	108
PU after 10h of UV	74

Three droplets (10 μl each) of deionized (DI) water were placed on the surface of interest. The contact angles were determined for each droplet and the WCA of the surface was calculated as the average of these measurements. To measure the WCA, the KSV CAM 200 Optical Contact Angle Meter was used. The results for each material[1] are shown in **Table 2.2**. The complete results, along with images of the water droplet on the surfaces, are shown in Appendix A.

2.3.3. Surface roughness measurements

Surface roughness was measured to assess the texture of each material. Surface roughness quantifies the variations in surface topography and affects properties such as adhesion and wettability. Roughness measurements were made with confocal microscopy, which is a basic non-destructive imaging technique, and with 10x magnification. For this thesis, a Keyence VK-X1000 confocal scanning microscope was used. The arithmetical mean height (Sa) and the maximum height (Sz) values were calculated form these measurements and are summarized in **Table 2.3**, while the overall results can be found in Appendix B. The first parameter (Sa) represents the difference in height of each point relative to the arithmetical mean of the surface. It is the surface equivalent of the arithmetical mean height along a line (Ra). The maximum height (Sz) is the sum of the deepest pit and the highest peak within a defined area. Since Sz emphasizes the effect of the deepest pits and highest peaks, this parameter is more directly related to the mechanical interlocking that occurs between the ice and the surface. The concept of these two parameters is shown in **Figure 2.9**.

[1]The WCA of the particles was measured using surfaces made of the corresponding materials.

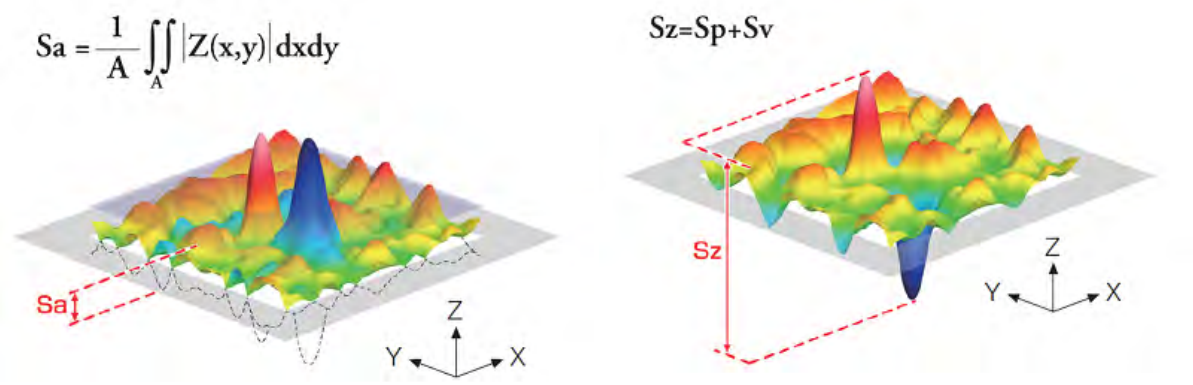

Figure 2.9: Arithmetical mean height (Sa) and maximum height (Sz) of a surface [60].

Table 2.3: Sa and Sz of materials.

Material	Sa [μm]	Sz [μm]
AA-6082 unpolished	2.61	24.23
AA-6082 polished	0.42	7.71
Teflon	1.27	24.49
Polypropylene	4.45	49.51
Polyurethane	0.25	6.09
PP after 5h of UV	4.50	43.24
PP after 10h of UV	3.70	42.26
PU after 10h of UV	0.21	6.18

2.4. Experimental procedure to determine ice adhesion strength

As described in section 1.3, ice adhesion strength can be assessed using various methods. The set-up used in the experiments is a home-built horizontal shear test set-up, inspired by the setup developed by Robert Biro [61]. The aim of this set-up is to be accurate and versatile, to be able to quantify and compare the ice adhesion strength of different materials. This means that the tests should be controllable and reproducible. To ensure consistency and reliability, the differences between tests should be minimal, i.e. the parameters and environmental conditions between two tests should be as similar and controllable as possible.

The experimental set-up has five main components:

- **Housing chamber:** its function is to help control temperature and humidity. The chamber is made of stainless steel and is isolated from the outside environment. It contains 5 sample holders arranged horizontally so that when an ice column breaks, it will not hit the other moulds and affect the other results. The housing chamber allows for the placement of the alignment block, which holds the moulds into which the water is injected to form the ice pillars. A representation of the housing chamber components with the alignment block can be seen in **Figure 2.10**.
- **Cooling and humidity system:** the purpose of the cooling system is to control the surface temperature of the specimens and to allow the water in the moulds to freeze to form the ice columns. This is achieved by means of a circulation chiller (LAUDA-ECO RE1050, shown in **Figure 2.11**), which is connected to the housing chamber by two silicone-insulated pipes through which the cooling fluid flows. A schematic diagram of

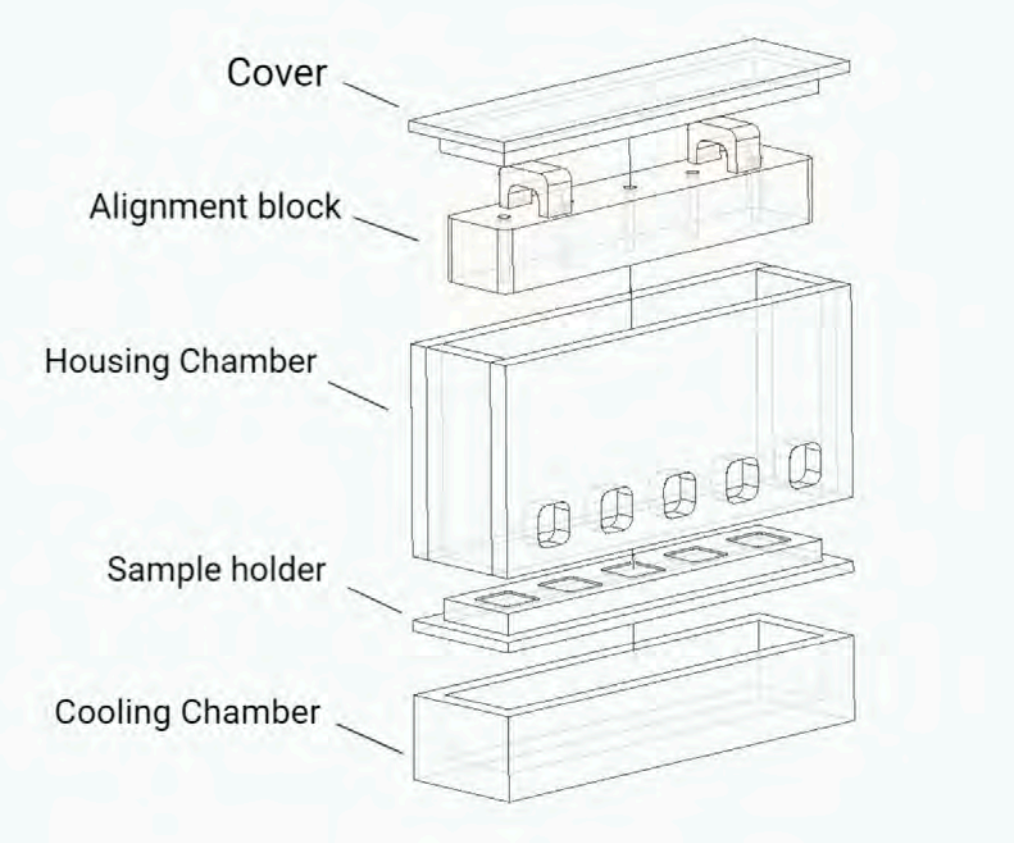

Figure 2.10: Housing chamber components and alignment block.

Figure 2.11: Circulation chiller LAUDA-ECO RE1050.

the housing chamber pipework is shown in **Figure 2.12**. The chiller has a temperature range of -50°C to 200°C, but the cooling fluid used is monoethylene glycol, which allows a minimum temperature of -32°C due to viscosity limitations. The humidity during the tests should be kept as low as possible, as the surfaces must be dry to prevent condensation frosting on the ice pillars. To realize this, a weak flow of nitrogen is connected to the housing chamber and the relative humidity can be kept below 10% during the tests.

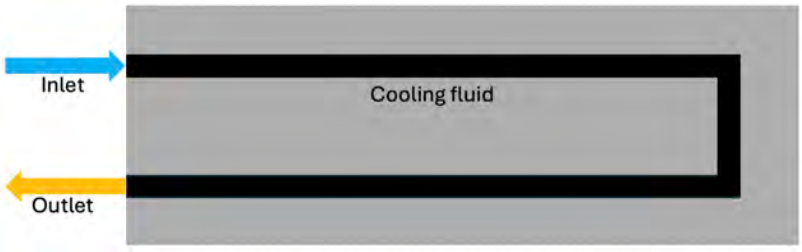

Figure 2.12: Illustration of the cooling fluid path through the housing chamber.

- **Actuator and load cell:** a linear actuator with a DC motor (LTA-HL integrated with CONEX-CC controller) is used to apply a force to the ice pillars. Its minimum speed is 0.01 mm/s, which allows testing in the quasi-static range, and a load capacity of 120 N. A pushing probe is used to push the moulds directly. The probe is made of polyoxymethylene (POM), which has high stiffness, good thermal stability and low sliding friction. It has a 2 mm flat-head tip in a half moon shape and an M6 female thread for mechanical connection to the load cell by a simple blot connection. As the load cell frame deforms, four strain gauges in a full bridge configuration record the deformation and the signal is amplified by an amplifier and read on an oscilloscope. The load cell is calibrated so that 1 V = 1 ÷ 0.002 kg.
- **Data acquisition (DAQ) system:** the DAQ system includes a signal amplifier and an oscilloscope to read the signal. The signal corresponds to a calibrated force value, which is read into a computer.
- **Moulds for the ice pillars:** they allow for the injection of the water, which it is assumed freezes instantly. The material used is Teflon for its hydrophobicity and the shape is cylindrical, with an inner diameter of 8 mm and an outer diameter of 13 mm. Their height is of 3 cm, to allow for a pushing height h of 1 mm, an ice pillar height H of 8 mm and an ice pillar diameter D of 8 mm (**Figure 2.13**).

An overall view of the set-up is shown in **Figure 2.14**. The operating procedure is described in subsection 2.4.1.

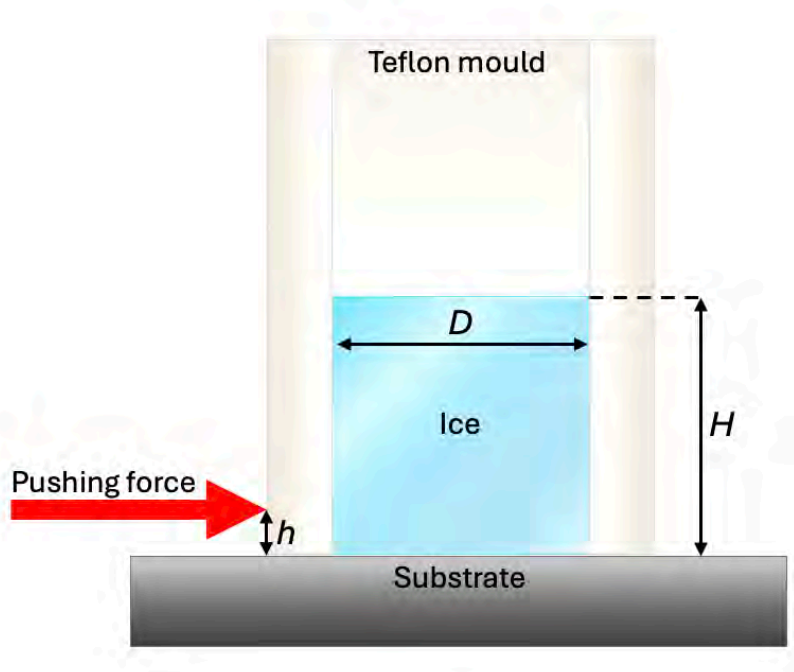

Figure 2.13: Representation of ice pillar and Teflon mould.

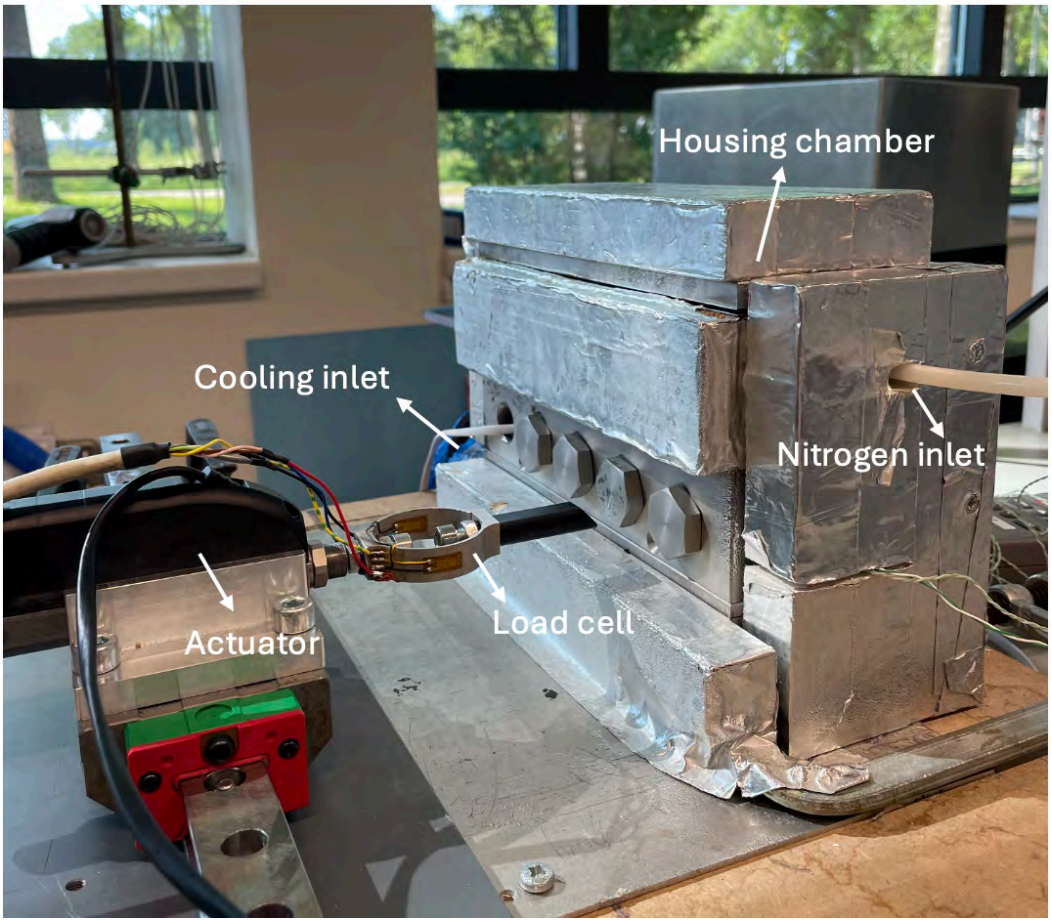

Figure 2.14: Set-up overview.

2.4.1. Testing method

To start the tests, the substrates to be tested was placed in the sample holders. Once the samples were in place, the chiller was started. The temperature set point was set between -18°C and -22°C. In order to achieve a relative humidity of less than 10%, the nitrogen flow was switched on.

When the desired temperature and relative humidity were reached (which were measured by placing temperature sensors on the surfaces of the samples, and by placing a humidity sensor in the chamber), the Teflon moulds were attached to the alignment block and placed in the housing chamber on top of the samples. The alignment pins were removed with pliers, the housing chamber was closed and left to return to the desired temperature and relative humidity. 400 μl of water was injected into the moulds to form the ice pillars. The waiting time for the ice pillars to form was about 30/35 minutes. As each test took about 5/10 minutes, it was necessary to wait 10 minutes before pouring the water into the next mould. The alignment block holding the moulds was removed and the actuator was manually positioned at the edge of the sample holder. The screws on the side of the actuator were tightened and the housing chamber was closed. When the actuator was positioned, the mould with the ice pillars was usually 4/5 mm away, so at a speed of 1 mm/s the actuator position could be set to 3.5 mm to speed up the test. The actual test began. The load cell speed was set to 0.01 mm/s and the end

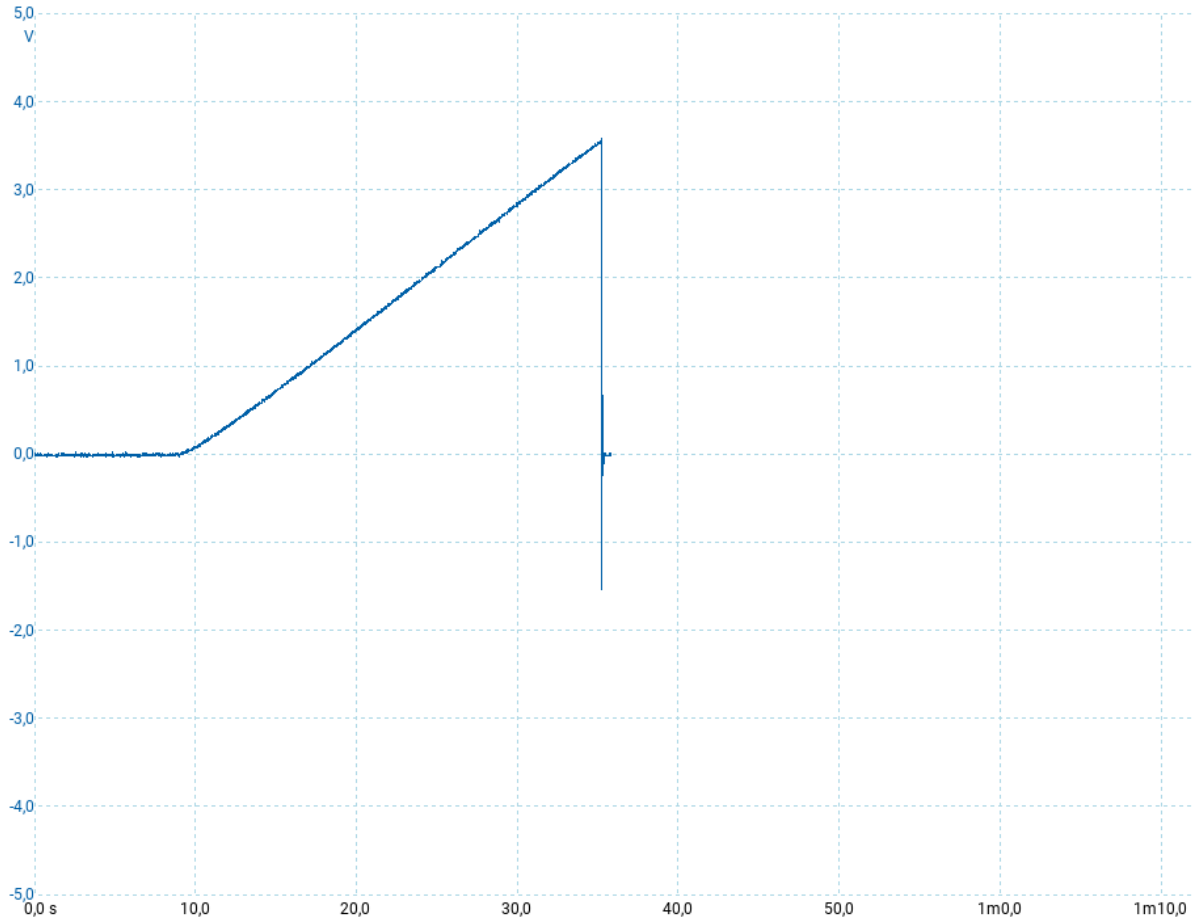

Figure 2.15: Graph resulting from the test. The electromotive force (in volts) is displayed on the y-axis and the time (in seconds) on the x-axis.

position to 7 mm and then the Picoscope measurement was started. As soon as the actuator starts to apply pressure to the mould, a visual response appeared on the Picoscope due to the

changing voltage, and data was collected until the ice pillar detached from the substrate. The graph showed the electromotive force (in volts) on the y-axis and the time (in seconds) on the x-axis. An example of the graph resulting from an adhesive failure of a 6082 aluminium alloy sample is shown in **Figure 2.15**. For a complete analysis, the ice pillar was also removed from the Teflon mould and observed before it melted.

To find the ice adhesion strength, which is defined as the ratio of the peak removal force to the interface area between the ice and the substrate, the highest value on the graph was multiplied by g (9.8067 m/s^2) to obtain the peak removal force. The resulting value (which is in Newtons) was then divided by the area, which is 0.0503 cm^2 (50.2655 mm^2). The resulting ice adhesion strength is in kPa. Any significant observations about the test run, fracture surface, ice type, etc. were noted. The actuator was returned to its zero position and moved to the next slot to start the next test.

3

Results and discussion

This chapter presents the results of the ice adhesion tests for different defect conditions on the samples. The results are divided into four main sections for clarity and detailed examination.

Section 3.1 discusses the ice adhesion strength of the bare samples, which are the unmodified samples without any addition of interfacial defects, providing a baseline for comparison with the following tests. Section 3.2 examines the impact of dust on the ice adhesion strength, offering insights into how particular parameters influence the adhesion between the ice and the substrates. In section 3.3, the effects on ice adhesion of adding lubricant oil to the samples are analysed. Finally, section 3.4 compares the ice adhesion strength of the bare samples with that of the samples after 10 hours of UV radiation exposure, assessing the potential effects of environmental factors on ice adhesion.

Together, these results contribute to a deeper understanding of the factors affecting ice adhesion strength across different surfaces. A discussion on these results is provided in section 3.5.

3.1. Ice adhesion strength of bare surfaces

The samples are tested as described in subsection 2.4.1 and tests are repeated multiple times per material to ensure accurate results, with the environmental conditions for each test being kept as similar as possible. The ice adhesion strength was calculated and the results plotted in the graphs shown in **Figure 3.1**. The ice adhesion strength values shown are the peak stresses reached before failure of the ice-substrate interface.

The differences in ice adhesion strength between the materials tested are quite significant. Teflon has a very low ice adhesion strength (with an average of 81.5 kPa), which can be attributed to its known high hydrophobicity, making it one of the most icephobic materials. Polyurethane (PU) shows the highest ice adhesion strength among the polymer substrates with an average of 824.2 kPa, which could be attributed to its relatively low water contact angle, compared to the other polymers. Polypropylene (PP) has an average ice adhesion strength of 171 kPa, which is slightly higher than Teflon, probably due to its lower water contact angle, but significantly lower than PU. This makes polypropylene a promising candidate for anti-icing applications.

The aluminium alloy samples show a high ice adhesion strength, with the polished aluminium alloy samples demonstrating a lower ice adhesion strength (with an average of 381.3 kPa) compared to their unpolished counterparts (which have an average of 745.7 kPa). This difference is attributed to the difference in surface roughness, as the unpolished AA6082

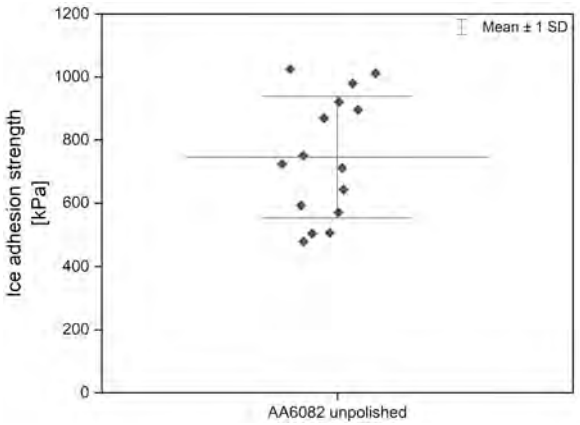

(a) Ice adhesion strength of AA6082 unpolished.

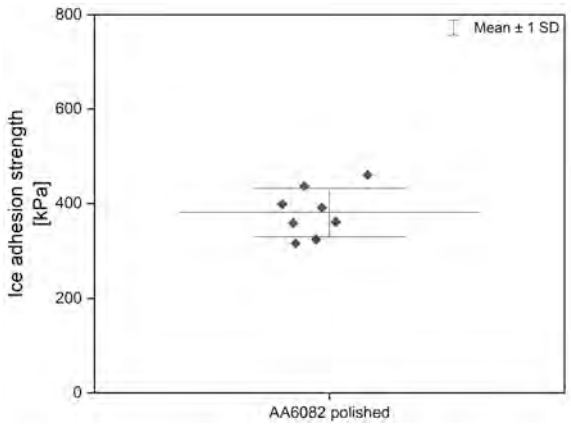

(b) Ice adhesion strength of AA6082 polished.

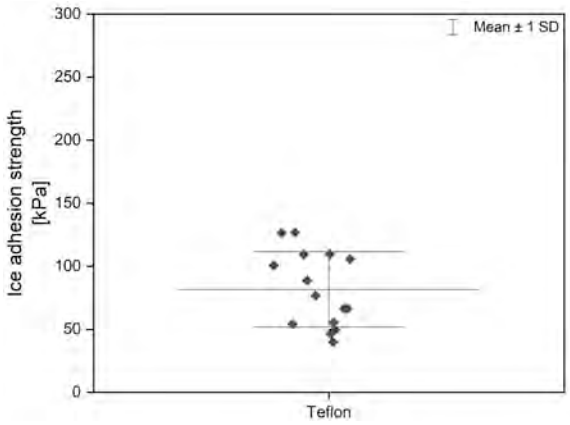

(c) Ice adhesion strength of Teflon.

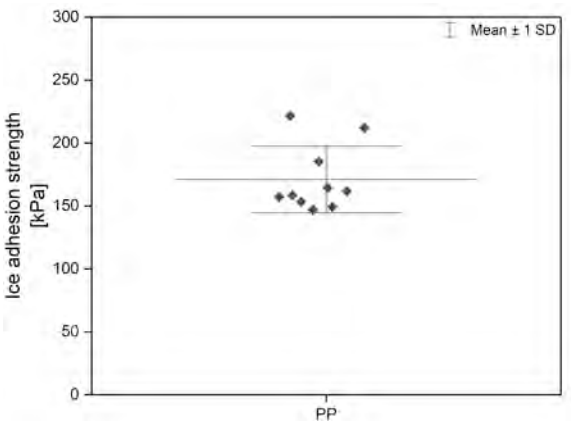

(d) Ice adhesion strength of PP.

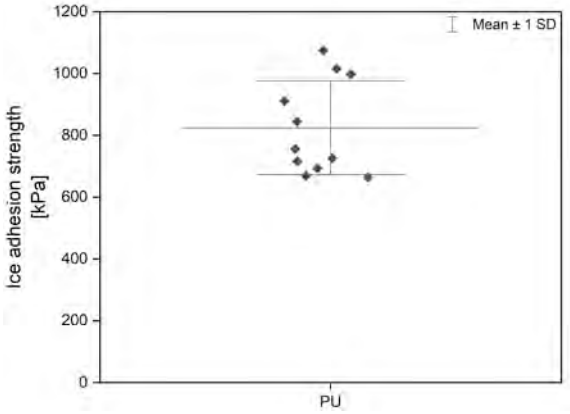

(e) Ice adhesion strength of PU.

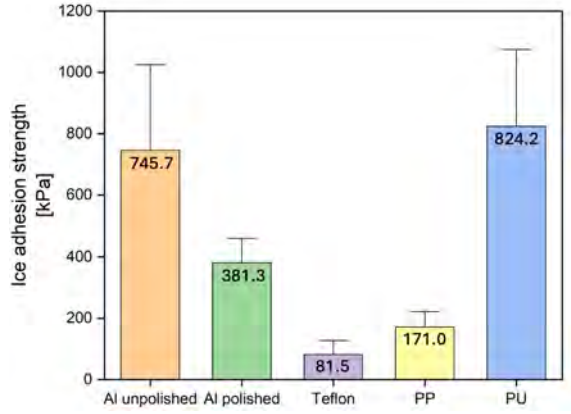

(f) Mean values of ice adhesion strength for all the materials.

Figure 3.1: Ice adhesion strength of the (a) unpolished AA6082, (b) polished AA6082, (c) Teflon, (d) polypropylene, and (e) polyurethane substrates. The mean ice adhesion strength values are shown in (f) for a comparison between the materials.

substrates have higher roughness, resulting in mechanical interlocking between the ice and the rough surface.

3.2. Effect of dust contamination on ice adhesion strength

This section analyses the ice adhesion strength of the surfaces with the addition of dust particles. The dust-contaminated surfaces are tested according to the test procedure discussed in section 2.4, and tests are repeated multiple times for each material, with the differences between the tests being as small as possible in order to obtain comparable data and to have better control of the variables involved. The ice adhesion strength is measured with the addition of PVC and SiO_2 particles. For a comparison with the ice adhesion strength of the bare samples, the data from the dust-contaminated surfaces are plotted together with the data from the bare surfaces.

3.2.1. Aluminium surfaces

The data for the unpolished and polished samples of AA6082 is shown in **Figure 3.2** and **Figure 3.3**, respectively.

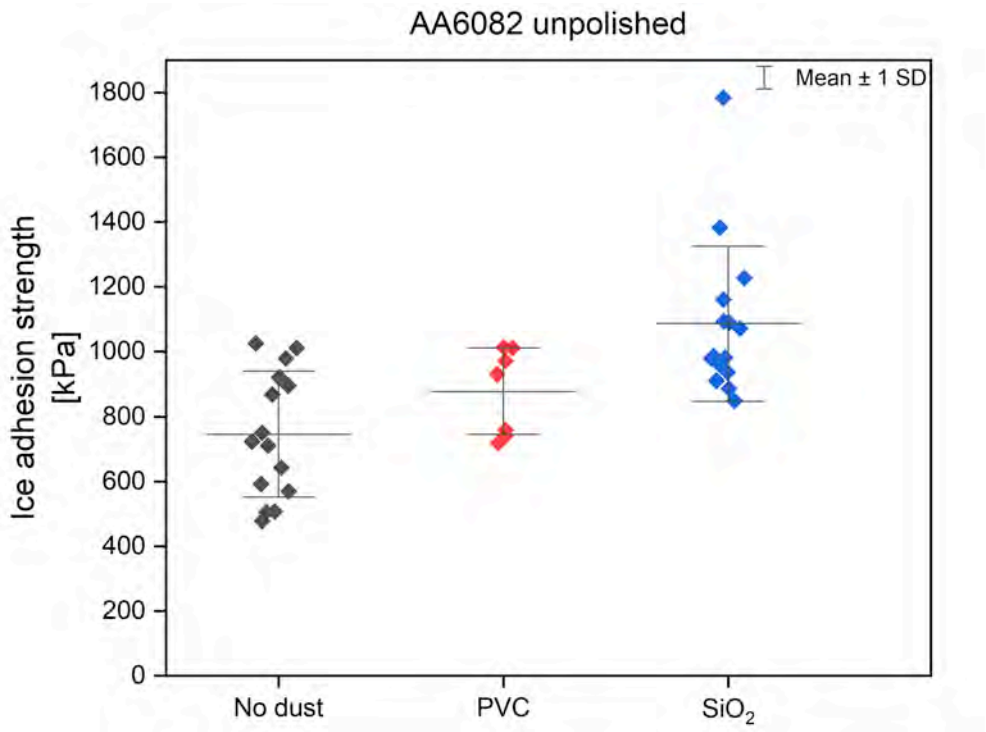

Figure 3.2: Comparison between ice adhesion strength of bare surfaces and dust-contaminated surfaces for unpolished AA6082.

These graphs indicate that the mean ice adhesion strength for the bare substrates is the lowest when compared to the dust-contaminated surfaces. This trend suggests that the presence of dust particles increases the ice adhesion strength.

This behaviour can be explained by the contact splitting hypothesis (CSH). According to this hypothesis, splitting a large contact area between two materials into multiple smaller contact points enhances the adhesion by increasing energy dissipation during the detachment process [62]. A well-known biological example of this phenomenon is seen in the fibrillar structures (called setae) on gecko feet, which allow for increased adhesion. This principle

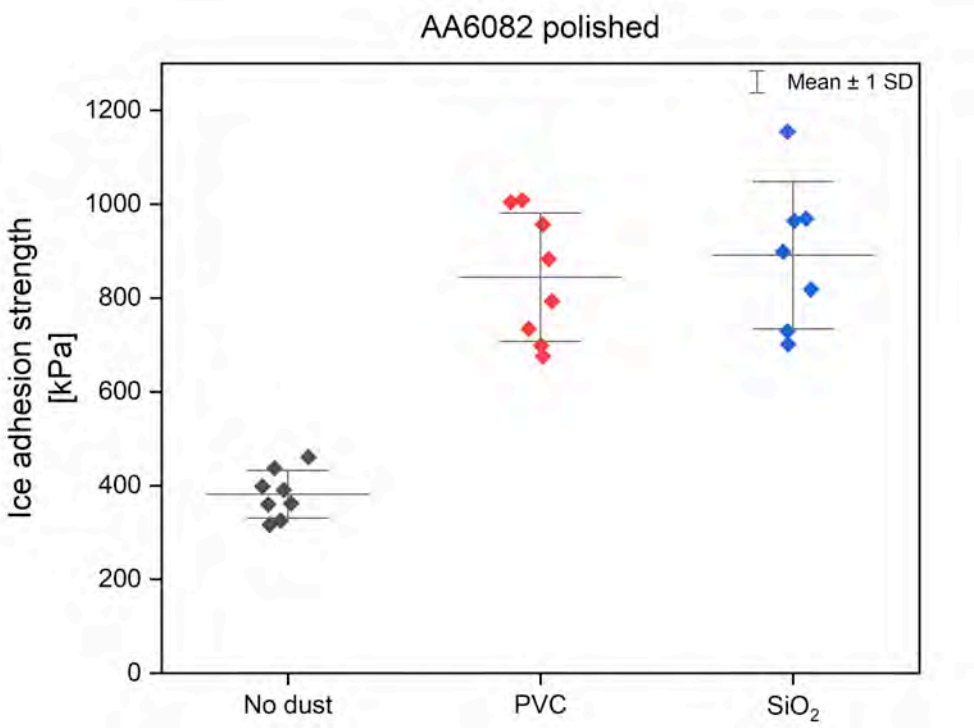

Figure 3.3: Comparison between ice adhesion strength of bare surfaces and dust-contaminated surfaces for polished AA6082.

has been used in designing advanced adhesive materials [63]. The mechanism behind this increased adhesion is related to the repeated interruption and re-initiation of the detachment process at each contact point, which require additional force. This process increases the separation force, which scales with the number of contact points, thereby increasing the overall adhesive strength.

The increase in ice adhesion strength observed in the previous graphs can be attributed to a similar detachment mechanism. Initially, a crack forms at the ice-substrate interface and propagates until it encounters a dust particle, at which point the detachment occurs between the particle and the substrate, and subsequently, crack propagation between the ice and the substrate re-starts, until it reaches another particle. This preferential detachment between the particle and the substrate, as opposed to the detachment between the particle and the ice, occurs due to the hierarchy of adhesion forces at play: the adhesion between the particles and the substrate is lower than that between the substrate and the ice, while the strongest adhesion is between the ice and the particles. The reason is that dust particles have a highly rough surface, which increases ice adhesion due to the increased mechanical interlocking at the interface. Consequently, the detachment process favors the separation between the particle and the substrate, as it requires less energy than separating the ice from the particles. A schematic representation of the adhesion forces is provided in **Figure 3.4**.

To confirm this relationship between the adhesion forces, during the experiments it was observed that the dust particles (both PVC and SiO_2) remained attached to the ice pillar after detachment. This behaviour was captured after the detachment by the Keyence VR 5000 digital microscope in **Figure 3.5**, which shows SiO_2 particles on the ice pillar. Additionally, tactile verification confirmed the presence of particles on the ice surface, further supporting this observation. This confirms that the adhesion between the ice and the particles is stronger than the adhesion between the particles and the substrate. Consequently, when detachment

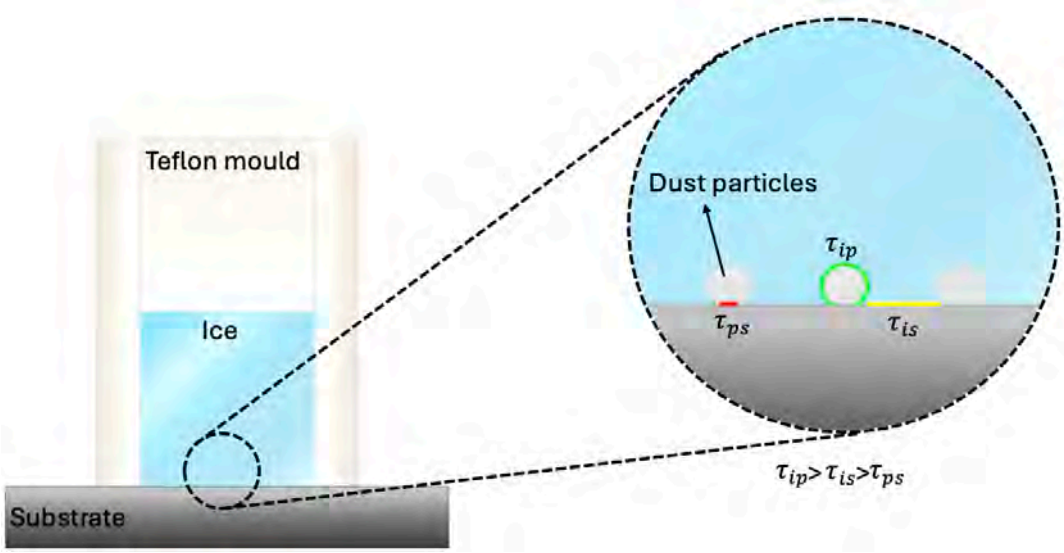

Figure 3.4: Schematic representation of the three adhesion strengths involved when dust particles are introduced: τ_{ip} represents the adhesion strength between ice and dust particles, τ_{is} represents the adhesion strength between ice and substrate, and τ_{ps} the adhesion strength between dust particles and substrate.

Figure 3.5: SiO_2 particles attached to the ice pillar after detachment. Picture taken with Keyence VR 5000 digital microscope.

occurs between the particles and the substrate, a new crack between must initiate at the interface between the ice and the substrate.

This phenomenon of enhanced toughness through mechanisms that resist crack propagation is also observed in other contexts, such as the toughening of epoxy resins and the mechanics of matrix cracking in fiber-reinforced composites. In epoxy resins, the introduction of nanoparticles improves the fracture toughness and the fatigue crack propagation resistance [64]. The presence of nanoparticles results in various fracture mechanisms, such as crack pinning, plastic deformation, and crack deflection, which lower the rate of crack propagation compared to neat epoxy [65]. Similarly, in fiber-reinforced composites, the fibers help to slow down or stop a crack from propagating, increasing the material toughness [66].

In the context of ice adhesion, the introduction of particles at the interface inhibits crack propagation by requiring multiple crack openings in the ice/substrate interface, thereby increasing the force required for detachment. If there is a crack propagation along the interface, the fracture mechanism is no longer stress-dominated (as in the bare samples) but toughness-dominated and is influenced by the toughness of the interface, i.e. the resistance to crack growth. Interfacial toughness can be assumed to be equal to the work of adhesion, which is the energy required to create free surfaces from two bonded surfaces, and is given by the following formula:

$$W_A = \gamma_1 + \gamma_2 - \gamma_i \tag{3.1}$$

where γ_1 and γ_2 are the surface free energies of the two adhering materials and γ_i is the free energy of the interface. In reality, however, every fracture involves some form of energy dissipation, whether through plastic deformation at the crack tip or by frictional forces. Therefore, interfacial toughness is defined as the practical work of adhesion, expressed as:

$$\Gamma = W_{A,P} = W_A + U_1 + U_2 + U_{friction} \tag{3.2}$$

where U_1 and U_2 are the energy losses due to plastic deformation of the ice and the substrate, and $U_{friction}$ is the energy dissipated by friction.

The energy loss due to friction depends on the normal force, which in turn depends on the mass of the ice pillar. The normal force can be calculated as follows:

$$N = mg = \rho V g = 917\,kg/m^3 \cdot 4.021 \cdot 10^{-7}\,m^3 \cdot 9.80665\,m/s^2 = 3.61596 \cdot 10^{-3}\,N \tag{3.3}$$

The resulting value is so small that, when multiplied by the coefficient of kinetic friction and the distance over which the force is applied, the resulting energy loss due to friction is considerably smaller than the other terms in Equation 3.2 for the interfacial toughness. Consequently, the contribution of frictional energy dissipation to the total interfacial toughness is negligible and is not considered in further analysis.

This means that what differentiates the ice adhesion strength between bare surfaces and dust-contaminated ones relies on the difference in energy dissipation through plastic deformation at the crack tip. The maximum stress required for crack opening occurs at the crack tip, and repeated crack openings increase the difficulty of crack propagation, resulting in higher interfacial toughness and, consequently, a higher adhesion between the ice and the substrate.

To gain deeper insights into the graphs presented in **Figure 3.2** and **Figure 3.3**, the data distribution and variability can be observed. This is particularly valuable for interpreting the data points from the dust-contaminated samples with the lowest ice adhesion strength.

One of the factors considered to explain this is how the ice adhesion strength varies with the percentage of area covered by dust particles. For the unpolished samples, the area covered by PVC particles ranges from 5% to 20%, while for SiO_2 particles, it ranges from 20% to 40%.

For the polished samples, the percentage of area covered by PVC particles ranges from 15% to 25%, whereas for SiO_2 particles, it ranges from 10% to 30%. However, it was observed that, as the percentage of the surface covered by both PVC and SiO_2 particles increased, there was no linear correlation with the ice adhesion strength. This can be attributed to the fact that the particles present on the surface can hinder the detachment of the ice from the surface, but this depends on how they are distributed on the surface itself.

If the particles are more concentrated in the region far from the pushing edge of the ice-substrate interface (as shown in **Figure 3.6**), the initial detachment area will contain fewer particles that could hinder the detachment process. As a result, the fracture mechanism remains toughness-dominated, governed primarily by the interfacial toughness, however, due to the reduced particle presence in the critical detachment zone, the particles will have a reduced impact on increasing the interfacial toughness.

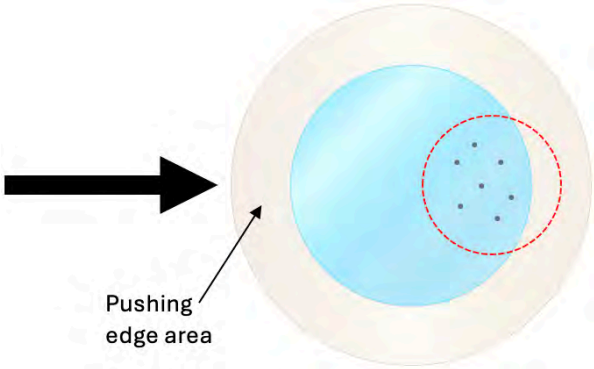

Figure 3.6: Distribution of particles concentrated in the area far from the pushing edge of the ice-substrate interface. The black arrow indicates the pushing force.

On the other hand, if the particles are mostly distributed near the pushing edge of the interface (as illustrated in **Figure 3.7**), or evenly distributed across the surface area (as shown in **Figure 3.5**), the initial detachment area will contain a significant number of particles. Their presence can effectively hinder the detachment process by introducing additional resistance to crack propagation, as the detachment is repeatedly interrupted by these particles. This increases the energy dissipation during the fracture process, thereby increasing the overall interfacial toughness and resulting in higher ice adhesion strength, as explained above.

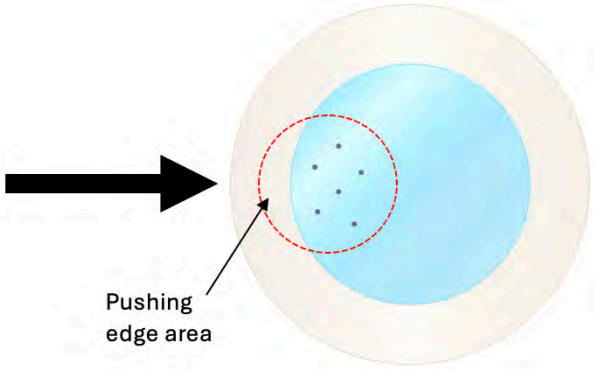

Figure 3.7: Distribution of particles concentrated near the pushing edge area of the ice-substrate interface. The black arrow indicates the pushing force.

The variability in particle distribution between the samples can therefore be a key factor in explaining the differences in ice adhesion strength observed in the graphs for the dust-

contaminated samples.

Another observation from the graphs in **Figure 3.2** and **Figure 3.3**, is that the increase in ice adhesion strength observed in the polished aluminium samples with the addition of dust particles is higher compared to the unpolished aluminium samples, indicating that surface smoothness may enhance the impact of particles on ice adhesion. It was already observed on the bare aluminium samples that the surface roughness plays a significant role in influencing ice adhesion. In fact, under hydrophilic conditions (as in this case, see the water contact angle data in section 2.1), as previously discussed in section 1.2, the hydrophilicity of a surface tends to increase with its roughness. When dust particles are added to the unpolished aluminium samples, the overall surface texture does not significantly change. On the other hand, the addition of dust particles on the polished aluminium substrates increases their surface roughness, resulting in a considerably higher ice adhesion strength compared to the pre-contaminated samples.

In summary, dust particles increase ice adhesion strength, particularly on polished aluminium surfaces where surface roughness increases. The distribution of particles plays a critical role in altering the fracture mechanism at the ice-substrate interface, which becomes toughness-dominated when crack propagation is hindered by the repeated crack openings caused by the presence of the dust particles. This results in higher interfacial toughness and higher ice adhesion strength. To further validate this hypothesis, an additional experiment was conducted, using SiO_2 particles with a size of 100 μm, in contrast to the initial size range of 40-60 μm.

Investigation of ice adhesion strength with larger SiO_2 particles (100 μm)

To confirm the previously discussed hypothesis explaining the behaviour of ice adhesion strength on aluminium samples, larger SiO_2 particles were used. The size used was 100 μm, whereas the particles used previously had a size of 40-60 μm. The larger particles were applied to the aluminium samples using the same preparation method as previously described. The tests were also replicated under similar conditions to maintain consistency. By comparing the ice adhesion strength results of aluminium surfaces with 100 μm SiO_2 particles to those obtained with the smaller particles, the aim is to assess whether similar trends are observed. If the results show consistency between the two particle sizes, this would provide evidence to support the validity of the hypothesis, demonstrating that, since the particles-substrate contact does not change considerably with increasing particle size, the presence of the particles acts as an obstacles to crack propagation, causing the crack to stop intermittently and increasing the interfacial toughness and the ice adhesion strength.

The percentage of area covered by SiO_2 particles with a size of 100 μm ranges from 25% to 45% for the unpolished samples and from 15% to 35% from the polished samples. The area coverage for the smaller size of SiO_2 particles was slightly lower, indicating that the particles-substrate contact points should remain approximately the same as before, thus it is expected for the ice adhesion strength to have a similar behaviour to the one observed before.

The values for the ice adhesion strength are presented in **Figure 3.8** and **Figure 3.9**. From these figures, it can be observed that the ice adhesion strength of the aluminium surfaces with the addition of the SiO_2 particles with a size of 100 μm does not show any significant variation compared to the ice adhesion strength determined with the SiO_2 particles with a size of 40-60 μm. The mean values remain very similar, indicating that the change in particle size does not significantly affect the overall ice adhesion strength under the conditions tested.

This demonstrates the previously stated hypothesis, as the results obtained with the 100 μm SiO_2 particles are consistent with those observed with the 40-60 μm particles. This similarity in results indicates that during the detachment, crack propagation occurs along the interface between the ice and the substrate. As the crack encounters a SiO_2 particle (or any

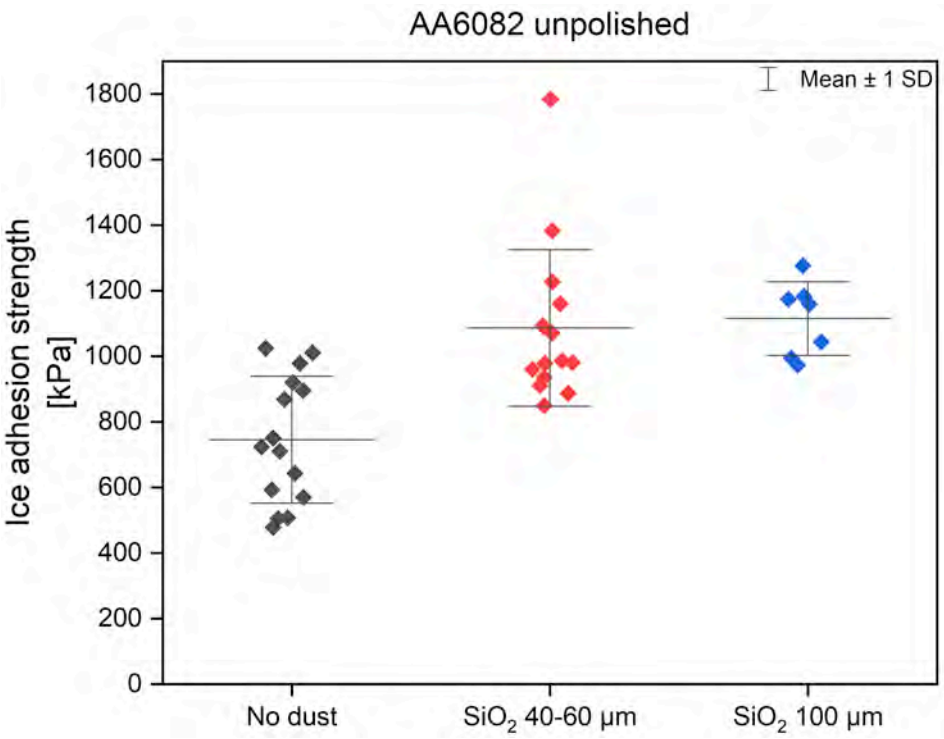

Figure 3.8: Comparison between ice adhesion strength of bare surfaces and dust-contaminated surfaces for unpolished AA6082.

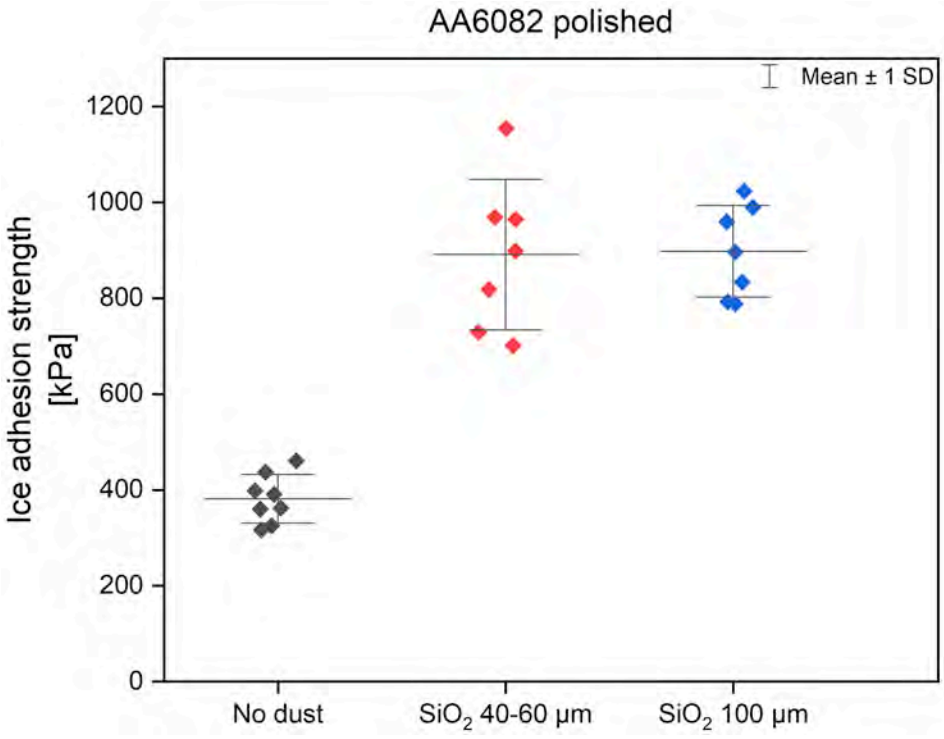

Figure 3.9: Comparison between ice adhesion strength of bare surfaces and dust-contaminated surfaces for polished AA6082.

other dust particle), it is temporarily stopped, forcing the crack to restart at a new location. This repeated interruption of the crack propagation increases the interfacial toughness, thereby increasing the overall ice adhesion strength. The presence of dust particles acts as a barrier to crack propagation, increasing the resistance to the ice detachment.

3.2.2. Polymer surfaces

The values of the ice adhesion strength for the bare and the dust-contaminated surfaces of Teflon, polypropylene, and polyurethane are shown in **Figure 3.10**, **Figure 3.11**, and **Figure 3.12**, respectively. For the Teflon samples the percentages of dust area coverage ranged from 5% to 15% and from 15% to 40% for the PVC particles and the SiO_2 particles respectively. For the PP samples it ranged from 5% to 25% for the PVC particles and from 10% to 30% for the SiO_2 particles. The percentage of area covered by the particles for the PU samples ranged from 10% to 40% for the PVC particles and from 25% to 60% for the SiO_2 particles.

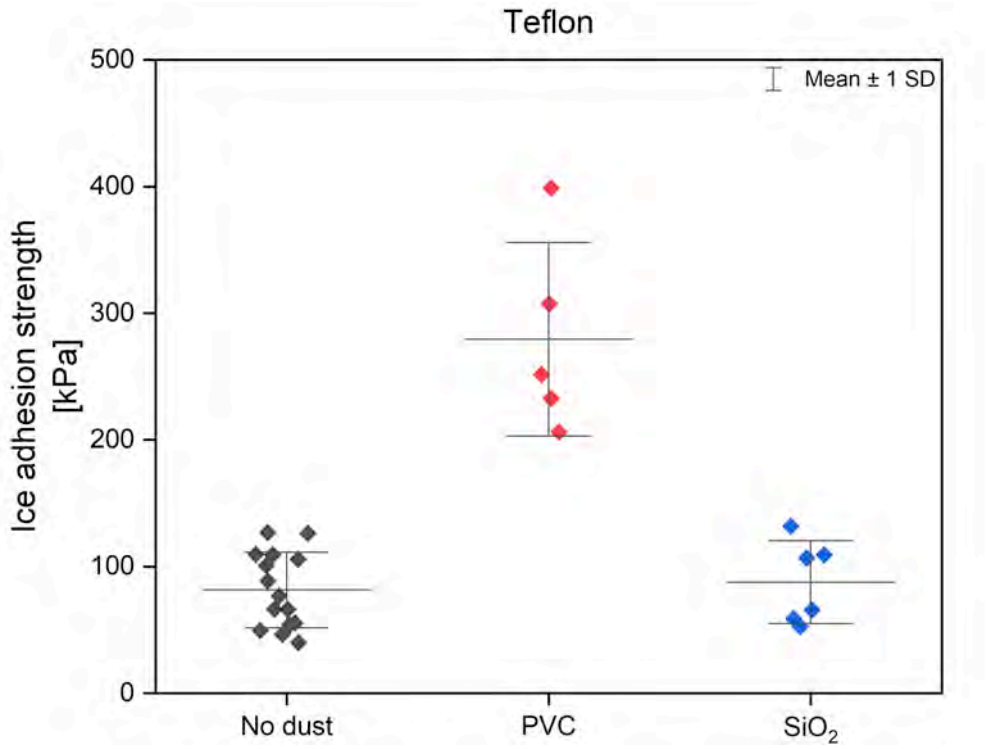

Figure 3.10: Comparison between ice adhesion strength of bare surfaces and dust-contaminated surfaces for Teflon.

Based on the previous analysis, it would be expected that the ice adhesion strength of dust-contaminated samples would be higher than that of bare samples due to the interfacial toughening effect introduced by the particles. This expected behaviour can be observed in the PU substrates, where there is a slight increase in the mean values of ice adhesion strength of the dust-contaminated samples, although the overall effect remains moderate. In contrast, the Teflon samples exhibit a noticeable increase in ice adhesion strength specifically with the addition of PVC particles, while the introduction of SiO_2 particles does not have any significant effect. Meanwhile, for the PP samples, a slight increase in ice adhesion strength is observed with the SiO_2 particles, but no significant change is detected with the addition of PVC particles.

This response was initially associated with the surface roughness of the samples. The PP samples exhibit a high surface roughness (Appendix B), which may lead to minimal changes

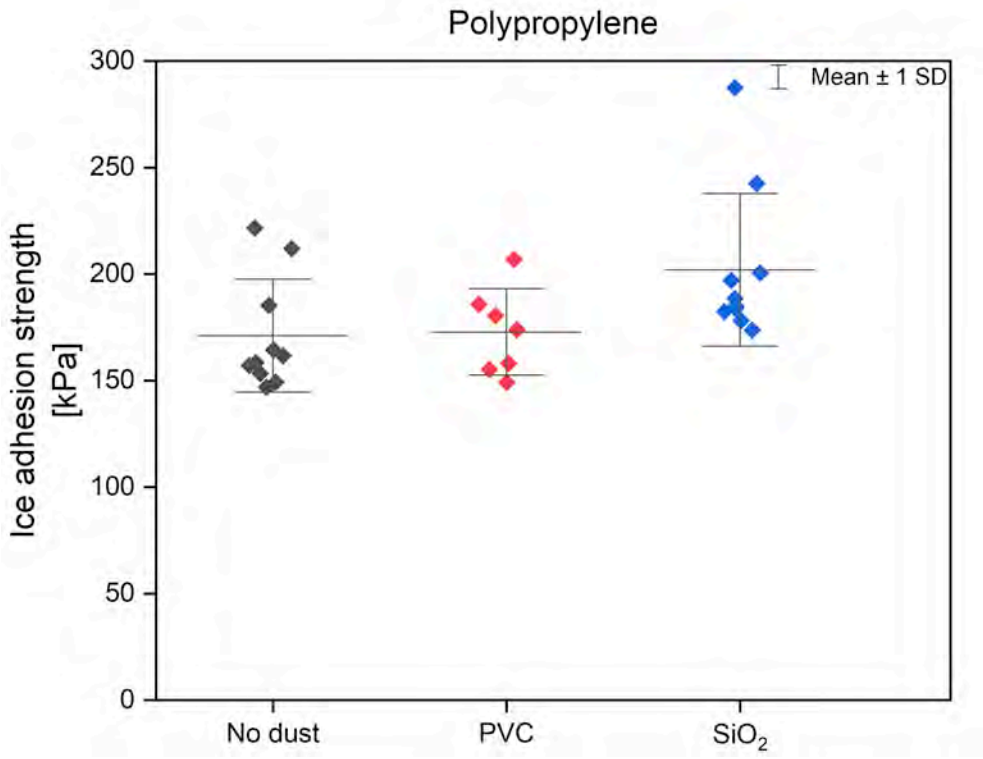

Figure 3.11: Comparison between ice adhesion strength of bare surfaces and dust-contaminated surfaces for polypropylene.

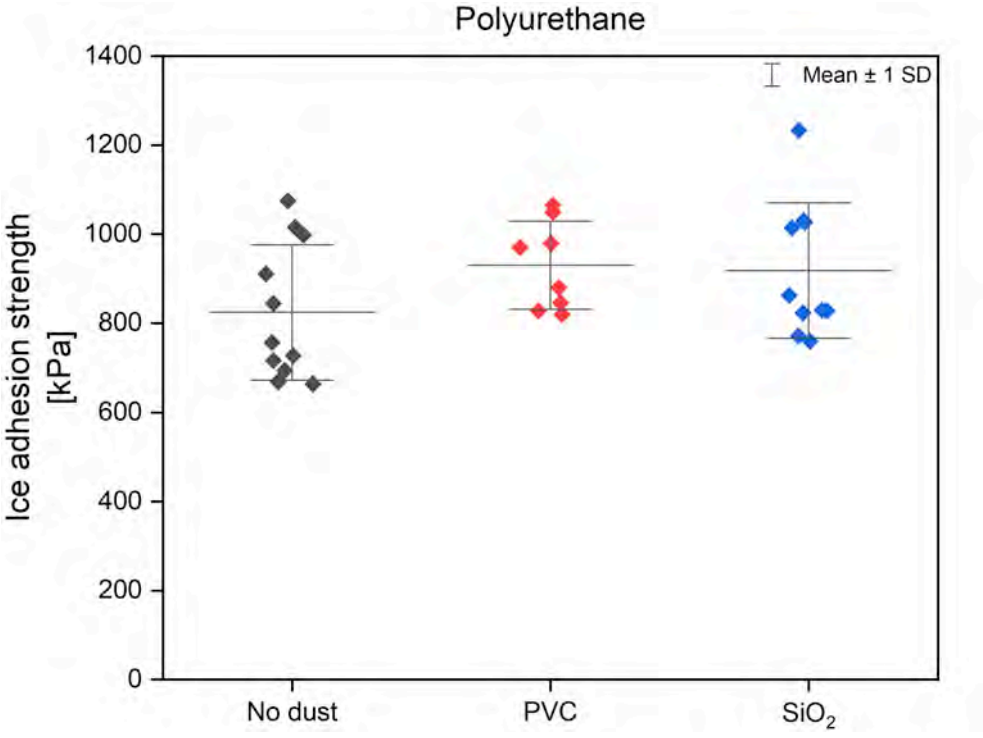

Figure 3.12: Comparison between ice adhesion strength of bare surfaces and dust-contaminated surfaces for polyurethane.

in surface texture after the PVC particles addition. This behaviour was also observed in the unpolished aluminium samples, suggesting a similar effect of surface roughness in reducing the impact of dust contamination on ice adhesion strength. On the other hand, the PU and Teflon samples demonstrate a low surface roughness, which may account for the observed increase in ice adhesion strength increases when PVC particles were introduced. However, this does not fully explain the results observed with the SiO_2 particles. In comparison to the bare samples, the ice adhesion strength remains unchanged for Teflon, while a slight increase is observed for both PP and PU samples.

An alternative explanation was attributed to the hydrophobicity of the materials involved, suggesting that some interactions between the particles, the polymer samples, and the ice may have occurred. The hydrophobicity of both the particles and the substrates was examined. The water contact angle (WCA) values are presented in **Table 2.2**. The PVC particles exhibit a WCA that is similar to that of the polypropylene substrates (96° compared to 101°). This similarity may account for the lack of significant difference in ice adhesion strength between the bare polypropylene substrates and those contaminated with PVC dust. On the other hand, the more pronounced differences in WCA between the PVC particles and the Teflon substrates (96° versus 111°) and between the PVC particles and the polyurethane substrates (96° versus 87°) are possibly contributing to the observed increase in ice adhesion strength when the PVC particles are introduced. These differences in surface energies suggest a different interaction between the particles and the substrate, ultimately leading to higher ice adhesion strength.

However, the increase in ice adhesion observed with the introduction of the SiO_2 particles on the PU and PP substrates, together with the lack of significant differences observed with the SiO_2 particles on the Teflon substrates compared to the ice adhesion of the bare samples, cannot be fully explained.

These results suggest that additional factors may play a critical role. To gain a deeper insight into this behaviour, the SiO_2 particles were surface modified to achieve a higher WCA, and the ice adhesion strength was measured and compared with previous results.

Investigation of ice adhesion strength with surface modified SiO_2 particles

The ice adhesion strength of the dust-contaminated surfaces with the modified SiO_2 particles is depicted in **Figure 3.13**, **Figure 3.14**, and **Figure 3.15** for the Teflon, polypropylene, and polyurethane substrates, respectively. The percentage of area covered by the surface-modified SiO_2 particles ranges from 12% to 27% for Teflon, from 12% to 25% for PP, and from 20% to 50% for PU.

The mean ice adhesion strength values show a slight increase for all the substrates, however no definitive conclusion about the influence of the WCA of the particles can be drawn from this observation.

The results of the tests suggest that the relatively weak effect of the particles on the ice adhesion strength observed for the polymer substrates, as compared to the aluminium samples, may be due to the particles not remaining attached to the substrates during the freezing process of the injected water. It is likely that, between the injection of the water and its subsequent freezing (which is typically considered to be instantaneous) a certain number of particles detach from the substrates and float in the water. An illustration of this scenario is provided in **Figure 3.16**.

This detachment results in a significant reduction in the number of particles present at the ice-substrate interface, thereby minimising their overall influence on ice adhesion strength. Many of the particles may instead become embedded in the ice rather than contributing to an increase in interfacial toughening and roughness.

The slight increase in ice adhesion strength observed with the introduction of silica (SiO_2) particles with higher WCA can be attributed to improved particle adhesion to the substrate

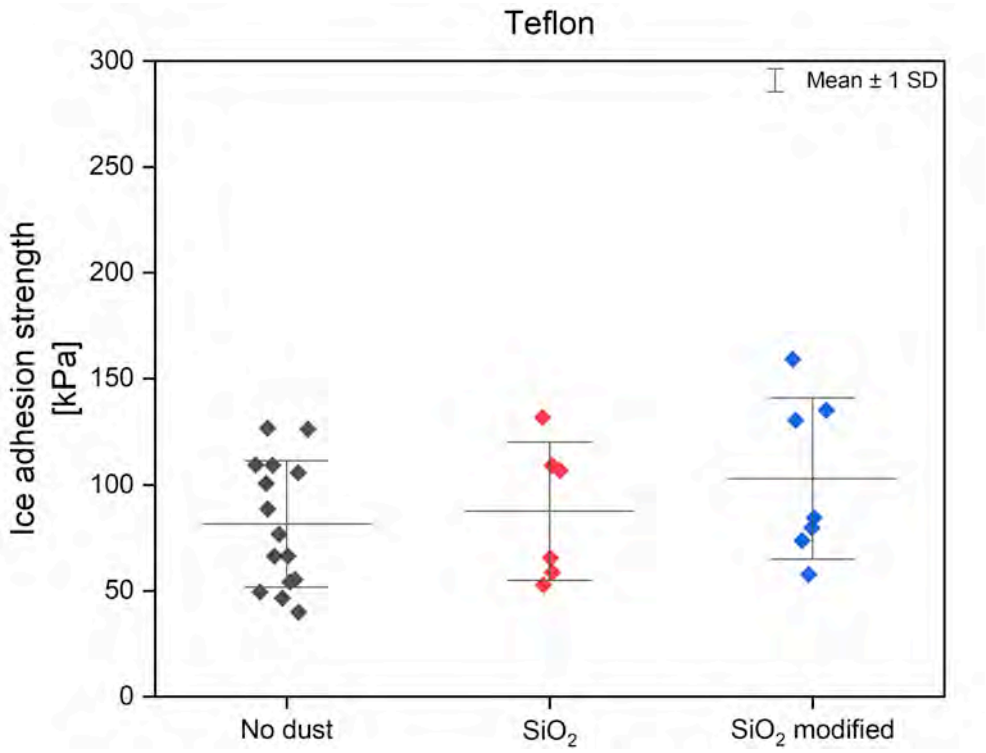

Figure 3.13: Comparison of ice adhesion strength between bare surfaces and dust-contaminated surfaces with unmodified and modified SiO_2 for Teflon.

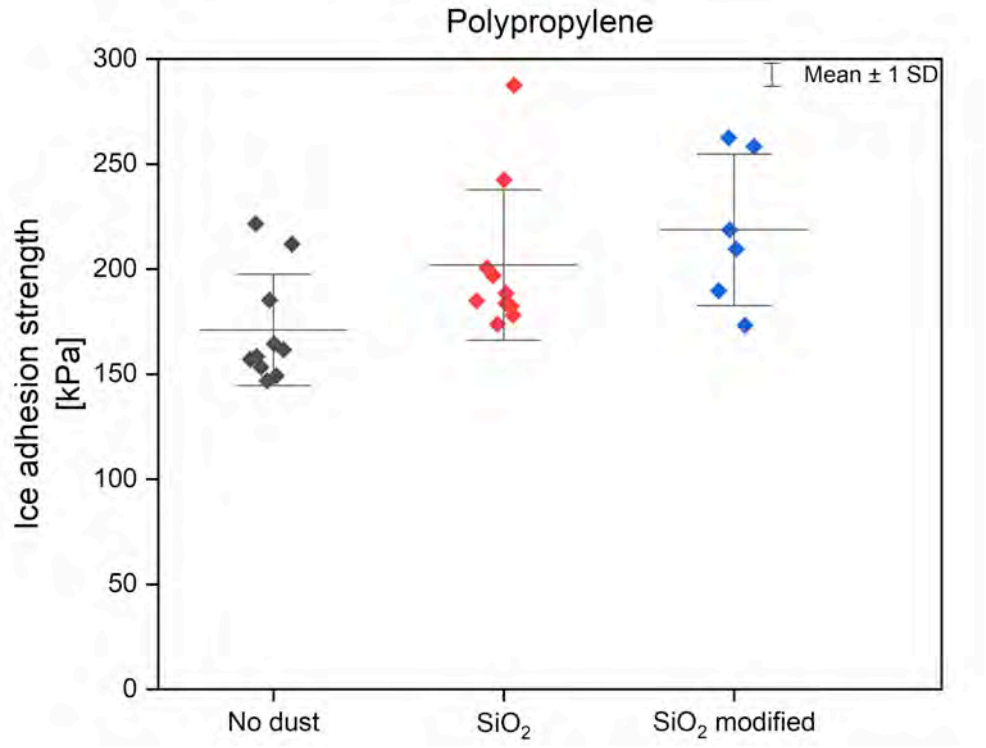

Figure 3.14: Comparison of ice adhesion strength between bare surfaces and dust-contaminated surfaces with unmodified and modified SiO_2 for polypropylene.

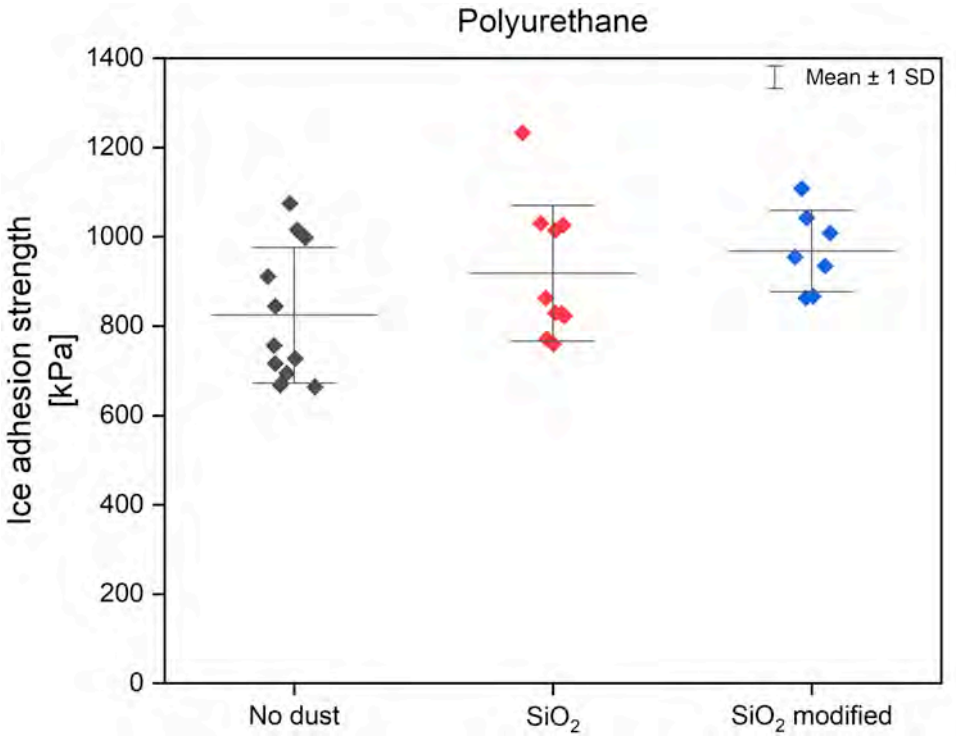

Figure 3.15: Comparison of ice adhesion strength between bare surfaces and dust-contaminated surfaces with unmodified and modified SiO_2 for polyurethane.

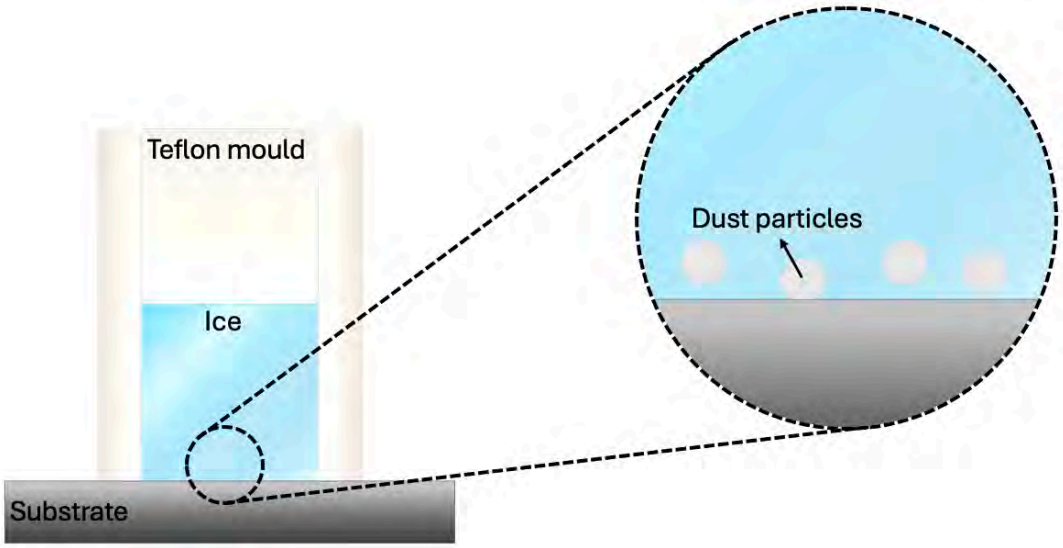

Figure 3.16: Illustration of particle detachment during the freezing process, showing how particles separate from the polymer substrate and float in the water prior to complete freezing.

surfaces, which is likely due to the increased hydrophobicity of the particles. This enhanced particle-substrate interaction may allow more particles to remain attached to the surfaces during freezing, thereby increasing interfacial toughening through repeated crack openings, similar to what was observed with the aluminium samples.

These findings indicate that the ice adhesion strength is dependent on the number of particles present at the interface (so on the number of particle-substrate contact points), which in turn is governed by the nature of their interaction with the substrates, in particular their ability to adhere to the surface. This interaction is governed by the particle attachment during the freezing process, which is influenced by the surface energies of both the particles and the substrates. Therefore, the difference in surface energy between the dust particles and the substrates plays a critical role in determining the extent to which the particles affect the ice adhesion strength.

Investigation of ice adhesion strength with different test procedure

In order to validate the hypothesis that the reduced adhesion between the particles and the substrates leads to their detachment during water injection, and consequently, to a reduced effect on ice adhesion strength, the test method was modified. The revised test method was designed to ensure that the particles remained attached to the substrates, preventing them from floating in the water prior to freezing. By maintaining the presence of particles at the ice-substrate interface, these tests aim to confirm that ice adhesion strength is indeed higher when particles are present, as they inhibit crack propagation. This is important in demonstrating the significant role that particle-substrate adhesion plays in increasing interfacial toughening and ice adhesion strength.

The modified tests were conducted exclusively on the PP samples with the introduction of SiO_2 particles (unmodified), and the results are assumed to be representative for the PU and Teflon substrates as well.

The modified test method eliminated the water injection step and instead placed an ice pillar directly on the sample. After the same waiting time as in the original method, to allow the ice to adhere to the substrate, the ice pillar was pushed with the probe using the same procedure as described in section 2.4. The purpose of this modification was to ensure that the particles remained on the substrate, thus providing a more accurate assessment of the ice adhesion strength. The ice adhesion strength was then calculated based on the force required to detach the ice pillar.

The comparison of ice adhesion strength between the bare PP substrates and those with the introduction of silica particles is presented in **Figure 3.17**. This comparison includes data from both the original and modified test methods, demonstrating the impact of the new method in assessing the role of dust particles in influencing ice adhesion strength. With the modified approach, the particles are forced to remain at the interface, allowing them to exert their influence on the crack propagation, similar to what was observed with the aluminium samples. The values shown in green in **Figure 3.17** represent the additional tests that were carried out on the bare PP samples using the new test method to assess if it would give similar results to the original method. The results indicate that, on average, the ice adhesion strength is slightly higher with the new method. However, the ice adhesion strength with the introduction of SiO_2 particles remains significantly higher compared to the bare substrates, even when both are tested using the new method.

These results highlight another important factor influencing ice adhesion strength: the way in which ice forms on surfaces. As shown, this factor significantly impacts the effect of dust particles on ice adhesion, as when the ice pillar was placed directly on the samples, the particles remained at the interface, increasing the difficulty of ice detachment. In addition, the ice formation process also plays a crucial role in the ice adhesion strength of bare surfaces,

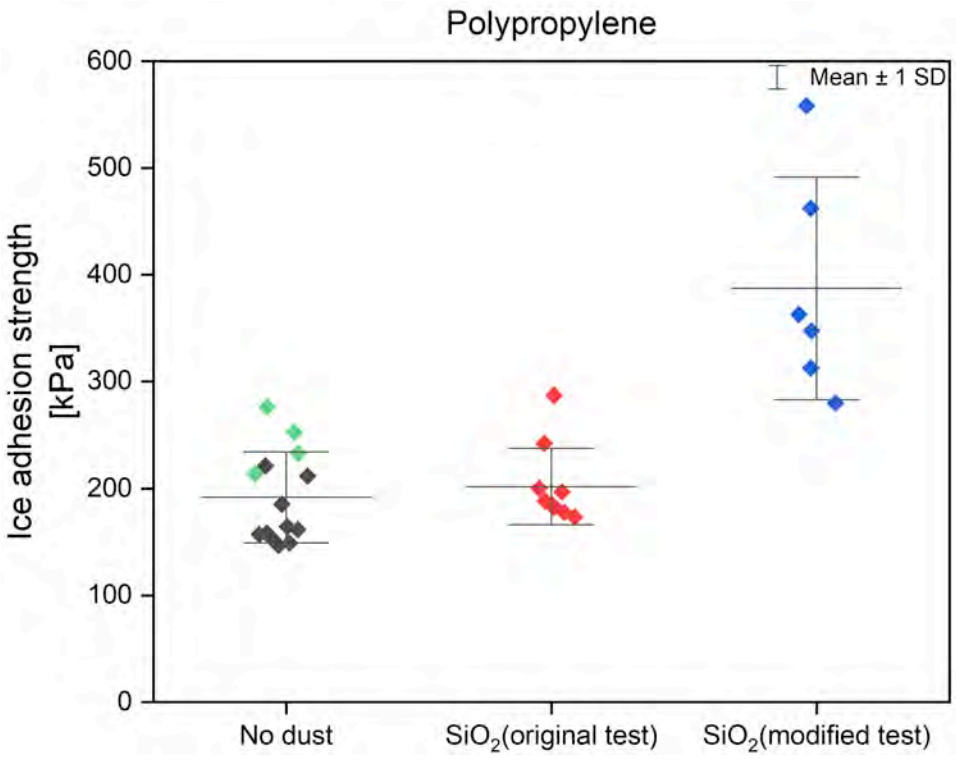

Figure 3.17: Comparison of ice adhesion strength between bare surfaces and dust-contaminated surfaces with SiO_2 for polypropylene with the original and modified test procedures. The green data points represent the ice adhesion strength values obtained with the modified test for the bare PP samples.

which was found to be slightly higher when the ice was placed directly on the samples rather than when water froze on the surfaces.

This finding suggests that variations in the ice formation process affect the ice adhesion strength, an aspect that needs to be carefully considered in the development of anti-icing technologies and experimental methodologies.

3.3. Effect of silicone oil droplets on ice adhesion strength

This section presents the results of the experiments conducted to evaluate the ice adhesion strength of samples with oil droplets added on the surfaces. The goal is to understand how the presence of oil droplets affects the ice adhesion strength of the previously studied samples. Silicone oil was chosen due to its common role as a lubricant, is highly hydrophobic, and has good wetting properties. Due to its low surface tension, silicone oil can spread on surfaces, covering them with a water repellent film.

The samples were tested according to the procedure described in section 2.4. For each material, repeated tests were conducted and the ice adhesion strength was calculated. The values are plotted and, for comparison, the data are shown alongside the data from the bare surfaces.

First, the adhesion between ice and the aluminium surfaces is discussed. Following this, the results for the polymer surfaces are presented, together with a discussion of the observed ice adhesion behaviour.

3.3.1. Aluminium surfaces

Figure 3.18 and **Figure 3.19** show how the ice adhesion strength varies with the introduction of silicone oil droplets on the aluminium surfaces.

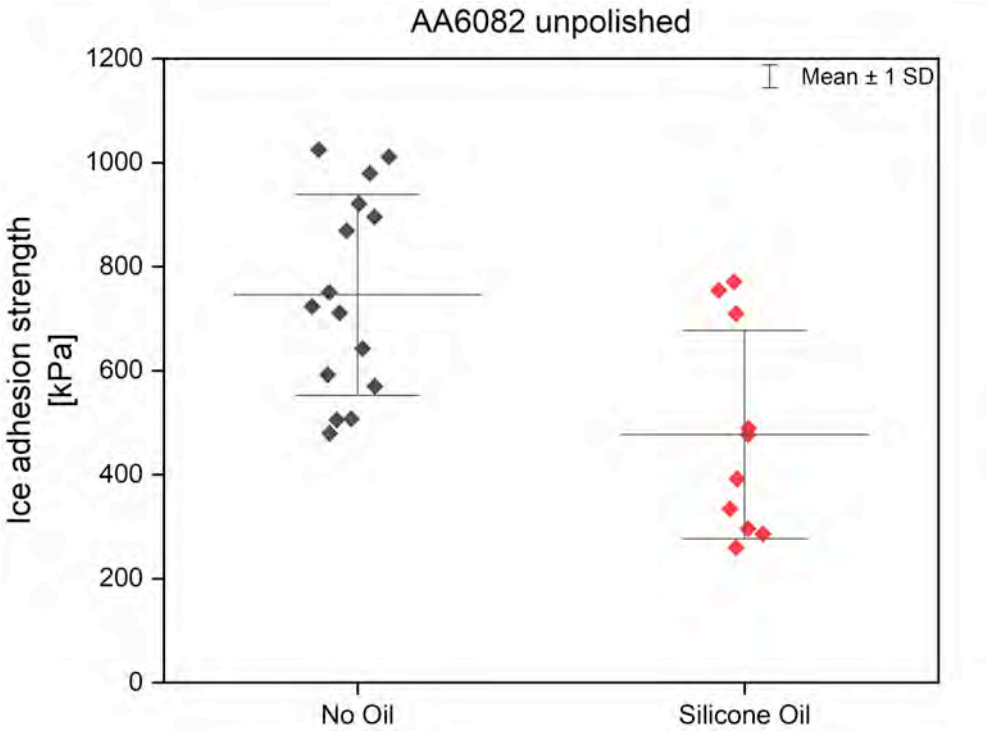

Figure 3.18: Comparison between ice adhesion strength of bare surfaces and surfaces with silicone oil droplets for unpolished AA6082.

The results for the ice adhesion strength of both the polished and unpolished aluminium samples clearly demonstrate a reduction in ice adhesion when silicone oil droplets are present on the surface. The introduction of these droplets creates liquid-solid interfaces between the oil and the ice, which are the primary factor contributing to the reduced ice adhesion strength. By acting as hydrophobic liquid barriers on the substrate, the silicone oil droplets also minimise the contact area between the ice and the surface, which also contributes to the reduction in ice adhesion strength.

This outcome aligns with expectations, given the hydrophobic nature of silicone oil, and that it remains liquid at low temperatures, creating liquid-solid interfaces that prevent ice to adhere to the substrate. By decreasing the effective contact area required for strong adhesion, the silicone oil droplets substantially reduce the force needed to detach the ice, resulting in a reduction in ice adhesion strength.

However, while the results generally show a decrease in ice adhesion strength with the addition of silicone oil droplets, there are some values that are inconsistent with the overall trend and require further evaluation. Although the overall trend indicates that the presence of silicone oil droplets reduces the ice adhesion strength, these unexpected results show adhesion strengths similar to those of the bare samples. These anomalies may be attributed to two factors: the uneven distribution of silicone oil droplets on the surfaces, and the variability in the experimental conditions and the possibility of error during testing. The distribution of the silicone oil droplets on the surface may not have been uniform, resulting in areas where the droplets did not sufficiently cover the surface and therefore did not effectively reduce the contact area between the ice and the substrate.

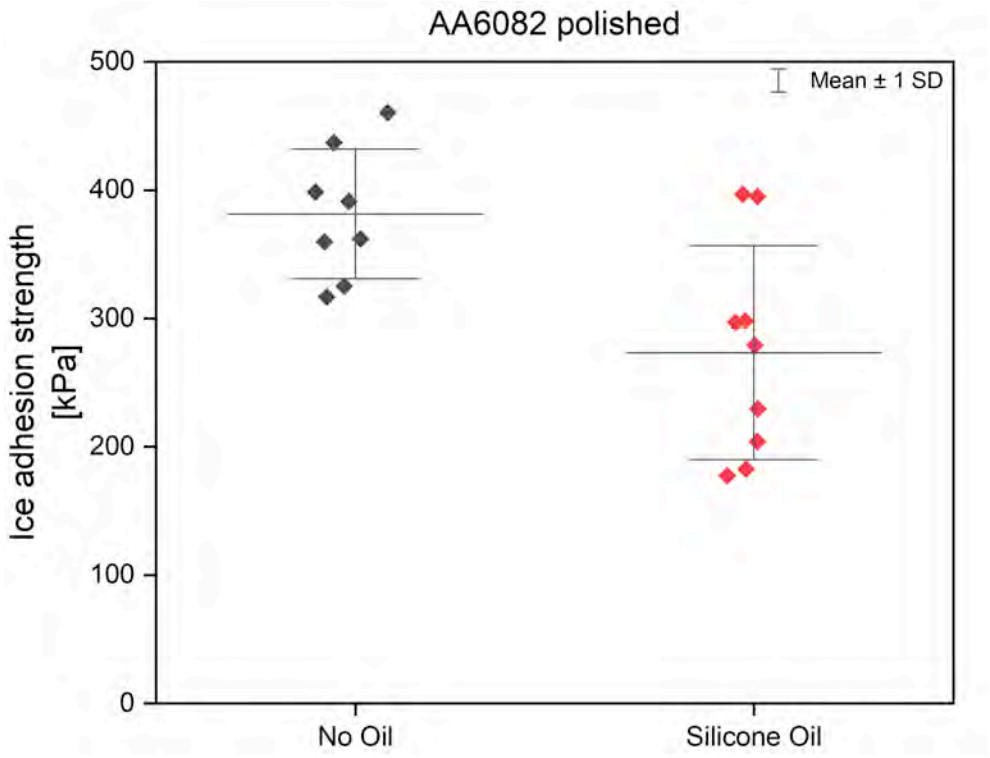

Figure 3.19: Comparison between ice adhesion strength of bare surfaces and surfaces with silicone oil droplets for polished AA6082.

This behaviour is consistent with the observations made for the ice adhesion strength on dust-contaminated aluminium surfaces. In particular, when the concentration of dust particles was located far from the pushing edge of the ice-substrate interface, the detachment region behaved similarly to that of the bare surfaces. As a result, the fracture mechanism in these cases was stress-dominated, leading to a sudden detachment of the ice similar to that observed in the bare surfaces. This suggests that if the dust particles or silicone oil droplets are not concentrated near the critical interface region, their effect on adhesion strength is reduced.

The fact that this behaviour occurred more frequently on the dust-contaminated surfaces than on those with oil droplets can be attributed to differences in the way the dust particles and oil droplets were applied. The distribution of the dust particles on the surfaces was less controlled due to the spin coating technique, resulting in a more uneven distribution across the surface. This increases the possibility of dust particles being concentrated away from the pushing edge of the ice-substrate interface. On the other hand, the application of silicone oil droplets were applied manually, which allows for greater precision and consistency, resulting in a more uniform distribution across the surface.

This, together with the natural variability of the environment and potential errors, provides plausible explanations for the unexpected results observed in these tests.

3.3.2. Polymer surfaces

The ice adhesion strength of the Teflon surfaces was found to be extremely low. In fact, the force required to detach the ice block was so minimal that it was comparable to zero. As a result, the force was below the detection threshold of the experimental set-up used, making it impossible to obtain accurate measurements of the ice adhesion strength for these substrates. These results are attributed to the hydrophobic nature of the added silicone oil droplets. Their

presence reduces the contact area to which the ice adheres, thereby significantly reducing the ice adhesion strength.

Given the hydrophobicity of the silicone oil droplets and their ability to significantly reduce the effective contact area required for strong ice attachment, it is reasonable to expect that similar reductions in ice adhesion strength would be observed across the other polymer surfaces.

Figure 3.20 and **Figure 3.21** show the ice adhesion strength of bare surfaces and surfaces with the addition of silicone oil droplets for PP and PU, respectively.

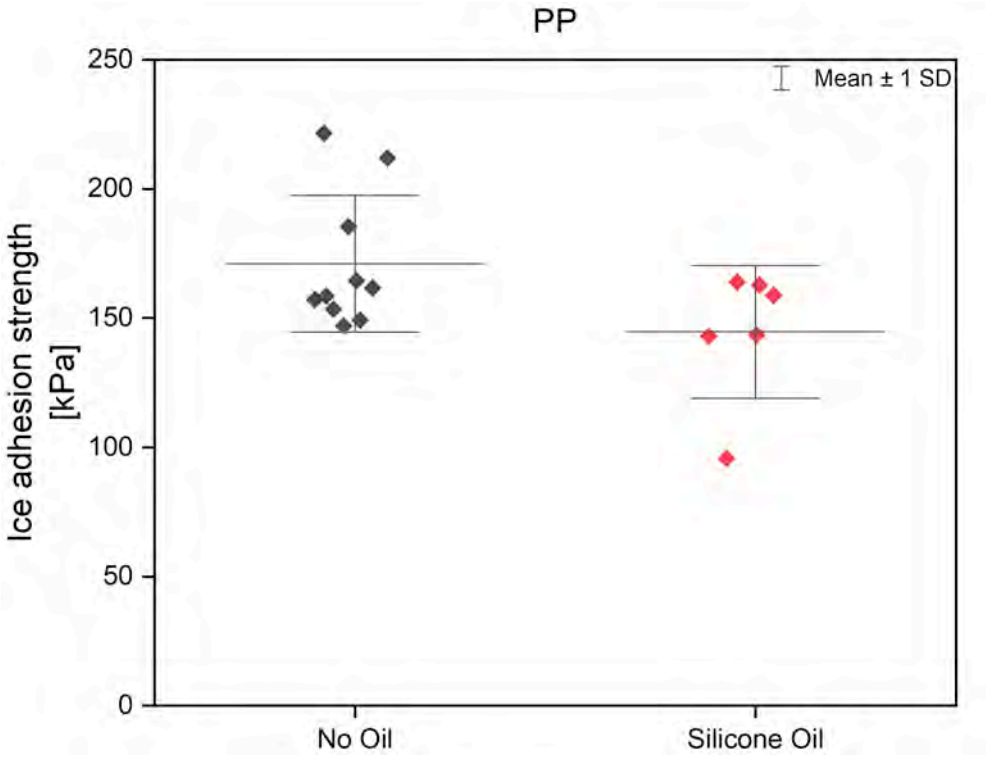

Figure 3.20: Comparison between ice adhesion strength of bare surfaces and surfaces with silicone oil droplets for PP.

Both graphs indicate a decrease in the mean ice adhesion strength following the addition of silicone oil droplets. However, this reduction is more pronounced for the PU samples, with a significant decrease of approximately 200 kPa, while the reduction in the PP samples is relatively minimal. The limited reduction for PP suggests that the silicone oil has little effect in lowering the ice adhesion strength on this material.

A possible explanation for this observation could come from the interaction mechanisms between the silicone oil and the PP samples, which appear to differ from those observed with other materials. Unlike other surfaces, where droplets are clearly visible, the PP surface shows less distinct droplet formation. This is evident in **Figure 2.6**, which shows that while the PP surface is wet, clear droplet formation is absent. This suggests that the spreading dynamics of silicone oil on PP differ from those on aluminium, Teflon, and PU samples, potentially reducing the efficacy of silicone oil in minimising ice adhesion strength.

A second factor that may contribute to the observed results is the uneven distribution of silicone oil across the surface, a phenomenon also observed in the aluminium samples. If the oil droplets fail to sufficiently cover the entire surface - particularly in critical areas near the pushing edge - direct contact between the ice and the substrate may persist, preventing the expected reduction in adhesion strength.

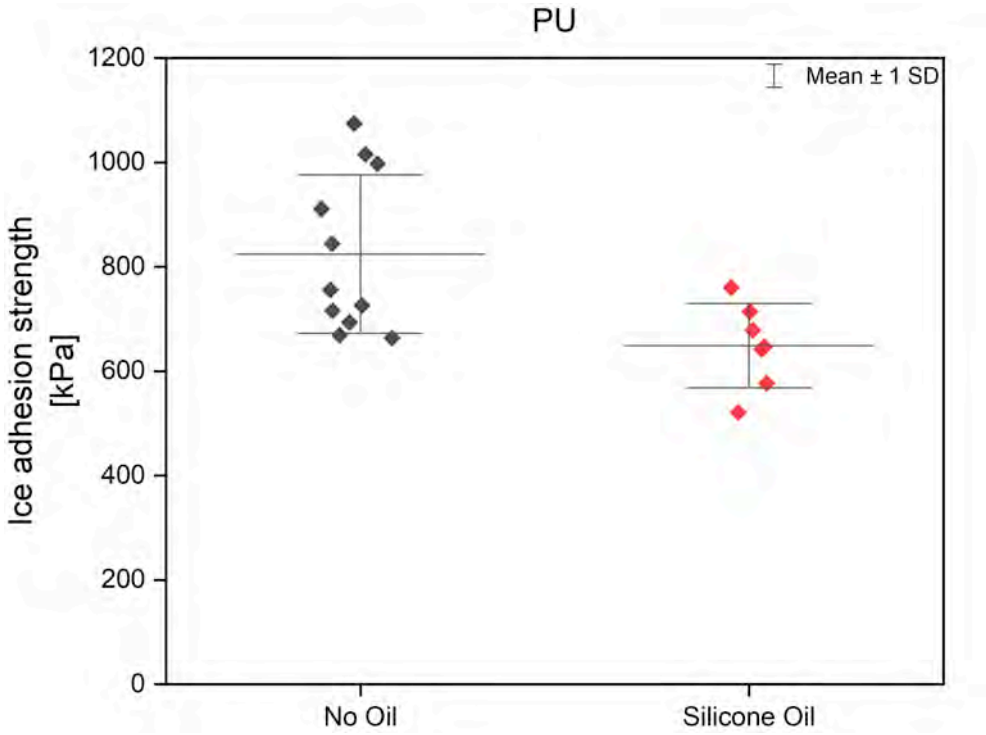

Figure 3.21: Comparison between ice adhesion strength of bare surfaces and surfaces with silicone oil droplets for PU.

This highlights the importance of ensuring a more uniform distribution of oil droplets in future experiments, to obtain more consistent results. Additionally, changing the hydrophobic oil could guarantee the formation of the droplets on the polypropylene substrates.

3.4. Effect of UV radiation exposure on ice adhesion strength

This section examines the impact of exposure to ultraviolet (UV) radiation on the ice adhesion strength of polypropylene and polyurethane. The samples were exposed to UV radiation to simulate environmental ageing, and the changes in their physical and chemical properties were analysed using Fourier-Transform Infrared spectroscopy (FTIR), confocal scanning microscopy (to determine the surface roughness), and WCA measurements.

The discussion focuses on how the UV induced changes in the chemical and physical properties affect the ice adhesion strength of PP after 5 and 10 hours and of PU after 10 hours. Comparisons are made with non-exposed samples to illustrate the extent of the effect of UV radiation, which is of interest for applications where UV exposure is expected. Before discussing the results, the following paragraph provides a brief overview of the implications of UV radiation on the properties of polymers.

Influence of UV radiation on polymers

Exposure to UV radiation can rapidly accelerate degradation processes in polymers. The main damage mechanism is oxidative photodegradation (called also photooxidation), which is a process initiated by light when oxygen is present in the environment [67]. This process is defined as the degradation of photodegradable molecules caused by the absorption of UV photons by chromophores (molecules that absorb light at a certain wavelengths). Photodegradation causes chain scission and the generation of free radicals and new chemical bonds, leading to a loss of molecular weight, surface discoloration, and loss of mechanical

strength.

UV exposure can also cause the introduction of new functional groups, such as carbonyl (C=O) and hydroxyl (OH) groups, which can alter the surface energy and affect the wettability. Additionally, Lu et al. [68] reported that UV exposure reduces the surface roughness of polymers, leading to smoother surfaces that further influence wettability.

3.4.1. Ice adhesion strength of polypropylene after 5 and 10 hours of UV radiation exposure

After 5 and 10 hours of UV radiation exposure, the ice adhesion strength of polypropylene was measured. The data is shown in **Figure 3.22**.

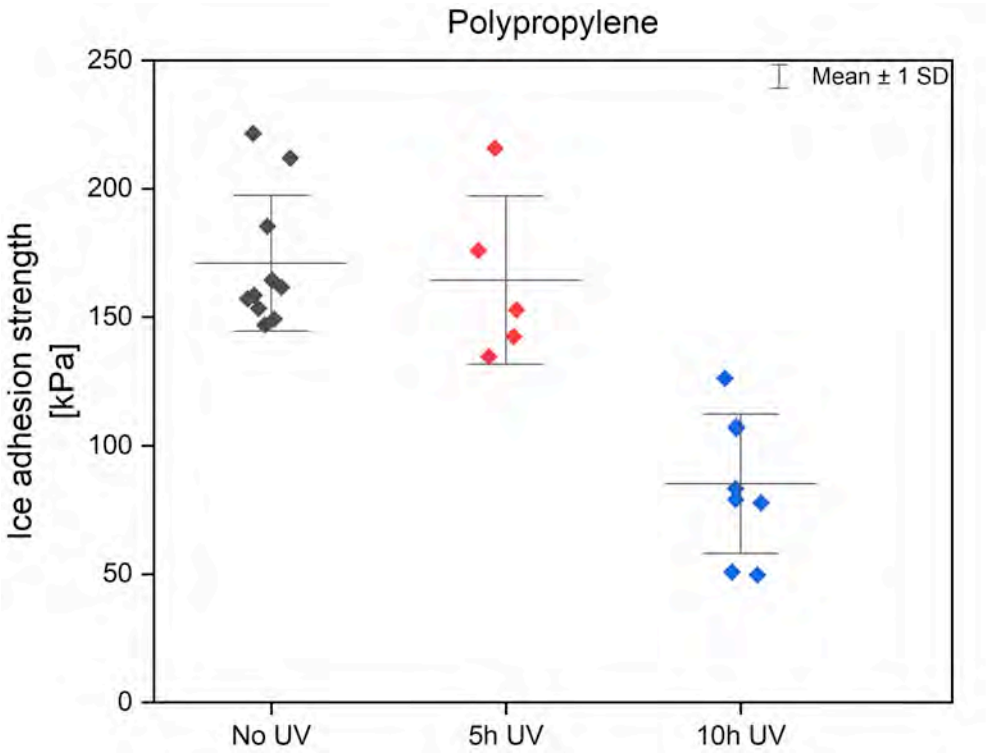

Figure 3.22: Comparison between ice adhesion strength of non-exposed PP surfaces and PP surfaces after 5 and 10 hours of UV radiation exposure.

The graph demonstrates a reduction in ice adhesion strength after 10 hours of UV exposure, whereas no considerable change is observed after 5 hours of exposure. The mean values of ice adhesion strength for the bare and the exposed samples are presented in **Table 3.1**, along with the WCA and surface roughness values (only the maximum height is shown, as it is more directly related to the mechanical interlocking between the ice and the surface than the arithmetical mean height).

This result was unexpected and a more detailed surface analysis was required.

The WCA measurements showed an initial decrease in WCA after 5 hours of UV exposure, followed by an increase after 10 hours. Surface roughness decreased after 5 hours of UV exposure and the value remained constant after an additional 5 hours, suggesting that UV exposure leads to a reduction in surface roughness. The observed decrease in WCA and surface roughness after 5 hours of UV exposure explains the small change in ice adhesion strength. The reduction in WCA counteracts the effect of the decrease in surface roughness, so that the ice adhesion strength remains comparable to that of the bare samples. However, after

Table 3.1: Mean ice adhesion strength, WCA, and maximum height (Sz) values for polypropylene after 5 and 10 hours of UV exposure.

Hours of exposure [h]	Mean ice adhesion strength [kPa]	WCA [°]	Sz [μm]
0	171.0	101	49.51
5	164.3	87	43.24
10	85.2	108	42.26

10 hours of exposure, the increase in WCA explains the decrease in ice adhesion strength. This decrease is attributed to the combined effect of the reduced surface roughness (relative to the original substrates) and the increase in WCA, which together reduce ice adhesion.

The decrease in surface roughness was expected, as UV radiation is known to reduce surface roughness. However, the initial decrease followed by a subsequent increase in WCA was unexpected and suggest the need for further investigation. This behaviour is in accordance with a phenomenon known as hydrophobic recovery (or the ageing effect), exhibited by some polymers, where they revert to a more hydrophobic state over time after initial UV exposure. This results from a disequilibrium in the surface properties caused by surface treatments [69], resulting from the generation of hydrophilic groups, such as hydroxyl (OH) and carbonyl (C=O) groups, and their re-orientation away from the surface. This effect, known as “overturn” of polar groups, is caused by thermodynamic relaxation.

This phenomenon was investigated by Wan et al. [70], who performed water contact angle measurements on several plastics before and after ageing. Their findings indicated an initial decrease followed by a subsequent increase in the WCA of PP, which was attributed to the rearrangement of surface molecular chains during the ageing process. In contrast, polycarbonate (PC) showed very little hydrophobic recovery, probably due to its intrinsic thermal stability, while polystyrene (PS) exhibited almost complete hydrophobic recovery, similar to PP. Hydrophobic recovery can be further enhanced by changes in surface topography, such as reduced surface roughness, which was also observed in the UV-exposed PP samples in this thesis.

3.4.2. Ice adhesion strength of polyurethane after 10 hours of UV radiation exposure

The ice adhesion strength of polypropylene was measured after 10 hours of UV radiation exposure and the values are shown in **Figure 3.23**.

The graph shows that the ice adhesion strength remain similar after 10 hours of UV exposure. To understand the cause of this, the WCA and the surface roughness were measured. **Table 3.2** presents the mean values of ice adhesion strength, the WCA, and the maximum height (Sz) for both the unexposed and exposed samples.

Table 3.2: Mean ice adhesion strength, WCA, and maximum height (Sz) values for polyurethane after 10 hours of UV exposure.

Hours of exposure [h]	Mean ice adhesion strength [kPa]	WCA [°]	Sz [μm]
0	824.2	87	6.09
10	872.7	74	6.18

Despite no evident change in surface roughness, the WCA decreased, indicating that

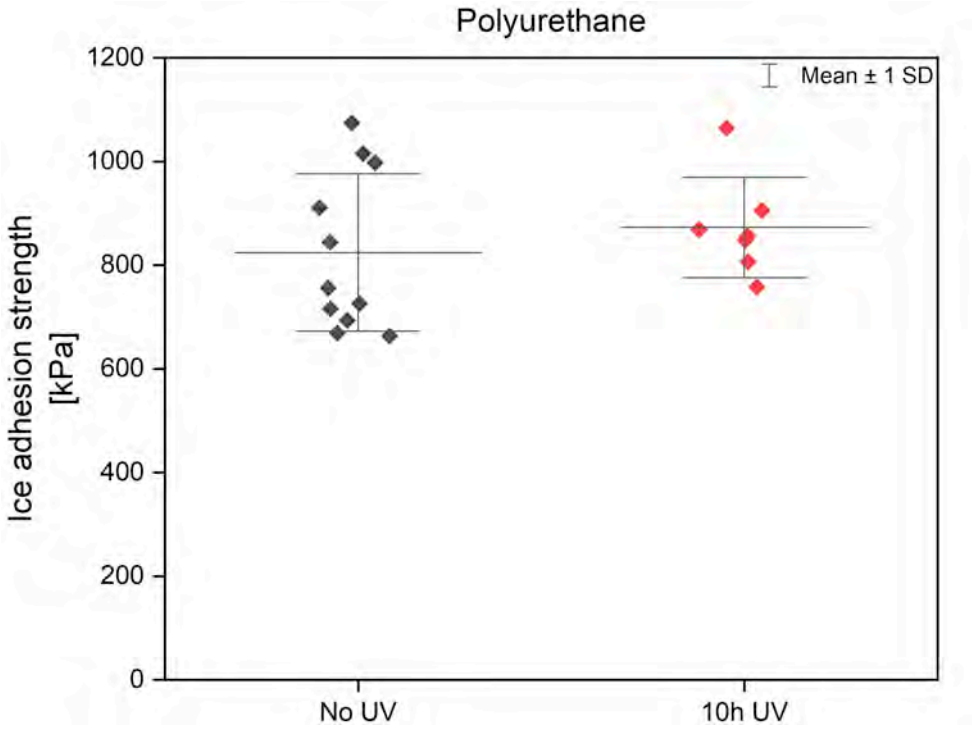

Figure 3.23: Comparison between ice adhesion strength of non-exposed PU surfaces and PU surfaces after 10 hours of UV radiation exposure.

the surfaces became more hydrophilic. Unlike the polypropylene samples, no hydrophobic recovery was observed, which is consistent with the literature, as this phenomenon has not been observed for polyurethane. With the surface roughness remaining unchanged and the WCA decreasing, an increase in ice adhesion strength would be expected due to the more hydrophilic nature of the substrates. However, the observed increase in ice adhesion strength was minimal, only about 5.9%. This suggests that surface roughness plays a more significant role in influencing ice adhesion strength, as its constancy is likely to have mitigated the effect of the increased hydrophilicity.

3.5. Discussion

This sections examines the interpretation and the analysis of the results presented previously. The goal is to explore the implications of the experimental results regarding ice adhesion strength across different materials and under various defect conditions. Here, the results are examined to understand how each defect affects ice adhesion strength.

The first defect identified as influencing ice adhesion strength is the presence of dust particles at the ice-substrate interface, which affect the interfacial toughness and increase the difficulty of ice detachment. In more detail, if the adhesion strength between the dust particles and the substrate is low enough to facilitate easy detachment, and the adhesion strength between the dust particles and the ice is high enough to keep the particles attached to the ice, the ice-substrate interface can be considered to be split into multiple contact points. As a result, crack propagation at the interface is intermittently arrested by the dust particles, which act as barriers to the advancing crack, leading to repeated interruptions. Each time the crack is arrested, it must overcome additional resistance to re-initiate, as the maximum stress required for crack opening occurs at the crack tip. This process of crack initiation and arrest increases the interfacial toughness and consequently the overall ice adhesion strength, making it much

more difficult for the ice to detach from the substrate.

To gain a deeper understanding of the phenomenon, the detachment curves were analysed. These curves results from the experimental tests, as illustrated in **Figure 2.15**, and they provide an insight of the detachment process. From the data of these curves the time difference between the start of the recording of the electromotive force and the moment when the ice pillar detaches from the substrate was measured. It represents the displacement of the ice pillar, which begins when the probe starts to exert pressure on it. This displacement can be determined by knowing the speed of the probe, which is constant at 0.01 mm/s. When the fracture mechanism is stress-dominated, resulting in a sudden fracture, the displacement (and corresponding time difference) is expected to be lower compared to a toughness-dominated fracture.

The analysis of these parameters focused on the aluminium samples, as they provided the most reliable and clear results. **Table 3.3** presents the mean values of the time differences and displacements.

Table 3.3: Mean time difference and displacement for unpolished and polished AA6082 samples.

AA6083	Type of test	Time difference [s]	Displacement [mm]
Unpolished	Bare surfaces	21.5	0.215
	Surfaces with PVC	31.5	0.315
	Surfaces with SiO_2 (40-60)	32.2	0.322
	Surfaces with SiO_2 (100)	33.1	0.331
Polished	Bare surfaces	16.8	0.168
	Surfaces with PVC	31.6	0.316
	Surfaces with SiO_2 (40-60)	28.9	0.289
	Surfaces with SiO_2 (100)	29.2	0.292

The analysis showed that the displacement measured for the bare samples was lower than that for the dust-contaminated samples. This trend was observed in both unpolished and polished aluminium samples. The increased displacement in the dust-contaminated samples indicates an increase in interfacial toughness. This toughness, represented by the area under the force-displacement curve, suggests that the fracture mechanism in these cases is toughness-dominated, with crack propagation occurring at the interface. **Figure 3.24** highlights the displacement and the crack propagation at the interface during the detachment of the ice pillar.

In particular, for the polished aluminium substrates, the displacement measured for the bare samples was approximately half that of the dust-contaminated samples. This trend was not observed for the unpolished aluminium substrates, where the displacement for the bare samples was approximately two thirds of the displacement for the dust-contaminated samples. This can be attributed to the smoother surface of the polished aluminium samples, where dust particles increase the mechanical interlocking and the resistance to detachment. In contrast, the unpolished aluminium samples, with their inherently rougher surface, already exhibits strong ice adhesion strength. As a result, the relative effect of dust contamination is less pronounced, as was explained before. This difference highlights the importance of surface roughness in governing the impact of interfacial defects on ice adhesion strength.

Figure 3.25 visually illustrates these trends, showing that surface roughness significantly influences the extent to which the ice adhesion strength increases in the presence of dust particles at the interface, compared to the bare substrates.

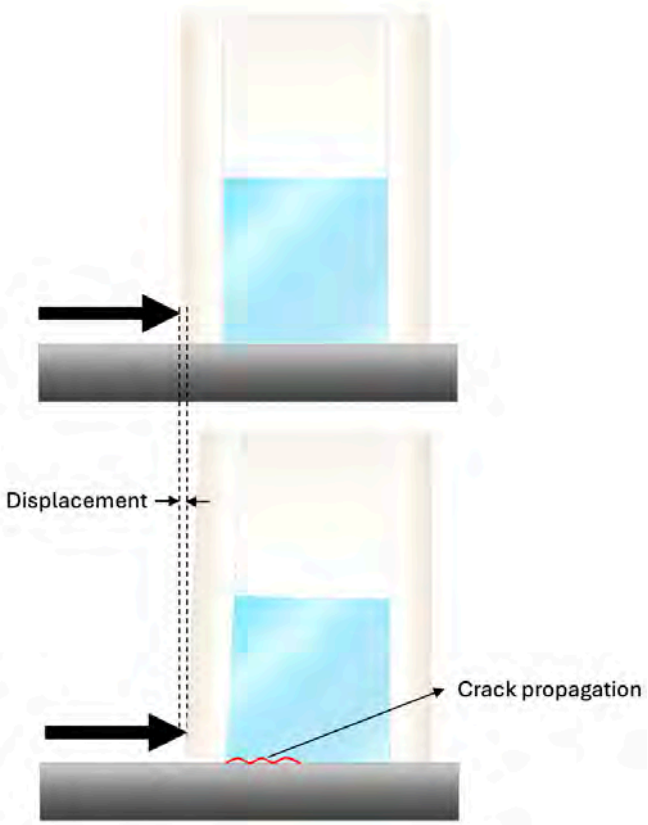

Figure 3.24: Schematic of a toughness-dominated fracture between an ice pillar and a substrate.

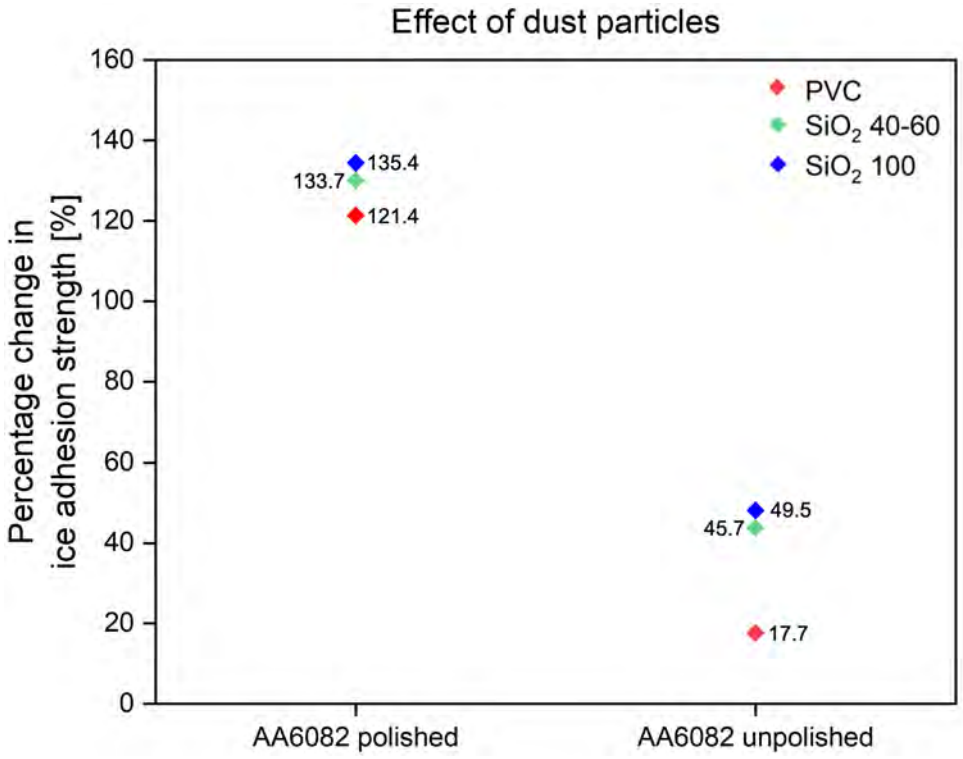

Figure 3.25: Effect of dust particles contamination on ice adhesion strength of AA6082 (polished and unpolished).

It is important to note that the mean ice adhesion strength of the bare unpolished aluminium samples is comparable to that of dust-contaminated polished aluminium samples, even though it is still slightly lower. Despite the significant increase in ice adhesion strength observed with the introduction of dust particles on polished aluminium, these surfaces demonstrate a better performance compared to the unpolished aluminium surfaces, regardless of the presence of dust particles on the former and the cleanliness of the latter. This suggests that a polished aluminium surface is preferable to an unpolished one when minimising ice adhesion is the desired outcome.

Another factor that can be analysed is the distribution of ice adhesion strength values following the introduction of dust particles on the substrates. As previously discussed, the variability in ice adhesion strength is influenced by the distribution of the particles at the ice-substrate interface. The detachment curves can provide valuable insight into how this particle distribution impacts the variation in ice adhesion strength values. Specifically, lower adhesion strength is recorded when fewer particles are present near the pushing edge, whereas higher adhesion strength is observed when more particles are concentrated in this area. This correlation is illustrated by the detachment curves in **Figure 3.26** and **Figure 3.27**, which compare samples with different particle distributions.

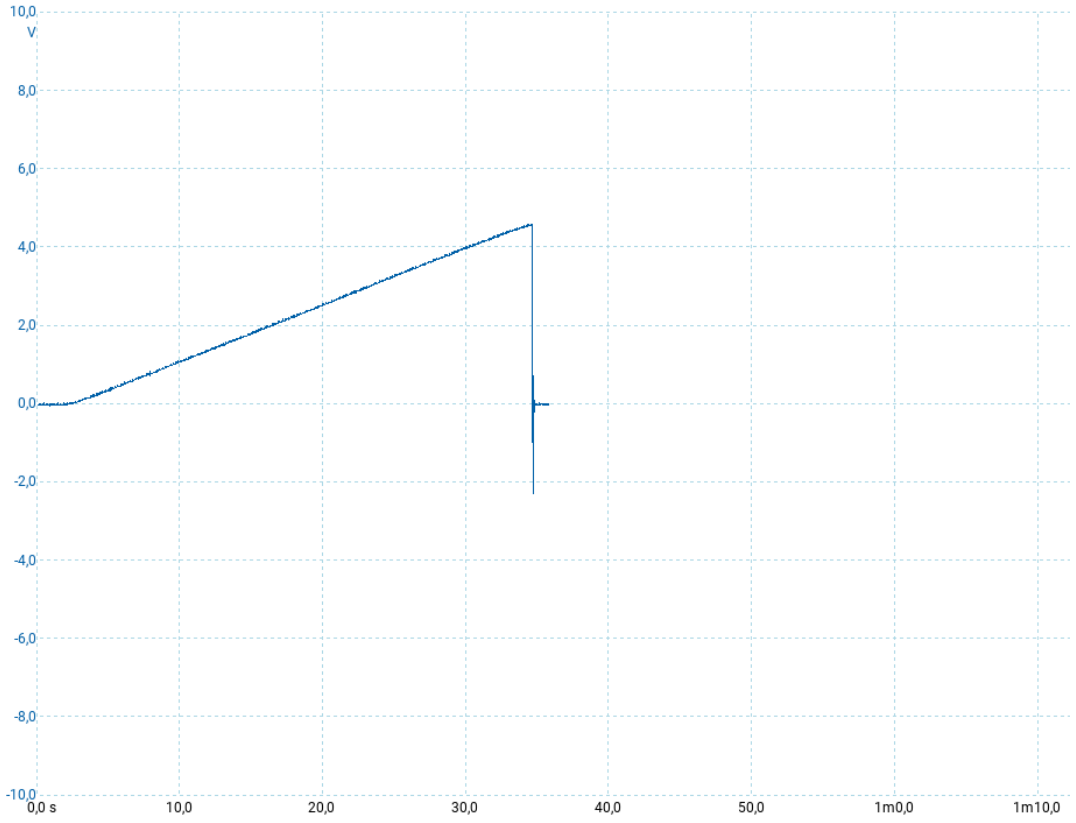

Figure 3.26: Detachment curve for an aluminium substrate with particles primarily distributed away from the pushing edge of the interface.

In **Figure 3.26**, an aluminium sample with fewer particles near the pushing edge exhibits a lower adhesion strength, whereas in **Figure 3.27**, a sample with a greater concentration of particles near the pushing edge shows a higher adhesion strength. From these curves, the displacement can be visualised through the time difference between the initiation of the applied force and the point at which detachment occurs. The graph displaying the lower ice adhesion strength (from the sample with fewer particles near the pushing edge) also shows a

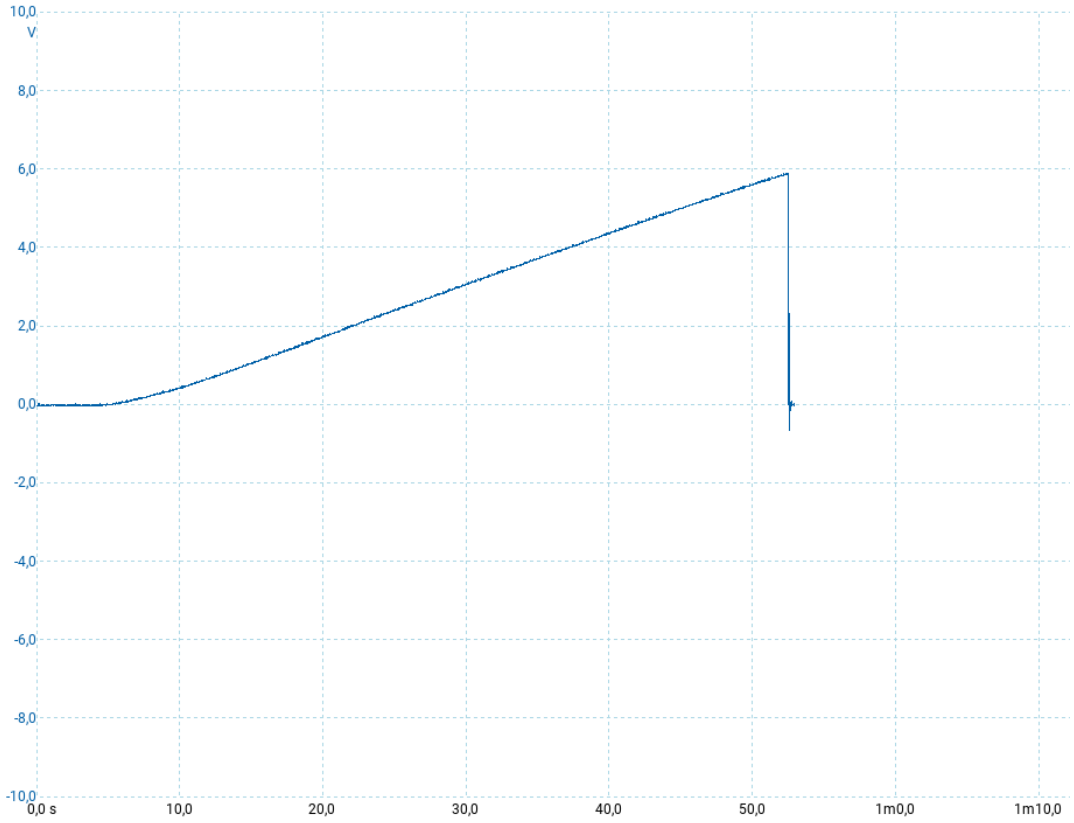

Figure 3.27: Detachment curve for an aluminium substrate with particles mainly distributed near the pushing edge of the interface.

shorter time difference, indicating that the displacement prior to the detachment is smaller. This suggests that the interfacial toughness is higher and that it is more difficult for the ice pillar to detach from the substrate when the particles are concentrated near the pushing edge, resulting in a higher ice adhesion strength. These results highlight the role of particle distribution in the ice adhesion strength and show that ice detachment can depend on multiple factors.

The graphs also indicate that the PVC particles increase the ice adhesion strength by a smaller extent compared to the SiO_2 particles. This difference can be attributed to the difference in particle size. When calculating the percentage of surface area covered by the particles, it is not the area of the effective contact points that is determined, but rather the projection of the particles onto the substrate. As a result, the number of PVC particle-substrate contact points is lower than that of SiO_2 particles, for the same percentage of surface area coverage. This reduced number of contact points of the PVC particles compared to the SiO_2 particles may be the reason for the lower contribution of the PVC particles on the ice adhesion strength.

For the polymer substrates, the interaction between the dust particles used and the samples, together with the way the ice formed, played an important role in determining how the ice adhesion strength changed. It was observed that for certain samples, the introduction of dust particles resulted in little to no significant change in ice adhesion strength. This was later shown to be due to a detachment of the particles from the substrates when the water was injected prior to the start of the test, significantly reducing the number of particles at the ice-substrate interface and minimising their influence on the ice adhesion strength. When the test procedure was adjusted to ensure that the particles remained at the ice-substrate interface, an increase in ice adhesion strength was observed, as happened with the aluminium samples. This means that the way in which ice forms on surfaces, as well as the adhesion between the substrate and the introduced dust particles, significantly influences how surface defects affect the ice adhesion strength of ice.

Consequently, understanding the influence of ice formation on surfaces is crucial to fully analyse the mechanisms of ice adhesion and to develop effective mitigation strategies based on the conditions under which ice forms.

The second type of defect analysed is the presence of hydrophobic liquid droplets (specifically silicone oil droplets). These droplets created localised liquid-solid interfaces within the ice adhesion area and, as a result, ice did not adhere to these regions, reducing the effective contact area between the ice and the substrate and decreasing the ice adhesion strength. The effect of the silicone oil can be seen in **Figure 3.28**, where the reduction in percentage compared to bare surfaces is shown.

The third factor investigated was the impact of UV radiation on the ice adhesion strength of polypropylene and polyurethane samples. UV exposure altered the surface roughness and surface energy, leading to changes in ice adhesion strength. This is illustrated in **Figure 3.29**, which displays the percentage change relative to the original samples.

It was observed that the effect of UV exposure varies according to the type of polymer. Polypropylene undergoes a phenomenon known as hydrophobic recovery, where the water contact angle initially decreases and then increases due to the re-orientation of the hydrophilic groups away from the surface. This process, coupled with a reduction in surface roughness, results in a significant reduction in ice adhesion strength of approximately 50.2%. The simultaneous reduction in both surface roughness and surface energy in the PP samples is likely to account for the observed reduction in ice adhesion strength. In contrast, polyurethane does not show any hydrophobic recovery, as indicated by a decrease in WCA. Despite this, the ice adhesion strength remains relatively stable, probably due to the unchanged surface roughness, which helps to maintain consistent ice adhesion strength.

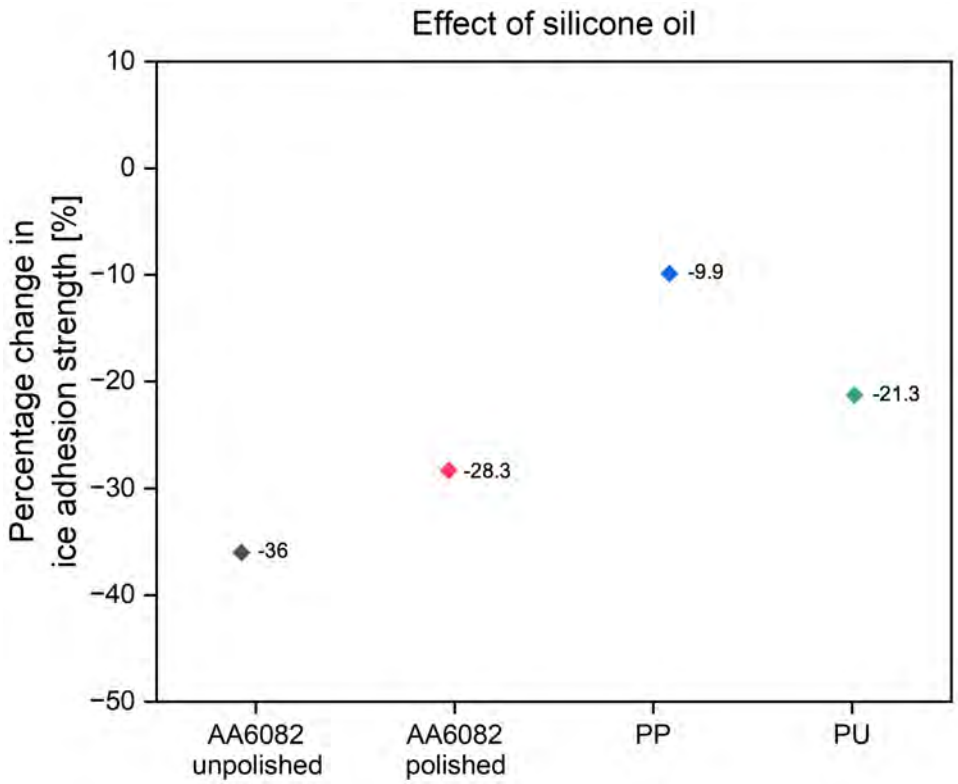

Figure 3.28: Effect of silicone oil on ice adhesion strength of AA6082 (polished and unpolished), PP, and PU.

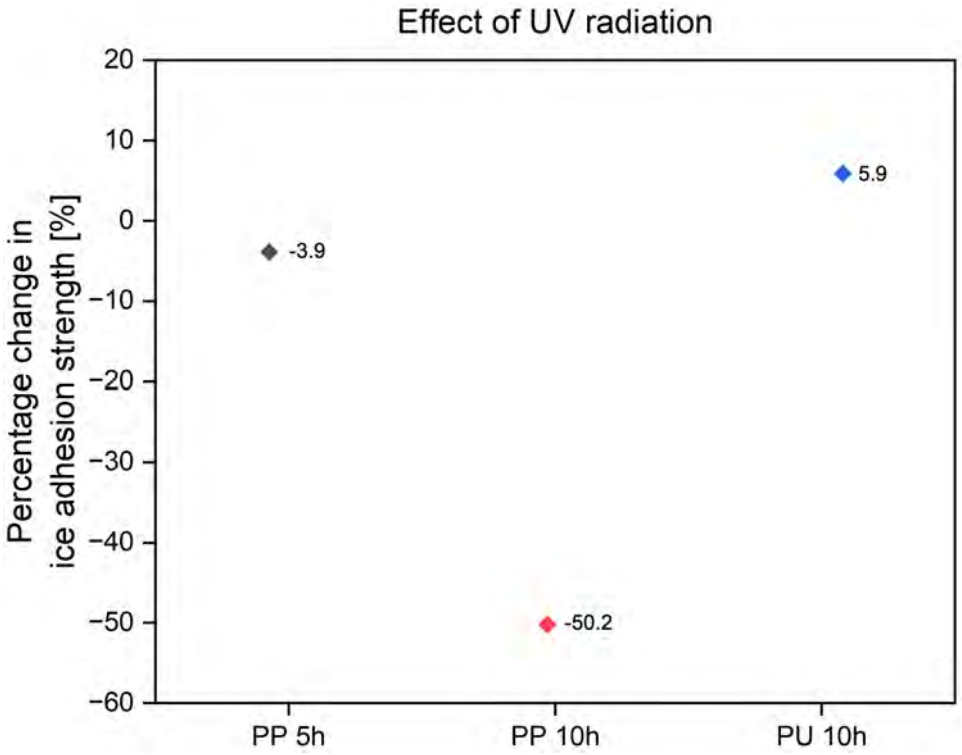

Figure 3.29: Effect of UV radiation on ice adhesion strength of PP and PU.

It is important to consider that ice adhesion strength is also highly sensitive to various external factors, including environmental conditions (e.g. temperature and humidity), the chosen testing method, and specific experimental parameters, such as the pushing height and the dimensions of the ice pillar. These variables can significantly influence the outcomes of ice adhesion measurements and should be carefully controlled in experimental tests.

4

Conclusion and recommendations

Due to the significant risks that ice accumulation poses to various industries, particularly in aerospace, there has been a growing interest in understanding the mechanisms of ice adhesion to surfaces and in developing anti-icing strategies by selecting materials with inherently low ice adhesion strength. The focus of this thesis was to gain a deeper understanding of the mechanisms behind ice adhesion on different materials and to explore the factors that influence this adhesion. By investigating how surface properties, such as surface roughness and hydrophobicity, and the presence of defects, such as dust particles, oil droplets and exposure to UV radiation, affect ice adhesion, this thesis aims to support the development of more effective anti-icing technologies and materials.

In this thesis, the impact of interfacial defects on the ice adhesion strength of different materials, specifically Teflon, polypropylene (PP), polyurethane (PU), and 6082 aluminium alloy, has been analysed and discussed. The results obtained showed that the interfacial defects analysed, i.e. dust particles, oil droplets, and UV radiation, influence the ice adhesion strength. This thesis contributes valuable knowledge to the field of ice adhesion research, particularly in understanding the effects of interfacial defects. The results provide a basis for future studies and practical applications aimed at reducing the risks associated with ice formation on critical infrastructure.

This chapter provides a summary of the key findings of this study, followed by a discussion of their implications. In addition, it will present potential areas for future research, providing ideas on how to extend the current research and explore new possibilities.

4.1. Summary of findings and discussion

The results from the bare samples indicated that Teflon and polypropylene exhibited the lowest ice adhesion strength compared to the polyurethane and aluminium alloy samples. This finding highlights the significant role of hydrophobicity, and therefore surface energy, in reducing the ice adhesion of these materials. Surface roughness also plays a critical role, as demonstrated by the difference in adhesion strength between polished and unpolished aluminium alloy samples. The results clearly show that the ice adhesion strength decreases significantly for the polished aluminium samples, which is attributed to their reduced surface roughness.

When dust particles were introduced, both PVC and SiO_2 particles were found to increase the ice adhesion strength on the aluminium samples. This increase can be explained by the contact splitting hypothesis, which states that splitting a large contact area into many smaller contact points increases the adhesion between the two materials in contact. This is due to the repeated process of crack arrest and re-initiation, which increases the difficulty of crack

propagation. As previously discussed, each time the crack encounters a particle, it is arrested because the adhesion between the ice and the particle is stronger than that between the particle and the substrate. This behaviour was confirmed by examining the ice pillar after detachment from the aluminium samples, where t was noticed that the particles remained adhered to the ice. A similar pattern was observed in polypropylene samples after modifying the test method. When the crack is stopped by a foreign particle, the detachment occurs between the particle and the substrate rather than between the ice and the particle, forcing the crack to restart between the ice and the substrate. This process increases the interfacial toughness, leading to an increase in ice adhesion strength.

Another observation from the experimental results was that the distribution of dust particles on the surface had a significant effect on the ice adhesion strength. Specifically, when particles were evenly distributed across the surface or concentrated near the pushing edge, the ice adhesion strength was higher compared to samples where particles were predominantly located on the opposite side. This can be attributed to the fact that a higher concentration of particles near the detachment initiation area promotes crack arrest and re-initiation, which increases interfacial toughness and consequently ice adhesion strength. On the other hand, with fewer particles concentrated near the pushing edge, there are fewer obstacles to impede crack propagation in the initial stages, resulting in lower ice adhesion strength. In addition, particles located further away from the pushing edge have a reduced effect as most of the interface has already detached by this point, so the final phase of detachment occurs rapidly, with minimal effect from the remaining particles. This reduces their overall contribution to the increase in interfacial toughness and ice adhesion strength.

This effect was also observed in polymer samples (except for the Teflon samples with the PVC particles). In these cases, the interaction between the substrates and the dust particles resulted in partial or complete detachment of the particles before the freezing of the water, reducing the number of particles at the ice interface during the test. Consequently, the number and location of the particles are critical factors in determining their effect on ice adhesion. Another important observation is that the influence of dust particles also depends on how the ice forms on the surface. Specifically, when the ice pillar was placed directly on the sample, the dust particles remained in place throughout the test. However, when the water froze directly on the surface, the number of particles at the interface was significantly reduced.

Hydrophobic liquid oil droplets were then added to the samples. Silicone oil was chosen since it is stable over a wide range of temperatures and it is commonly used as a lubricant or as a protective sheath on aircraft. As expected, the presence of the oil droplets resulted in a reduction in the ice adhesion strength. This reduction in the force required to detach the ice pillar can be attributed to the formation of thin hydrophobic liquid layers on the surface, which create liquid-solid interfaces between the oil and the ice. These interfaces reduce the contact area between the ice and the substrate, thereby reducing the total adhesion area and consequently the ice adhesion strength of the surfaces tested.

This thesis also examined the effect of UV radiation exposure on ice adhesion to polypropylene (PP) and polyurethane (PU). The exposure to UV radiation induced changes in both surface roughness and surface energy, which affected ice adhesion.

Specifically, for PP, a decrease in ice adhesion strength was observed after 10 hours of UV exposure. This reduction was attributed to changes in surface roughness, and chemical composition. The changes in chemical composition resulted in an increase in WCA, which in turn increased hydrophobicity and decreased ice adhesion strength. This behaviour is attributed to the phenomenon known as hydrophobic recovery, where certain polymers, such as PP, exhibit a transient decrease in hydrophobicity followed by a recovery phase. This process is driven by oxidative photodegradation caused by UV exposure. To further investigate

this phenomenon, PP samples were analysed after 5 hours of UV exposure. At this point, a decrease in WCA and surface roughness were observed, which correlated with a slight increase in ice adhesion strength. This suggests that the early stages of UV exposure initiate changes that temporarily reduce hydrophobicity, without significantly affecting adhesion, before the hydrophobic recovery process takes effect.

For PU samples, a decrease in WCA was observed after 10 hours of UV exposure, but not changes were detected in surface roughness. Unlike PP, this led to a slight increase in ice adhesion strength, indicating that the ”overturn” of polar groups, typically responsible for hydrophobic recovery, did not occur in PU. This suggests that the response to UV-induced oxidative photodegradation varies between different polymer types, influencing their respective ice adhesion behaviour.

The findings of this study provide valuable insights into the influence of interfacial defects on ice adhesion strength, specifically focusing on the presence of dust particles and oil droplets, and UV radiation exposure. This thesis advances the current understanding by highlighting the specific effects of these different types of defects. For example, the observed change in ice adhesion strength following the introduction of dust particles emphasizes the importance of considering environmental factors when designing icephobic coatings.

4.2. Recommendations for future research

Based on the conclusions of this thesis, there are several key areas where further research and improvements are necessary to improve the understanding of ice adhesion and to develop more effective anti-icing solutions.

Firstly, while this thesis has focused primarily on the effects of UV radiation exposure on polymer substrates after a fixed amount of hours, it would be valuable to extend this research to examine its effects over a longer period of time. This could include investigating how ice adhesion strength evolves over time with prolonged exposure, as well as how surface roughness and surface energy are affected. To continue the study of the effect of liquid droplets on ice adhesion strength, it would be beneficial to test ice adhesion strength with the introduction of droplets of a non-hydrophobic liquid. This could serve as a contrast to the effects observed with silicone oil and provide insight into how different types of liquids affect ice adhesion.

Moreover, studying the effect of different types of interfacial defects, such as mechanical damage or solvent exposure, on ice adhesion would provide a more complete understanding of the factors that influence ice adhesion strength. Studying the impact of environmental conditions, such as temperature, humidity, and the way in which ice forms on surfaces, would also provide valuable insights into the mechanisms of icing under different atmospheric conditions. The durability of icephobic coatings over multiple icing and de-icing cycles is another area of interest. Investigating how different materials perform over time, particularly under repeated icing conditions, would provide important information on their long-term effectiveness and potential degradation.

Ice adhesion remains a complex phenomenon that is not yet fully understood, and understanding the effect of different factors on it will reduce the risk of ice formation on surfaces. It is essential to test and compare different materials and potential icephobic coatings to identify the most effective solutions. To advance this research, it is crucial to improve the experimental set-up, for example by modifying the cooling fluid path in the housing chamber to achieve a more uniform temperature distribution, which would lead to more accurate and consistent data. On a broader scale, future research should prioritise the development of standardised test procedures across different laboratories. This would improve the comparability of results and accelerate the development of effective anti-icing technologies, ultimately contributing to

safer and more reliable solutions in industries where ice accumulation poses significant risk.

Finally, developing a finite element model (FEM) of the ice-substrate system could significantly improve the analysis of stress concentrations and interactions at the interface. Further modelling of crack initiation and propagation through the interface would also be of great interest, providing deeper insights into the mechanisms that govern ice adhesion and detachment.

In conclusion, future research into the understanding of ice adhesion is vital to reduce the significant risks present in various industries, such as aerospace, due to ice accumulation.

References

[1] Erlend Andenæs et al. “The influence of snow and ice coverage on the energy generation from photovoltaic solar cells”. In: *Solar Energy* 159 (Jan. 2018), pp. 318–328. ISSN: 0038-092X. DOI: 10.1016/J.SOLENER.2017.10.078.

[2] Rupp Carriveau et al. “Ice adhesion issues in renewable energy infrastructure”. In: *Journal of Adhesion Science and Technology* 26.4-5 (Mar. 2012), pp. 447–461. ISSN: 01694243. DOI: 10.1163/016942411X574592.

[3] Charles C. Ryerson. “Ice protection of offshore platforms”. In: *Cold Regions Science and Technology* 65.1 (Jan. 2011), pp. 97–110. ISSN: 0165-232X. DOI: 10.1016/J.COLDREGIONS.2010.02.006.

[4] Yihua Cao, Wenyuan Tan, and Zhenlong Wu. “Aircraft icing: An ongoing threat to aviation safety”. In: *Aerospace Science and Technology* 75 (Apr. 2018), pp. 353–385. ISSN: 1270-9638. DOI: 10.1016/J.AST.2017.12.028.

[5] Richard Menini and Masoud Farzaneh. “Elaboration of Al2O3/PTFE icephobic coatings for protecting aluminum surfaces”. In: *Surface and Coatings Technology* 203.14 (Apr. 2009), pp. 1941–1946. ISSN: 02578972. DOI: 10.1016/j.surfcoat.2009.01.030.

[6] Masoud Farzaneh. *Atmospheric icing of power networks*. London, United Kingdom: Springer Science & Business Media, 2008.

[7] Dennis A. Crider. “Accident lessons for stall upset recovery training”. In: *AIAA Guidance, Navigation, and Control Conference*. 2010. ISBN: 9781600869624. DOI: 10.2514/6.2010-8003.

[8] Filomena Piscitelli. “Special Issue ”Superhydrophobic and Icephobic Coatings as Passive Ice Protection Systems for Aeronautical Applications””. In: *Appl. Sci* 2024 (2024), p. 1288. DOI: 10.3390/app14031288.

[9] Kevin Petty and Carol D Floyd. “A statistical review of aviation airframe icing accidents in the US”. In: *Proceedings of the 11th Conference on Aviation, Range, and Aerospace Hyannis* (2004), pp. 623–628.

[10] Linyue Gao and Hui Hu. “Wind turbine icing characteristics and icing-induced power losses to utility-scale wind turbines”. In: *Proceedings of the National Academy of Sciences of the United States of America* 118.42 (Oct. 2021). ISSN: 10916490. DOI: 10.1073/pnas.2111461118.

[11] George William Kent Moore. “A climatology of vessel icing for the subpolar North Atlantic Ocean”. In: *International journal of climatology* 33.11 (2013), pp. 2495–2507. DOI: 10.1002/joc.3604. URL: https://rmets.onlinelibrary.wiley.com/doi/10.1002/joc.3604.

[12] Lasse Makkonen. “Models for the growth of rime, glaze, icicles and wet snow on structures”. In: *Philosophical Transactions of the Royal Society of London. Series A: Mathematical, Physical and Engineering Sciences* 358.1776 (2000), pp. 2913–2939. DOI: 10.1098/rsta.2000.0690. URL: https://royalsocietypublishing.org/.

[13] Christian Stenroos. *Properties of icephobic surfaces in different icing conditions*. Tech. rep. Tampere University of Technology, 2015.

[14] Susan Frankenstein and Andrew M Tuthill. “Ice Adhesion to Locks and Dams: Past Work; Future Directions?” In: *Journal of Cold Regions Engineering* 16.2 (2002), pp. 83–96.

[15] Olivier Parent and Adrian Ilinca. “Anti-icing and de-icing techniques for wind turbines: Critical review”. In: *Cold Regions Science and Technology* 65.1 (Jan. 2011), pp. 88–96. ISSN: 0165232X. DOI: 10.1016/j.coldregions.2010.01.005.

[16] Neda Dalili, Afsaneh Edrisy, and Rupp Carriveau. *A review of surface engineering issues critical to wind turbine performance*. Feb. 2009. DOI: 10.1016/j.rser.2007.11.009.

[17] Yizhou Shen et al. “Icephobic materials: Fundamentals, performance evaluation, and applications”. In: *Progress in Materials Science* 103 (June 2019), pp. 509–557. ISSN: 0079-6425. DOI: 10.1016/J.PMATSCI.2019.03.004.

[18] Peyman Irajizad, Sina Nazifi, and Hadi Ghasemi. “Icephobic surfaces: Definition and figures of merit”. In: *Advances in Colloid and Interface Science* 269 (July 2019), pp. 203–218. ISSN: 0001-8686. DOI: 10.1016/J.CIS.2019.04.005.

[19] Yizhi Zhuo et al. “Polysiloxane as icephobic materials – The past, present and the future”. In: *Chemical Engineering Journal* 405 (Feb. 2021), p. 127088. ISSN: 1385-8947. DOI: 10.1016/J.CEJ.2020.127088.

[20] Luyao Bao et al. “A significant reduction of ice adhesion on nanostructured surfaces that consist of an array of single-walled carbon nanotubes: A molecular dynamics simulation study”. In: *Applied Surface Science* 437 (Apr. 2018), pp. 202–208. ISSN: 0169-4332. DOI: 10.1016/J.APSUSC.2017.12.096.

[21] Qiangqiang Sun et al. “Reduction of atomistic ice tensile stress by graphene–carbon nanotube coating”. In: *Applied Surface Science* 565 (Nov. 2021), p. 150562. ISSN: 0169-4332. DOI: 10.1016/J.APSUSC.2021.150562.

[22] Marco Marengo and Joel De Coninck. *The Surface Wettability Effect on Phase Change*. Springer International Publishing, 2022. DOI: 10.1007/978-3-030-82992-6.

[23] Regina Rekuviene et al. *A review on passive and active anti-icing and de-icing technologies*. Aug. 2024. DOI: 10.1016/j.applthermaleng.2024.123474.

[24] Sigrid Rønneberg et al. “The effect of ice type on ice adhesion”. In: *AIP Advances* 9.5 (May 2019). ISSN: 21583226. DOI: 10.1063/1.5086242.

[25] Saurabh Nath, S. Farzad Ahmadi, and Jonathan B. Boreyko. *A Review of Condensation Frosting*. Apr. 2017. DOI: 10.1080/15567265.2016.1256007.

[26] Jeffrey Brandon Dooley. *Determination and characterization of ice propagation mechanisms on surfaces undergoing dropwise condensation*. Texas A&M University, 2010.

[27] Guy Fortin and Jean Perron. “Ice adhesion models to predict shear stress at shedding”. In: *Journal of Adhesion Science and Technology* 26.4-5 (Mar. 2012), pp. 523–553. ISSN: 01694243. DOI: 10.1163/016942411X574835.

[28] Thomas Young. “An essay on the cohesion of fluids”. In: *Philosophical transactions of the royal society of London* (1805), pp. 65–87.

[29] Kai Schennetten, Matthias M Meier, and Markus Scheibinger. “Non-sticking drops”. In: *Reports on Progress in Physics* 68.68 (2005). DOI: 10.1088/0034-4885/68/11/R01.

[30] Barthlott Wilhelm and Neinhuis Christoph. *Purity of the sacred lotus, or escape from contamination in biological surfaces*. Tech. rep. Planta, 1997, pp. 1–8.

[31] Andrey V Kudryavtsev. *3D Reconstruction in Scanning Electron Microscope : from image acquisition to dense point cloud*. Tech. rep. Université Bourgogne Franche-Comté, 2017. URL: https://tel.archives-ouvertes.fr/tel-01930234.

[32] Dipak Sarkar and Masoud Farzaneh. "Superhydrophobic Coatings with Reduced Ice Adhesion". In: *Journal of Adhesion Science and Technology* 23.9 (2009), pp. 1215–1237. DOI: 10.1163/156856109X433964. URL: https://www.tandfonline.com/action/journalInformation?journalCode=tast20.

[33] Bo Liu et al. "Strategies for anti-icing: low surface energy or liquid-infused?" In: *RSC advances* 6.74 (2016), pp. 70251–70260. DOI: 10.1039/c6ra11383d. URL: www.rsc.org/advances.

[34] Sergei Kulinich and Masoud Farzaneh. "How Wetting Hysteresis Influences Ice Adhesion Strength on Superhydrophobic Surfaces". In: *J. Adhes. Sci. Technol* 25.16 (2009), pp. 4056–4060. DOI: 10.1021/la901439c. URL: https://pubs.acs.org/sharingguidelines.

[35] Richard Menini, Zahira Ghalmi, and Masoud Farzaneh. "Highly resistant icephobic coatings on aluminum alloys". In: *Cold Regions Science and Technology* 65.1 (Jan. 2011), pp. 65–69. ISSN: 0165232X. DOI: 10.1016/j.coldregions.2010.03.004.

[36] Jinlong Song et al. "Inexpensive and non-fluorinated superhydrophobic concrete coating for anti-icing and anti-corrosion". In: *Journal of Colloid and Interface Science* 541 (Apr. 2019), pp. 86–92. ISSN: 10957103. DOI: 10.1016/j.jcis.2019.01.014.

[37] Vittorio Vercillo et al. "Design Rules for Laser-Treated Icephobic Metallic Surfaces for Aeronautic Applications". In: *Advanced Functional Materials* 30.16 (2020). DOI: 10.1002/adfm.201910268. URL: https://doi.org/10.1002/adfm.201910268..

[38] Jing Chen et al. "Superhydrophobic surfaces cannot reduce ice adhesion". In: *Applied Physics Letters* 101.11 (Sept. 2012). ISSN: 00036951. DOI: 10.1063/1.4752436.

[39] Kripa K. Varanasi et al. "Frost formation and ice adhesion on superhydrophobic surfaces". In: *Applied Physics Letters* 97.23 (Dec. 2010). ISSN: 00036951. DOI: 10.1063/1.3524513.

[40] Srinivas Bengaluru Subramanyam et al. "Low Ice Adhesion on Nano-Textured Superhydrophobic Surfaces under Supersaturated Conditions". In: *ACS Applied Materials and Interfaces* 8.20 (May 2016), pp. 12583–12587. ISSN: 19448252. DOI: 10.1021/acsami.6b01133.

[41] Samaneh Heydarian, Reza Jafari, and Gelareh Momen. *Recent progress in the anti-icing performance of slippery liquid-infused surfaces*. Feb. 2021. DOI: 10.1016/j.porgcoat.2020.106096.

[42] Shuqing Yang et al. "Research on the icephobic properties of fluoropolymer-based materials". In: *Applied Surface Science* 257.11 (Mar. 2011), pp. 4956–4962. ISSN: 01694332. DOI: 10.1016/j.apsusc.2011.01.003.

[43] Rainer Lohmann et al. "Are Fluoropolymers Really of Low Concern for Human and Environmental Health and Separate from Other PFAS?" In: (2020). DOI: 10.1021/acs.est.0c03244. URL: https://dx.doi.org/10.1021/acs.est.0c03244.

[44] Peyman Irajizad et al. "Stress-localized durable icephobic surfaces †". In: 6 (2019), p. 758. DOI: 10.1039/c8mh01291a.

[45] Ghazaleh Gharib et al. *Antifreeze Proteins: A Tale of Evolution From Origin to Energy Applications*. Feb. 2022. DOI: 10.3389/fbioe.2021.770588.

[46] Xiaojun Wu et al. *Antifreeze proteins and their biomimetics for cell cryopreservation: Mechanism, function and application-A review*. Dec. 2021. DOI: 10.1016/j.ijbiomac.2021.09.211.

[47] S. Farzad Ahmadi et al. “Passive Antifrosting Surfaces Using Microscopic Ice Patterns”. In: *ACS Applied Materials and Interfaces* 10.38 (Sept. 2018), pp. 32874–32884. ISSN: 19448252. DOI: 10.1021/acsami.8b11285.

[48] Jonathan B. Boreyko et al. “Controlling condensation and frost growth with chemical micropatterns”. In: *Scientific Reports* 6 (Jan. 2016). ISSN: 20452322. DOI: 10.1038/srep19131.

[49] Laforte C. and Beisswenger A. “Icephobic-Materials-Centrifuge-Adhesion-Test”. In: *11th International Workshop on Atmospheric Icing on Structures (IWAIS)* (June 2005), pp. 1–5.

[50] Kevin Golovin et al. “Low-interfacial toughness materials for effective large-scale deicing”. In: *Science* 364.6438 (2019), pp. 371–375. URL: https://www.science.org.

[51] Luca Stendardo et al. “Reframing ice adhesion mechanisms on a solid surface”. In: *Applied Surface Science* 641 (Dec. 2023), p. 158462. ISSN: 0169-4332. DOI: 10.1016/J.APSUSC.2023.158462.

[52] Sigrid Rønneberg, Jianying He, and Zhiliang Zhang. *The need for standards in low ice adhesion surface research: a critical review*. Feb. 2020. DOI: 10.1080/01694243.2019.1679523.

[53] Andrew Work and Yongsheng Lian. *A critical review of the measurement of ice adhesion to solid substrates*. Apr. 2018. DOI: 10.1016/j.paerosci.2018.03.001.

[54] Marzhan Sypabekova et al. *Review: 3-Aminopropyltriethoxysilane (APTES) Deposition Methods on Oxide Surfaces in Solution and Vapor Phases for Biosensing Applications*. Jan. 2023. DOI: 10.3390/bios13010036.

[55] Khaled Ziani et al. “Microplastics: A Real Global Threat for Environment and Food Safety: A State of the Art Review”. In: (2023). DOI: 10.3390/nu15030617. URL: https://doi.org/10.3390/nu15030617.

[56] Sajid Naseem et al. “Different transition metal combinations of LDH systems and their organic modifications as UV protecting materials for polypropylene (PP)”. In: *RSC Advances* 8.52 (2018), pp. 29789–29796. ISSN: 20462069. DOI: 10.1039/c8ra05447a.

[57] Guido Grause, Mei Fang Chien, and Chihiro Inoue. *Changes during the weathering of polyolefins*. Nov. 2020. DOI: 10.1016/j.polymdegradstab.2020.109364.

[58] Svetlana Butylina, Marko Hyvärinen, and Timo Kärki. “A study of surface changes of wood-polypropylene composites as the result of exterior weathering”. In: *Polymer Degradation and Stability* 97.3 (Mar. 2012), pp. 337–345. ISSN: 01413910. DOI: 10.1016/j.polymdegradstab.2011.12.014.

[59] Xiu Li et al. “UV LED curable epoxy soybean-oil-based waterborne PUA resin for wood coatings”. In: *Progress in Organic Coatings* 151 (Feb. 2021). ISSN: 03009440. DOI: 10.1016/j.porgcoat.2020.105942.

[60] Olympus IMS. *”Surface Roughness Measurement Portal: Parameters.* URL: https://www.olympus-ims.com/en/metrology/surface-roughness-measurement-portal/parameters/#!cms%5Bfocus%5D=cmsContent14709.

[61] Robert A. Biro, Eric C. Tyrode, and Esben Thormann. “Reducing Ice Adhesion to Polyelectrolyte Surfaces by Counterion-Mediated Nonfrozen Hydration Water”. In: *ACS Applied Materials and Interfaces* (2024). ISSN: 19448252. DOI: 10.1021/acsami.4c02434.

[62] Edwin P. Chan et al. “Designing model systems for enhanced adhesion”. In: *MRS Bulletin* 32.6 (2007), pp. 496–503. ISSN: 08837694. DOI: 10.1557/mrs2007.84.

[63] Hong Hu et al. “Revisiting the contact splitting hypothesis: An effective route for enhancing adhesion on rough surface”. In: *Journal of the Mechanics and Physics of Solids* 170 (Jan. 2023). ISSN: 00225096. DOI: 10.1016/j.jmps.2022.105121.

[64] Bernd Wetzel et al. “Epoxy nanocomposites - fracture and toughening mechanisms”. In: *Engineering Fracture Mechanics* 73.16 (Nov. 2006), pp. 2375–2398. ISSN: 00137944. DOI: 10.1016/j.engfracmech.2006.05.018.

[65] Aldobenedetto Zotti et al. “Fracture Toughening Mechanisms in Epoxy Adhesives”. In: *Adhesives - Applications and Properties*. InTech, Nov. 2016. DOI: 10.5772/65250.

[66] AG Evans and FW Zok. “The physics and mechanics of fibre-reinforced brittle matrix composites”. In: *Journal of Materials science* 29 (1994), pp. 3857–3896.

[67] Emad Yousif and Raghad Haddad. *Photodegradation and photostabilization of polymers, especially polystyrene: review*. Tech. rep. 2013. URL: http://www.springerplus.com/content/2/1/398.

[68] T. Lu et al. “UV degradation model for polymers and polymer matrix composites”. In: *Polymer Degradation and Stability* 154 (Aug. 2018), pp. 203–210. ISSN: 01413910. DOI: 10.1016/j.polymdegradstab.2018.06.004.

[69] Benedikt Hünnekens et al. “Hydrophobic recovery of atmospheric pressure plasma treated surfaces of Wood-Polymer Composites (WPC)”. In: *European Journal of Wood and Wood Products* 75.5 (Sept. 2017), pp. 761–766. ISSN: 1436736X. DOI: 10.1007/s00107-017-1175-x.

[70] Grace Wan, Colin Li Pi Shan, and Shaoguang Feng. “Advances in bonding plastics”. In: *Advances in Structural Adhesive Bonding, Second Edition*. Elsevier, Jan. 2023, pp. 327–358. ISBN: 9780323912143. DOI: 10.1016/B978-0-323-91214-3.00009-0.

A

Appendix A

WCA results

Table A.1: Water contact angles.

Material				**Mean WCA [°]**
AA-6082 unpolished	84.8	83.9	84.2	84.3
AA-6082 polished	97.8	96.4	99.3	97.8
Teflon	111.7	110.8	110.5	111.0
Polypropylene	99.4	100.4	101.6	100.6
Polyurethane	87.6	86.2	86.5	86.8
PVC	94.3	96.9	96.2	95.8
SiO_2	27.7	28.3	27.2	27.7
Surface modified SiO_2	47.2	48.8	46.2	47.4
PP after 5h of UV exposure	86.1	81.7	91.3	86.4
PP after 10h of UV exposure	107.0	107.3	108.2	107.5
PU after 10h of UV exposure	75.6	73.4	72.1	73.7

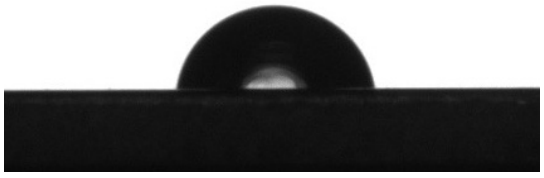

Figure A.1: Water droplet (10 μl) on the AA-6082 unpolished surface.

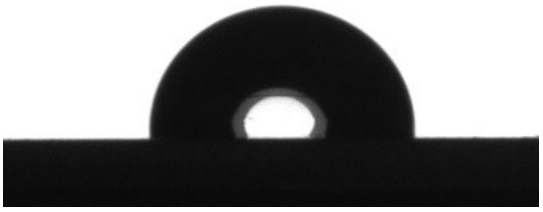

Figure A.2: Water droplet (10 μl) on the AA-6082 polished surface.

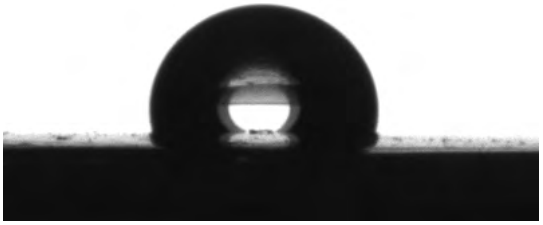

Figure A.3: Water droplet (10 μl) on the Teflon surface.

Figure A.4: Water droplet (10 μl) on the PP surface.

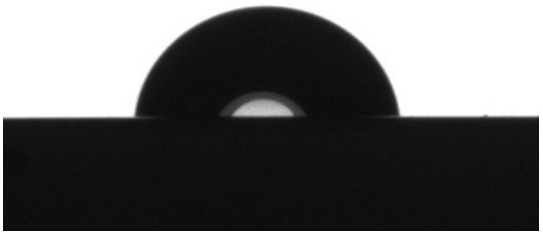

Figure A.5: Water droplet (10 μl) on the PU surface.

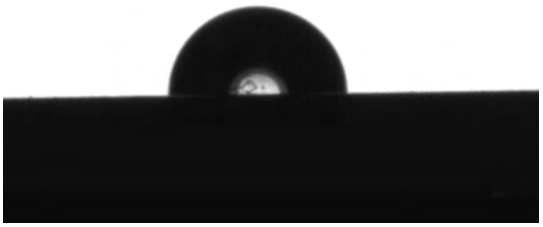

Figure A.6: Water droplet (10 μl) on the PVC surface.

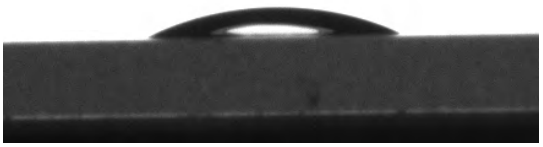

Figure A.7: Water droplet (10 μl) on the SiO_2 surface.

Figure A.8: Water droplet (10 μl) on the surface modified SiO_2 surface.

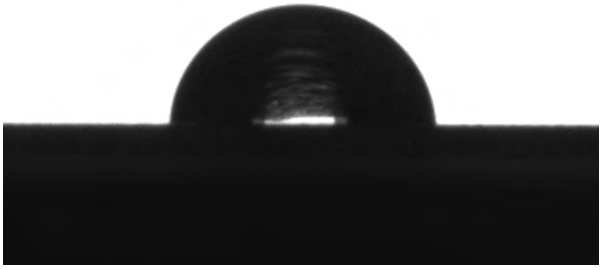

Figure A.9: Water droplet (10 μl) on the PP surface after 5 hours of UV radiation exposure.

Figure A.10: Water droplet (10 μl) on the PP surface after 10 hours of UV radiation exposure.

Figure A.11: Water droplet (10 μl) on the PU surface after 10 hours of UV radiation exposure.

B

Appendix B

Surface roughness results

Table B.1: Arithmetical mean height (Sa) of samples.

Material	Sa		
	Max. [μm]	Min. [μm]	Average [μm]
AA-6082 unpolished	2.72	2.29	2.61
AA-6082 polished	0.57	0.26	0.42
Teflon	1.69	0.84	1.27
Polypropylene	5.32	3.35	4.45
Polyurethane	0.27	0.24	0.25
PP after 5h of UV	5.18	3.69	4.50
PP after 10h of UV	4.52	2.60	3.70
PU after 10h of UV	0.24	0.16	0.21

Table B.2: Maximum height (Sz) of samples.

Material	Sz		
	Max. [μm]	Min. [μm]	Average [μm]
AA-6082 unpolished	28.68	20.60	24.23
AA-6082 polished	10.35	4.01	7.71
Teflon	25.75	23.33	24.49
Polypropylene	59.47	33.46	49.51
Polyurethane	8.08	4.64	6.09
PP after 5h of UV	48.90	34.25	43.24
PP after 10h of UV	55.11	30.46	42.26
PU after 10h of UV	7.24	4.51	6.18

C

Appendix C

Failed tests

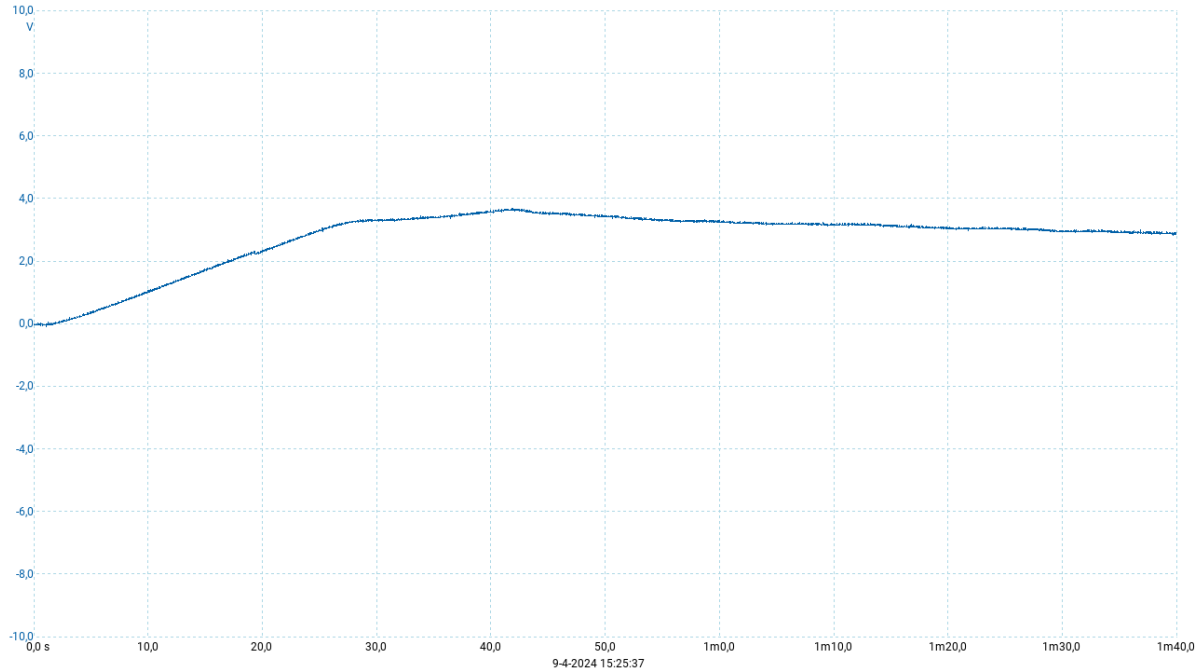

Figure C.1: Sliding of the ice pillar for AA6082 unpolished.

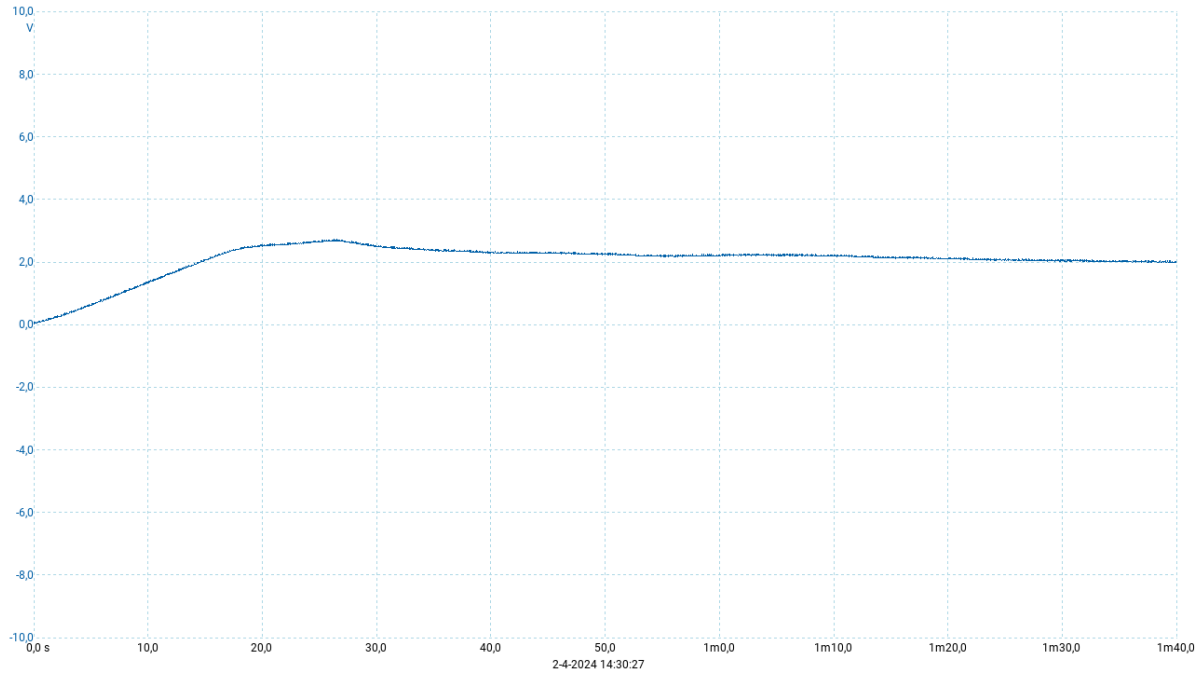

Figure C.2: Sliding of the ice pillar for PU.